

Abrasive Blasting with Post-Process and In-Situ Characterization

Robert Jeffrey Mills

Thesis submitted to the faculty of the Virginia Polytechnic Institute and State University
in partial fulfillment of the requirements for the degree of

Master of Science
In
Materials Science and Engineering

Gary R. Pickrell, Chair
Daniel S. Homa
Alan P. Druschitz
Thomas W. Staley

May 29, 2014
Blacksburg, VA

Keywords: (abrasive blasting, media, substrate, roughness, profilometry, temperature,
optical fibers,)

Copyright 2014, Robert J. Mills

Abrasive Blasting with Post-Process and In-Situ Characterization

Robert Jeffrey Mills

ABSTRACT

Abrasive blasting is a common process for cleaning or roughening the surface of a material prior to the application of a coating. Although the process has been in practice for over 100 years, the lack of a comprehensive understanding of the complex interactions that exist with the process can still yield an inferior surface quality. Subsequently, parts can be rejected at one of many stages of the manufacturing process and/or fail unexpectedly upon deployment. The objective of this work is to evaluate the effect of selected input parameters on the characteristics of the blasted surface characteristics so that a more useful control strategy can be implemented. To characterize surface roughness, mechanical profilometry was used to collect average roughness parameter, R_a . Decreasing blast distance from 6" to 4" gave $\Delta R_a = +0.22 \mu\text{m}$ and from 8" to 6" gave $\Delta R_a = +0.22 \mu\text{m}$. Increasing blast pressure from 42 psi to 60 psi decreased the R_a by $0.33 \mu\text{m}$. Media pulsation reduced R_a by $0.56 \mu\text{m}$ and the use of new media reduced R_a by $0.47 \mu\text{m}$. Although blasting under the same conditions and operator on different days led to ΔR_a due to shorter blast times, there was no statistically significant variance in R_a attributed to blasting on different days. Conversely, a $\Delta R_a = +0.46 \mu\text{m}$ was observed upon blasting samples with different cabinets. No significant ΔR_a was found when switching between straight and Venturi nozzles or when using different operators.

Furthermore, the feasibility of fiber optic sensing technologies was investigated as potential tools to provide real time feedback to the blast machine operator in terms of substrate temperature. Decreasing the blast distance from 6" to 4" led to $\Delta T = +9.2 \text{ }^\circ\text{C}$, while decreasing the blast angle to 45° gave $\Delta T = -11.6 \text{ }^\circ\text{C}$ for 304 stainless steel substrates. Furthermore, increasing the blast pressure from 40 psi to 50 psi gave $\Delta T = +15.3 \text{ }^\circ\text{C}$ and changing from 50 psi to 60 psi gave $\Delta T = +9.9 \text{ }^\circ\text{C}$. The blast distance change from 8" to 6" resulted in $\Delta T = +9.8 \text{ }^\circ\text{C}$ in thin stainless steel substrate temperature. The effects of substrate thickness or shape were evaluated, giving $\Delta T = +7.4 \text{ }^\circ\text{C}$ at 8" distance, $\Delta T = +20.2 \text{ }^\circ\text{C}$ at 60 psi pressure, and $\Delta T = -15.2 \text{ }^\circ\text{C}$ at 45° blasting when comparing thin stainless steel against 304 stainless steel (thick) temperatures. No significant ΔT in means was found when going from 6" to 8" distance on 304 stainless steel, 40 psi and 60 psi blasting of thin

SS, as well as angled and perpendicular blasting of thin SS. Comparing thick 304 and thin stainless steel substrates at a 6" blast distance gave no significant ΔT .

Acknowledgements

I would like to sincerely thank Dr. Gary Pickrell for his support, feedback, and allowing me to work in his research group these past four semesters. I have learned many things from working in his lab and with his research team. I'm appreciative of the support of Dr. Daniel Homa for his patience, encouragement, and inspiring work ethic on various research projects. I have increased my knowledge of abrasive blasting and optical fiber technologies through experiments in this research group also.

I would like to thank specific members of the research team. I want to thank Edward, Cary, and Taylor for helping me carry out experiments in the blast cabinet in the Hancock Lab. Their time and patience were invaluable and helped me obtain some of experimental results shown in this report. I appreciate the rest of the research team being cooperative and helpful when I used the blast cabinet, as it was loud and annoying at times.

Lastly, I want to thank everyone who helped me make it this far in my academic career. Without the support, encouragement, and love from my parents schoolwork, research, and thesis writing would not have been possible. My friends and other family helped encourage me along the way and I'm grateful for that as well.

I would also like to acknowledge and thank CCAM for their funding of the equipment and materials for the roughness testing portion of this work. I want to thank Norton Sandblasting as well for answering many questions related to maintaining the blasting equipment. LISA helped greatly with the statistical analysis of the results as well.

All photographs by author (Robert J. Mills), 2014.

Table of Contents

1	Introduction	1
1.1	Motivation	1
1.2	Research Approach	2
1.3	Thesis Scope and Organization	2
2	Background	4
2.1	Abrasive Blasting History and Advances	4
2.1.1	Various Blasting Methods	5
2.1.2	Control Systems	6
2.2	Abrasive Media	7
2.2.1	Abrasive Shape	7
2.2.2	Grit, Shot and Cylindrical	10
2.2.3	Abrasive Size & Size Distribution	11
2.2.4	Abrasive Hardness	14
2.2.5	Abrasive Density	16
2.2.6	Type (Metallic vs. Non-Metallic)	17
2.2.7	Fracture Strength	18
2.2.8	Impurities	19
2.3	Substrates	19
2.3.1	Substrate Material	20
2.3.2	Substrate Hardness	21
2.3.3	Substrate Thickness	21
2.3.4	Substrate Shape	21
2.3.5	Initial Surface Roughness	22
2.3.6	Pre-Blasting Strains and Stresses	23
2.3.7	Cleanliness	23
2.4	Blasting Environment	24
2.4.1	Temperature	24
2.4.2	Humidity	25
2.5	Blasting Process Parameters	26
2.5.1	Blasting Pressure and Media Flow Rate	26
2.5.2	Stand-off Distance	27
2.5.3	Blast Angle	29
2.5.4	Blast Time	30
2.5.5	Media Degradation/Fragmentation	32

2.5.6	Nozzle Type	33
2.6	Characterization Techniques	34
2.6.1	Mechanical Profilometry	34
2.6.2	Optical Profilometry/Microscopy	36
3	Experimental Methods	37
3.1	Roughness Experimental Procedure	37
3.1.1	Media, Substrate, and Parameter Selections	37
3.1.2	Cabinet Information	38
3.1.3	Substrate Preparation	39
3.1.4	Cabinet Preparation and Substrate Blasting	40
3.2	Post-Process Characterization	43
3.2.1	Mitutoyo SurfTest SJ-210 Mechanical Profilometer	43
3.2.2	HIROX Optical Microscopy	44
3.2.3	UVA ROST Optical Profilometry	44
3.3	Substrate Temperature Experimental Procedure	45
3.3.1	Optical Fiber Splicing, Adaptors, and Connectors	45
3.3.2	Optical Fiber Connection Cleanliness	46
3.3.3	Micron Optics SM125 Optical Sensing Interrogator	47
3.3.4	Temperature Sensor and Probe	47
3.3.5	Micron Optics Enlight Software	48
3.3.6	Sensor Attachment to Substrates	50
3.3.7	Temperature Blast Conditions	52
3.4	Statistical Analysis of Roughness and Temperature Data	52
4	Results and Discussion.....	54
4.1	Roughness Characterization Results	54
4.2	Effect of Process Parameters on Surface Roughness	56
4.3	Repeatability and Reproducibility	60
4.4	Temperature Sensor Measurements	62
4.5	Temperature Probe Measurements	64
5	Conclusions.....	71
6	Future Work.....	73
	References	74
	Appendices.....	78
	Appendix A Blast Media Chart	78
	Appendix B Nozzle Design	79
	Appendix C Roughness Testing Information	80

Appendix D Temperature Testing Information	83
Appendix E Sample F-test and t-test calculations	87
Appendix F Roughness F-tests and t-tests Data	89
Appendix G Temperature F-tests and t-tests data.....	92
Appendix H Figures and Tables Permissions	96

List of Tables

Table 2-1 ISO 12944-4 Blast cleaning methods. Momber A. <i>Blast Cleaning Technology: Chapter 1: Introduction</i> , 2008. p. 3. http://link.springer.com/chapter/10.1007%2F978-3-540-73645-5_2 (accessed March 31, 2013) Used with permission from Copyright Clearance Center, 2014.....	5
Table 2-2 Mohs hardness scale. Momber A. <i>Blast Cleaning Technology: Chapter 2: Abrasive Materials</i> , 2008. p. 14. http://link.springer.com/chapter/10.1007%2F978-3-540-73645-5_2 (accessed April 1, 2013) Used with permission from Copyright Clearance Center, 2014.....	14
Table 3-1 Media and substrate properties.....	38
Table 3-2 Cabinet specifications for roughness testing.....	38
Table 3-3 Blasting information during one experiment.....	40
Table 3-4 Experimental design sets for roughness testing.....	40
Table 3-5 Measurement information for roughness testing.....	43
Table 3-6 SJ-210 measurement settings.	43
Table 3-7 Experimental design sets for temperature testing.....	52
Table 4-1 SJ-210 Ra results with three types of standard deviation.....	54
Table 4-2 Hirox measurements for Sa & σ calculations of samples 2.10 and 3.10.....	55
Table 4-3 ROST Avg. Sa and measurement σ values.	55
Table 4-4 Comparison of R_a and σ_M for characterization techniques.....	56
Table 4-5 304 Stainless steel substrate temperature results.....	66
Table 4-6 Thin stainless steel substrate temperature results.	68
Table A-1 Blast media chart. No Author. “Blast Media Chart.” Norton Sandblasting Equipment. 2014. http://www.nortonsandblasting.com/nsbabrasives.html (accessed June 9, 2014) Used with permission from Norton Sandblasting Equipment, 2014.....	78

List of Figures

Figure 2.1 a. pre-blasting, b. blasting, and c. post-blasting surfaces. No Author. "Technical Reference: Surface Preparation." Blast One. 2014. http://www.blast-one.com/weekly-tips/the-difference-between-surface-profile-and-class-of-blast (accessed May 14, 2014) Used with permission from Blast One, 2014.	4
Figure 2.2 Suction and pressure blasting systems. No Author. "Blast Cabinets." Norton Sandblasting Equipment, 2014. http://www.nortonsandblasting.com/nsbcontact.html (accessed May 14, 2014) Used with permission from Norton Sandblasting Equipment, 2014.....	6
Figure 2.3 Media shape definitions; a. shape factor & circulatory factor, b. roundness, & sphericity, & c. elongation ratio & flatness ratio. Momber A. <i>Blast Cleaning Technology: Chapter 2: Abrasive Materials</i> , 2008. p. 19. http://link.springer.com/chapter/10.1007%2F978-3-540-73645-5_2 (accessed March 31, 2013) Used with permission from Copyright Clearance Center, 2014.....	8
Figure 2.4 a. Hansink's shape designations & b. garnet roundness-sphericity chart. Momber A. <i>Blast Cleaning Technology: Chapter 2: Abrasive Materials</i> , 2008. p. 21. http://link.springer.com/chapter/10.1007%2F978-3-540-73645-5_2 (accessed March 31, 2013) Used with permission from Copyright Clearance Center, 2014.	9
Figure 2.5 Shape, size, and type relationships. Momber A. <i>Blast Cleaning Technology: Chapter 2: Abrasive Materials</i> , 2008. p. 20. http://link.springer.com/chapter/10.1007%2F978-3-540-73645-5_2 (accessed March 31, 2013) Used with permission from Copyright Clearance Center, 2014.....	10
Figure 2.6 a. Grit image and b. shot image. Momber A. <i>Blast Cleaning Technology: Chapter 2: Abrasive Materials</i> , 2008. p. 18. http://link.springer.com/chapter/10.1007%2F978-3-540-73645-5_2 (accessed March 31, 2013) Used with permission from Copyright Clearance Center, 2014.10	
Figure 2.7 Distribution of sieve analysis. Momber A. <i>Blast Cleaning Technology: Chapter 2: Abrasive Materials</i> , 2008. p. 26. http://link.springer.com/chapter/10.1007%2F978-3-540-73645-5_2 (accessed March 31, 2013) Used with permission from Copyright Clearance Center, 2014.12	
Figure 2.8 Grit contamination vs. roughness. Day, James; Huang, Xiao; and Richards, N.L. "Examination of a Grit-Blasting Process for Thermal Spraying Using Statistical Methods." <i>Journal of Thermal Spray Technology</i> , 2005/Vol. 14, p. 477. http://link.springer.com/article/10.1361%2F105996305X76469 (accessed November 2012) Used with permission from Copyright Clearance Center, 2014.	13
Figure 2.9 Grit diameter vs. a. residual grit and b. penetration depth. Maruyama T, Akagi K, Kobayashi T. "Effects of Blasting Parameters on Removability of Residual Grit." <i>Journal of Thermal Spray Technology</i> . 2006/Vol. 15, no. 4. p. 820. http://link.springer.com/article/10.1361%2F105996306X147018 (accessed November 2, 2012) Used with permission from Copyright Clearance Center; letter attached.	14
Figure 2.10 Abrasive hardness effect on specific mass loss. Momber A. <i>Blast Cleaning Technology: Chapter 2: Abrasive Materials</i> , 2008. p. 11, 12. http://link.springer.com/chapter/10.1007%2F978-3-540-73645-5_2 (accessed March 31, 2013) Used with permission from Copyright Clearance Center, 2014.	16
Figure 2.11 a. Steel shot, b. steel grit, c. brown corundum, & d. demetalized steel slag. Makova, I., Sopko, M. "Effect of Blasting Material on Surface Morphology of Steel Sheets." <i>Acta Metallurgica Slovaca</i> . 2010/ Vol. 16, no. 2, p. 111. (accessed March 07, 2013) Used with permission from Acta Metallurgica Slovaca, 2014.....	17

Figure 2.12 Particle strength vs. a. Weibull function & b. vs. fracture strength. Momber A. <i>Blast Cleaning Technology: Chapter 2: Abrasive Materials</i> , 2008. p. 11, 12. http://link.springer.com/chapter/10.1007%2F978-3-540-73645-5_2 (accessed March 31, 2013) Used with permission from Copyright Clearance Center, 2014].	19
Figure 2.13 Temperature effects from blasting. Fang, C.K., Chuang, T.H. "Erosion of SS41 Steel by Sand Blasting." <i>Metallurgical and Materials Transactions A</i> . 1999/Vol. 30A, p. 944. (accessed January 11, 2013) Used with permission from Copyright Clearance Center, 2014.	25
Figure 2.14 Effect of humidity during blasting. Fang, C.K., Chuang, T.H. "Erosion of SS41 Steel by Sand Blasting." <i>Metallurgical and Materials Transactions A</i> . 1999/Vol. 30A, p. 944. (accessed January 11, 2013) Used with permission from Copyright Clearance Center, 2014.	25
Figure 2.15 Blasting pressure vs. grit flow rate. Mellalia, M., Grimaud, A., Leger, A.C., Fauchais, P., and Lu, J. "Alumina Grit Blasting Parameters for Surface Preparation in the Plasma Spraying Operation." <i>Journal of Thermal Spray Technology</i> . 1997/Vol. 6. No. 2. p 219. (accessed October 22, 2012) Used with permission from Copyright Clearance Center, 2014.	27
Figure 2.16 Blast pressure vs. compressive residual stress. Chander, K. Poorna, Vashita, M., Sabiruddin, Kazi, Paul, S., Bandyopadhyay, P.P. "Effects of Grit Blasting on Surface Properties of Steel Substrates." <i>Materials and Design</i> . 2009. p. 2901. (accessed November 2012) Used with permission from Copyright Clearance Center, 2014.	27
Figure 2.17 Surface roughness distance. Chander, K. Poorna, Vashita, M., Sabiruddin, Kazi, Paul, S., Bandyopadhyay, P.P. "Effects of Grit Blasting on Surface Properties of Steel Substrates." <i>Materials and Design</i> . 2009. p. 2899. (accessed November 2012) Used with permission from Copyright Clearance Center, 2014.	28
Figure 2.18 Surface roughness vs. blasting distance/substrate type. Mellalia, M., Grimaud, A., Leger, A.C., Fauchais, P., and Lu, J. "Alumina Grit Blasting Parameters for Surface Preparation in the Plasma Spraying Operation." <i>Journal of Thermal Spray Technology</i> . 1997/Vol 6. No. 2. p 221. (accessed October 22, 2012) Used with permission from Copyright Clearance Center, 2014.	29
Figure 2.19 a. Cross-sectional photographs & b. Angle vs. Ra. Amada, Shigeyasu, Hirose, Tohru. "Influence of grit blasting pre-treatment on the adhesion strength of plasma sprayed coatings: fractal analysis of roughness." <i>Surface and Coatings Technology</i> . 1998/Vol. 102. p. 134. http://dx.doi.org/10.1016/S0257-8972(97)00628-2 (accessed October 29, 2012) Used with permission from Copyright Clearance Center, 2014.	29
Figure 2.20 Erosion rate vs. incident angle. Carter, G., Bevan I.J., Katardjiev I.V., Nobes, M.J. "The Erosion of Copper by Reflected Sandblasting Grains." <i>Materials Science Engineering</i> . 1991/Vol. A. no. 132. P. 232. (accessed October 22, 2012) Used with permission from Copyright Clearance Center, 2014.	30
Figure 2.21 Time vs. roughness for Al ₂ O ₃ against stainless steel. Celik, E., Demirkiran, A.S., Avci, E. "Effect of Grit Blasting of Substrate on the Corrosion Behaviour of Plasma-Sprayed Al ₂ O ₃ Coatings." <i>Surface and Coatings Technology</i> . 1999/Vol 116-119. p. 1062. (accessed October 29, 2012) Used with permission from Copyright Clearance Center, 2014.	31
Figure 2.22 Blast time vs. grit residue. Wigren, Jan. "Technical Note: Grit Blasting as Surface Preparation Before Plasma Spraying." <i>Surface and Coatings Technology</i> . 1988/Vol 34. p. 107. (accessed January 15, 2013) Used with permission from Copyright Clearance Center, 2014.	32
Figure 2.23 Fracture mechanisms. Momber A. <i>Blast Cleaning Technology: Chapter 2: Abrasive Materials</i> , 2008. p. 38. http://link.springer.com/chapter/10.1007%2F978-3-540-73645-5_2 (accessed March 31, 2013) Used with permission from Copyright Clearance Center, 2014.	32

Figure 2.24 Number of cycles vs. disintegration #, a. substrate hardness & b. slag size. Momber A. <i>Blast Cleaning Technology: Chapter 2: Abrasive Materials</i> , 2008. p. 47, 48. http://link.springer.com /chapter/10.1007%2F978-3-540-73645-5_2 (accessed March 31, 2013) Used with permission from Copyright Clearance Center, 2014.	33
Figure 2.25 Mechanical profilometry. Tabenkin, Alex. "The Basics of Surface Finish Measurement." <i>Quality Magazine</i> . 2014. http://www.deterco.com/products/Mahr%20Federal/newsletter/finish_measure_10_19_04.htm (accessed May 14, 2014) Used with permission from Mahr Federal Inc., 2014.	35
Figure 2.26 Average roughness, Ra image. Pickrell, G., Homa, D, Mills, R. "Abrasive Blasting Deliverable No.3." CCAM. 2014. (accessed April 2, 2014) Used with permission from Robert Mills, 2014.	35
Figure 2.27 Surface roughness for Sa. Sosale, G., Hackling S.A., and Vengallatore, S. "Topography Analysis of Grit-Blasted and Grit-Blasted-Acid Etched Titanium Implant Surfaces Using Multi-scale Measurements and Multi-Parameter Statistics." <i>Journal of Materials Research</i> . 2011/Vol 23, Issue 10. p. 2709. (accessed June 6, 2014) Used with permission from Copyright Clearance Center; letter attached.	36
Figure 3.1 a. unclean substrate & b. clean substrate.	39
Figure 3.2 Example of sample labeling (experiment # followed by sample #).	39
Figure 3.3 a. Compressed air valve open & b. ball choke valve open.	41
Figure 3.4 a. Blast pressure regulator knob/gage & b. media flow regulator/handle.	42
Figure 3.5 SJ-210 surface measurement technique.	44
Figure 3.6 a. Fibers before & b. after fusion splicing.	46
Figure 3.7 a. Fiber connectors, b. connector for blue-yellow adaptors, & c. blue-blue connection.	46
Figure 3.8 F1-7020C connector end face cleaner.	47
Figure 3.9 Optical fibers connected to the SM125 Interrogator.	47
Figure 3.10 Epoxied temperature sensor and strain gage on Al 3003 substrate.	50
Figure 3.11 a. "TempProb2" attached to 304 SS substrate & b. blast platform pre-blasting.	51
Figure 3.12 a. 304 SS & b. Thin SS substrates during experiments.	51
Figure 4.1 Blast distances effects on Ra for 4" and 6" blasting.	57
Figure 4.2 Blast distance effects on Ra for 6" and 8" blasting.	57
Figure 4.3 Blast pressure effect on Ra for 42 psi and 60 psi blasting.	58
Figure 4.4 Nozzle type effect on Ra.	59
Figure 4.5 Media flow effect on Ra.	59
Figure 4.6 Media Recycling effect on Ra.	60
Figure 4.7 Repeatability of same blast conditions.	60
Figure 4.8 Cabinet type effect on Ra.	61
Figure 4.9 Operator effect on Ra.	62
Figure 4.10 a. Good coverage & b. bad coverage.	62
Figure 4.11 Adaptor effect on substrate temperature.	63
Figure 4.12 LED and halogen effect on substrate temperature.	63
Figure 4.13 Blast height effect on substrate temperature with "TempSens2"	64
Figure 4.14 Experiment #1 data.	65
Figure 4.15 Zeroed temperature experiment #1 data.	65
Figure 4.16 Blast distance effects on 304 SS temperature changes.	66
Figure 4.17 Pressure effect on 304 SS temperature.	67

Figure 4.18 Angle effect on 304 SS temperature.....	68
Figure 4.19 Blast distance effect on thin SS temperature.	69
Figure 4.20 Blast pressure effect on thin SS temperature.....	69
Figure 4.21 Blast angle effect on thin SS temperature.	70
Figure B.1 Nozzle descriptions. No Author. “Abrasive Blast Nozzles.” Kennametal Inc. 2012 page 9. http://www.kennametal.com/content/dam/kennametal/kennametal/common/Resourcess/Catalogs-Literature/Advanced%20Materials%20and%20Wear%20Components/B-12-02861_KMT_Blast_Nozzles_Catalog_EN.pdf (accessed June 9, 2014) Used with permission from Kennametal, Inc., 2014.....	79
Figure C.1 Pulsation elimination methods [71].	80
Figure C.2 SJ-210 Example sample results for SS304 7-01 V3 measurement.....	81
Figure C.3 Standard deviation calculations for experiment #2.....	81
Figure C.4 Hirox S _a and standard deviation measurements and calculations.....	82
Figure C.5 UVA ROST S _a and standard deviation measurements and calculations.....	82
Figure D.1 Optical fiber ready for fusion splicing.....	83
Figure D.2 “Acquisition” window of Enlight software.	83
Figure D.3 “Sensors” window.	84
Figure D.4 “TempSens2” information.....	84
Figure D.5 “TempProbe2” information.	85
Figure D.6 Charts window with live temperature data.....	85
Figure D.7 Edit sensors data saving option under “Save” window.	86
Figure D.8 Thin stainless steel substrate (0.09” x 1.378” x 4.2875”) pre-blasting.	86
Figure E.1 Sample F _{calc} and t _{calc} for F-test and t-test for 4” and 6” blasts on Ra comparison.	87
Figure E.2 Sample F _{calc} and t _{calc} for F-test and t-test for 4” and 6” blasts on 304 SS T comparison.	87
Figure F.1 F-test and t-test results for 4” and 6” blasts on Ra comparison.	89
Figure F.2 F-test and t-test results for 6” and 8” Ra comparison.	89
Figure F.3 F-test and t-test results for 42 psi and 60 psi Ra comparison.....	89
Figure F.4 F-test and t-test results for 5/16” straight and 3/16” Venturi nozzle Ra comparison..	90
Figure F.5 F-test and t-test results for no pulsation and pulsation Ra comparison.....	90
Figure F.6 F-test and t-test results for newer media and old (recycled media) Ra comparison. ..	90
Figure F.7 F-test and t-test results for Day A and Day B Ra comparison.	91
Figure F.8 F-test and t-test results for VT and CCAM cabinet Ra comparison.	91
Figure F.9 F-test and t-test results for Operator A and Operator B Ra comparison.	91
Figure G.1 F-test and t-test results for 4” and 6” blasts on 304 SS temperature comparison.....	92
Figure G.2 F-test and t-test results for 6” and 8” blasts on 304 SS temperature comparison.....	92
Figure G.3 F-test and t-test results for 40 psi and 50 psi blasts on 304 SS temperature comparison.....	92
Figure G.4 F-test and t-test results for 50 psi and 60psi blasts on 304 SS temperature comparison.	93
Figure G.5 F-test and t-test results for 45° and 90° blasts on 304 SS temperature comparison....	93
Figure G.6 F-test and t-test results for 6” and 8” blasts on thin SS temperature comparison.	93
Figure G.7 F-test and t-test results for 40 psi and 60 psi blasts on thin SS temperature comparison.....	94
Figure G.8 F-test and t-test results for 45° and 90° blasts on thin SS temperature comparison....	94
Figure G.9 F-test and t-test results for 6”, 40 psi blasts of both substrates for T comparison.....	94

Figure G.10 F-test and t-test results for 8", 40 psi blasts of both substrates for T comparison.... 95
Figure G.11 F-test and t-test results for 6", 60 psi blasts of both substrates for T comparison.... 95
Figure G.12 F-test and t-test results for 45°, 40 psi blasts of both substrates for T comparison.. 95

1 Introduction

1.1 Motivation

Grit blasting is used for various industrial applications. The purpose of this process is to roughen, clean, remove material, texture, and deburr substrates. For this process, various parameters are varied in order to generate a desired result. Some of these parameters are as follows:

- Media propellant – type of propulsion of media (pressure or suction). Using different types will affect the roughness and energy required to power the system.
- Control type- manual, automatic, or semi-automatic. These control types are selected prior to blasting based on the blasting application
- Media – properties of the abrasive in the process. These can be media size, shape, hardness, fracture strength, media type, and purity of media supply.
- Substrate- properties of the material being blasted. The material hardness, strength, size, thickness, cleanliness, and initial roughness influence media selection.
- Blast angle – nozzle angle with respect to the substrate during process.
- Blast distance- nozzle exit distance from the substrate.
- Blast pressure- pressure of the system set prior to blasting. This affects the media flow rate and velocity.

Process parameters are set by the operator prior to blasting. Characterization techniques occur at the surface of substrate (and sometimes media) upon completion of blasting. Subsequently, parts that are out of specification require re-work or are scrapped, both of which decrease yield and increase costs. Some of the common characterization properties are:

- Roughness characterization- noncontact microscopy, optical profilometry, and mechanical profilometry. These methods are used to gather information on various roughness parameters of blasted substrates.
- Cleanliness – microscopy, visual inspection, and impurity detection. These methods gather data on how well the surface was cleaned during blasting and how many residual debris are left behind.
- Removed Mass- 3-D mapping and weight of substrate post-blasting. This technique is used to see how effective blasting is on the erosion of the substrate mass.

- Strain- measurement with Almen gage with the amount of bending that occurred from the forces of the propelled media.

The experiments that follow show the effects of media/substrate combinations along with process parameters on the post-blasting surface roughness. The substrates were characterized via optical microscopy and contact profilometry. The problem arises since these are post-characterization techniques, and a better process control can be gathered from in-situ process analysis, which would reduce the amount of defective parts.

1.2 Research Approach

With the vast majority of the automated blasting systems, controls are a pivotal point of interest and process enhancement. Controls are in place for monitoring blast angle, blast rate, blasting distance, and blast pressure during the process. Media quality and flow rate can be monitored to improve process efficiencies. Manual blasting operations are utilized over automated system for various reasons such as an extremely large substrate or places that a larger robotic system cannot be moved too. The goal is to understand which manual blast parameters best influence the substrate quality. One area that needs further investigation is the live data acquisition from the substrate during the blasting process.

One method to analyze the process with live data acquisition is to measure the temperature change on the substrate from the media interaction with the substrate. The blasting process parameters should effect the substrate temperature in different intensities magnitudes. Along with the roughness characterization, optical fiber sensors can be utilized to understand the blasting process live and can help determine the temperature threshold of the substrate.

1.3 Thesis Scope and Organization

Section 1: Introduction - the motivation and research approach for the abrasive blasting process. Emphasis on surface roughness characterization (post-process) and temperature data acquisition (in-situ process).

Section 2: Background - this section focuses on the abrasive media properties and selection, various substrate properties and selection, blasting environment, process parameters, blasting systems (cabinets or rooms), and optical sensors for in-situ blasting measurements for temperature changes and applied strains, and noise recordings.

- Section 3: Experimental Methods - discussion of the operating procedures for the EMPIRE Pro-Finish 4848 blast cabinet, semi-controls on blasting parameters, set-up of the in-situ optical sensors system (temperature detection and definition).
- Section 4: Results and Discussion - numerous results based on the blasting parameters, mainly: angle, distance, time, and pressure including: alteration of surface roughness, in-situ temperature changes, and types of substrates subjected to the process. Explanation of how the blasting parameters affected the mentioned surface roughness and temperature changes through post process and in-situ characterization.
- Section 5: Conclusions - highlights of key results that are novel or contradict those discussed in the literature.
- Section 6: Future Work - reasoning for further investigation of the abrasive blasting process in-situ monitoring via optical sensors.

2 Background

2.1 Abrasive Blasting History and Advances

Tilghman patented a process known as abrasive (grit) blasting on October 18, 1870, defining the process as “cutting, boring, grinding, dressing, pulverizing, and engraving stone, metal, glass, wood, and other hard of solid substances, by means of sand or grains of quartz, or other suitable materials, artificially driven as projectiles rapidly against them by any suitable method of propulsion” [1]. A simple representation of the blasting process with an unblasted or “smooth” surface, during blasting, and a blasted “profiled” surface is shown in Figure 2.1.

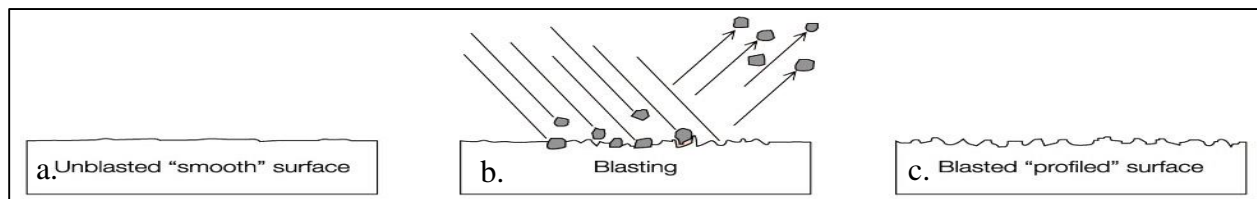


Figure 2.1 a. pre-blasting, b. blasting, and c. post-blasting surfaces. No Author. “Technical Reference: Surface Preparation.” Blast One. 2014. <http://www.blast-one.com/weekly-tips/the-difference-between-surface-profile-and-class-of-blast> (accessed May 14, 2014) Used with permission from Blast One, 2014.

The particles are propelled against the surface (substrate) via a flow of liquid and/or gas. Tilghman describes methods of propelling the particles against the substrate as follows, “by a rapid jet or current of steam, air, water, or other suitable gaseous or liquid media; but any direct propelling force may be used, as, for example, the blow of the blades of a rapidly-revolving fan, or a centrifugal force of a revolving drum or tube, or any other suitable machine” [1].

The industrial world started to use this blasting application to clean large surfaces in 1893. “Thomas Pangborn expanded on Tilghman’s ideas in 1904 to create a new machine that used compressed air, which it combined with an abrasive material like sand, in order to clean metal surfaces for further use” [3]. This newer sand blasting machine utilized the combination of a blasting nozzle and air compressor to better control the amounts of air and particles released during the process. An enclosure (cabinet) was first utilized in 1918 due to health concerns with silicosis caused by inhalation of tiny sand particles. The process continued to evolve, in 1939, with “particles derived from aluminum oxide, silicon carbide, quartz, glass beads, powdered abrasives, plastic abrasives, copper slag, steel grit, coconut shells, walnut shells, and fruit stones were put into use” [3]. Other safety enhancements that helped improve the blasting process for workers were glass viewing screens, dust collection systems, and use of hearing protection and respirators.

Along with media selection and process safety improvements, the abrasive process was eventually automated to produce better control of the process. In 1968, Progressive Engineering Company built its first automated abrasive grit blasting system and by 1972, the company had created its first pneumatic blasting product for the shot peening process [4]. The latest blasting process improvement was the introduction of the robotic, ultra-high pressure water stripping systems in 1992. Today, Wheelabrator (created with the help of Tilghman’s research and invention) and Empire are two large blasting cabinet manufacturers that have become world leaders in the abrasive blasting for the purposes of surface roughening, cleaning, material removal, texturing, and deburring.

2.1.1 Various Blasting Methods

There are various types of abrasive blasting media propulsion systems currently used in industry and research facilities. Table 2-1 includes a list of four types of blast cleaning methods, specified by ISO 12944-4. Each type of blast cleaning will be reviewed, with an emphasis on dry abrasive blast cleaning via compressed air.

Table 2-1 ISO 12944-4 Blast cleaning methods. Momber A. *Blast Cleaning Technology: Chapter 1: Introduction*, 2008. p. 3. http://link.springer.com/chapter/10.1007%2F978-3-540-73645-5_2 (accessed March 31, 2013) Used with permission from Copyright Clearance Center, 2014.

Dry abrasive blast cleaning	<ul style="list-style-type: none"> • Centrifugal abrasive blast cleaning • Compressed-air abrasive blast cleaning • Vacuum or suction-head abrasive blast cleaning
Moisture-injection abrasive blast cleaning	(No further subdivision)
Wet abrasive blast cleaning	<ul style="list-style-type: none"> • Compressed-air wet abrasive blast cleaning • Slurry blast cleaning • Pressurized-liquid blast cleaning
Particular applications of blast cleaning	<ul style="list-style-type: none"> • Sweep blast cleaning • Spot blast cleaning

Dry abrasive blasting is one of the most widely used blasting processes. The dry abrasive blasting technology includes the use of compressed-air (pressurized), suction, and centrifugal blasting media propulsion methods. Figure 2.2 shows an image of the design of the pressure and suction blasting systems.

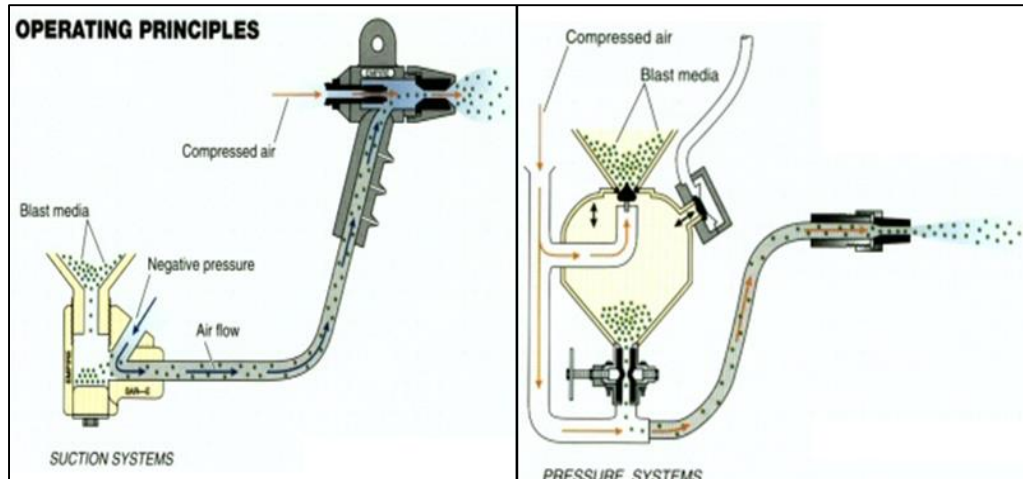


Figure 2.2 Suction and pressure blasting systems. No Author. "Blast Cabinets." Norton Sandblasting Equipment, 2014. <http://www.nortonsandblasting.com/nsbcontact.html> (accessed May 14, 2014) Used with permission from Norton Sandblasting Equipment, 2014.

In the pressurized blasting system, media is fed by gravity from a blast media pot into the air line through an orifice at the bottom of the pot. Advantages of pressurized media blasting include greater media velocity, quicker media mass flow, higher stand-off distance, and more productive than suction systems [7].

Suction blasting operates via the venturi principle to pull abrasive media from a non-pressurized hopper to the blast nozzle at which it is combined with the compressed air stream and propelled against a substrate [7]. Advantages of the suction blasting process include lower capital equipment cost, easier maintenance, and less air and abrasive demand (lower energy cost).

2.1.2 Control Systems

Generally, the abrasive blasting process has three levels of control: manual, automatic, and semi-automatic.

- Manual systems entail blasting the substrate by moving the nozzle (and possibly hose location) and media flow meter manually.
- Fully automatic systems tend to control the location of the nozzle with respect to the substrate, an automatic media flow regulation valve, and controls for the time or coverage area of blasting.
- Semi-automatic systems are often hybrids of manual and automatic systems, which could include the computer aided control of the nozzle with a manual media flow regulation unit or manual control of the nozzle with assistance from an automatic media flow regulator.

For small manual systems, the blasting operator utilizes the protected blast cabinet to control the blast nozzle location via gloves. These cabinet systems are used for smaller substrates and monitored from the protection viewing window. Disadvantages with the manual blasting systems include the lack of accuracy of attack angle detection, no readout for stand-off distance, uncontrolled or variable media flow rates that can alter, and no control of blasting time or coverage. Some applications that require better control employ automatic blasting systems. The use of an automatic media flow regulator can allow for better media to air flow ratios and optimize the blasting production rate. An automated nozzle controls along with programming, allow for: more accurate blast angle, distance, blasting rate (step size and traverse rates), full blasting time, and area coverage.

The abrasive blasting process can be fine-tuned and adjusted to create better results, save time, and improve the process yield. Unfortunately, some substrates are larger than a blast cabinet or blast room can accommodate and have to be blasted manually due to their size and possibly blasted on location. Manual blasting is more versatile in some scenarios and performed in smaller blasting locations or to blast uniquely shaped substrates with ease.

Semi-automated blasting units comprise both manual and automated blasting systems. This type of system could have the advantages of blasting in any environment, along with the ability for better control of the nozzle and media flow. Fixtures can be used to control the blast distance or angle, while the pressure is controlled via an automatic media flow regulator. Blast time can be controlled automatically, while still having the versatility of moving the nozzle at different angles to generate desired results. Another improvement would be to use a laser system to help monitor the nozzle distance from the substrate.

2.2 Abrasive Media

Different properties of the abrasive media play a role in material selection for blasting processes. Some of these properties are media shape, size, hardness, density, type, fracture strength, and presence of impurities. All of these mentioned properties or qualities will be discussed in the following section.

2.2.1 Abrasive Shape

The blasting media shape can be separated into different categories: round, irregular, globular, or cylindrical. Each shape of media can further defined by properties such as shape

factor, circularity factor, roundness, sphericity, elongation ratio, and flatness ratio. Equations for each of those properties are listed below. Figure 2.3 shows the diagrams for the determination of the six media shape definitions mentioned above.

Shape Factor $F_{shape} = \frac{d_{min}}{d_{max}}$ (1)

Circularity Factor $F_0 = \frac{4 \cdot \pi \cdot A_p}{Perimeter^2}$ (2)

Roundness $S_R = \frac{\sum^{2 \cdot r_{corner}}}{d_p}$ (3)

Sphericity $S_P = \frac{\sqrt{\frac{4}{\pi} \cdot b_p \cdot l_p}}{N_{corner}}$ (4)

Elongation ratio $r_E = \frac{l_p}{b_p}$ (5)

Flatness ratio $r_F = \frac{l_p}{t_p}$ (6)

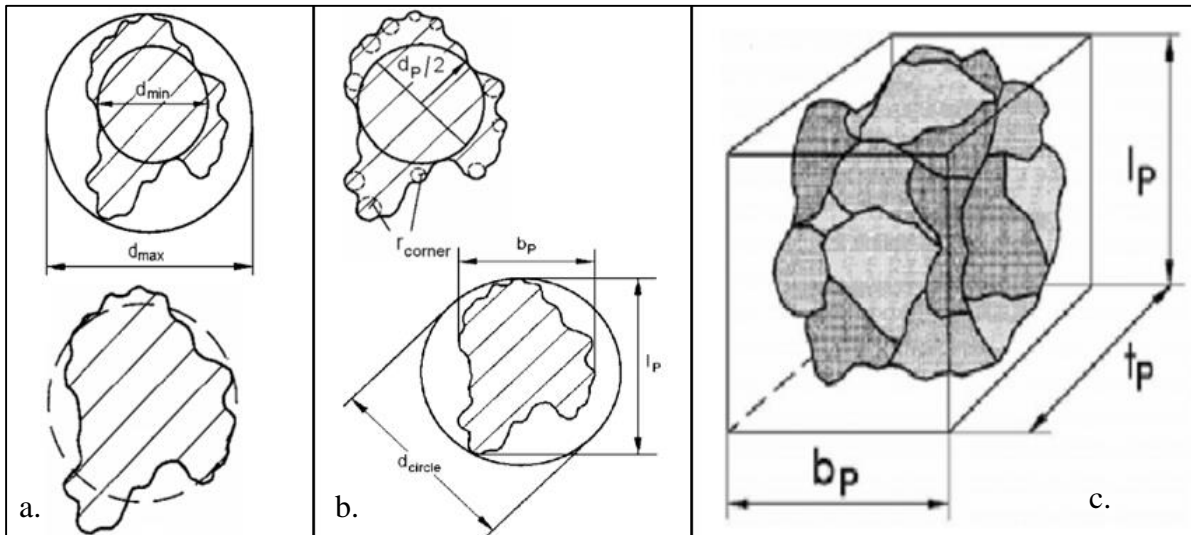


Figure 2.3 Media shape definitions; a. shape factor & circulatory factor, b. roundness, & sphericity, & c. elongation ratio & flatness ratio. Momber A. *Blast Cleaning Technology: Chapter 2: Abrasive Materials*, 2008. p. 19. http://link.springer.com/chapter/10.1007%2F978-3-540-73645-5_2 (accessed March 31, 2013) Used with permission from Copyright Clearance Center, 2014.

The particle shape can also be defined by the geometrical form, and the relative proportions of length, breadth, and thickness [8]. Shape factor, circularity factor, roundness and sphericity all refer to the geometrical form of the media. The shape factor is defined as the ratio of the small diameter particle (d_{min}) to the large diameter (d_{max}) particle [8, 9]. This simply means that as the

shape factor approaches unity, the particle is more spherical. The circularity factor takes the particle area and the particle perimeter into account. As the circularity factor approaches unity, a particle of spherical shape occurs similar to the shape factor. Gillepsie and Fowler showed that a circularity factor of $F_0 > 0.83$ classified a particle as shot media. As the circularity and shape factor values decrease, the particles become less spherical and more angular in shape.

The roundness of a particle can be defined as the sum of the corner diameter-core diameter ratio divided by the number of corners. A “round” particle has less corners or edges present, while a tetragonal would have four corners. The particle sphericity suggested by Wadell (1933) was determined by particle length and breadth (width), along with the diameter of a circle that the particle edges will touch, but not pass over [10]. Figure 2.4a shows another roundness scale, developed by Hansink, which defines particles as angular or round. Figure 2.4b demonstrates a relationship between sphericity and roundness. Particles can be round, spherical, a combination of both, or neither based on this roundness and sphericity chart.

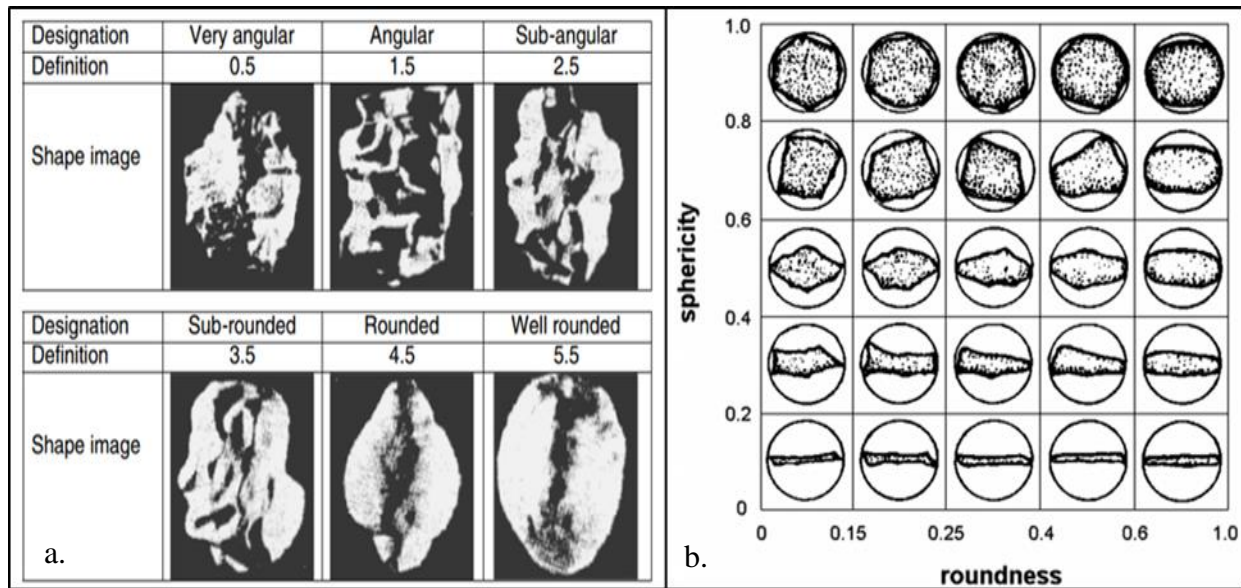


Figure 2.4 a. Hansink's shape designations & b. garnet roundness-sphericity chart. Momber A. *Blast Cleaning Technology: Chapter 2: Abrasive Materials*, 2008. p. 21. http://link.springer.com/chapter/10.1007%2F978-3-540-73645-5_2 (accessed March 31, 2013) Used with permission from Copyright Clearance Center, 2014.

Bahadur and Badruddin created the ratios for the purpose of determining the influence of abrasive particle shape on particle erosion processes [13]. The particle length to particle breadth ratio is the elongation ratio and the flatness ratio is the ratio of particle length to particle thickness. In either case, the particle is considered to be elongated or flat with a decrease of this value. A relationship between particle shape, type, and diameter is shown in Figure 2.5.

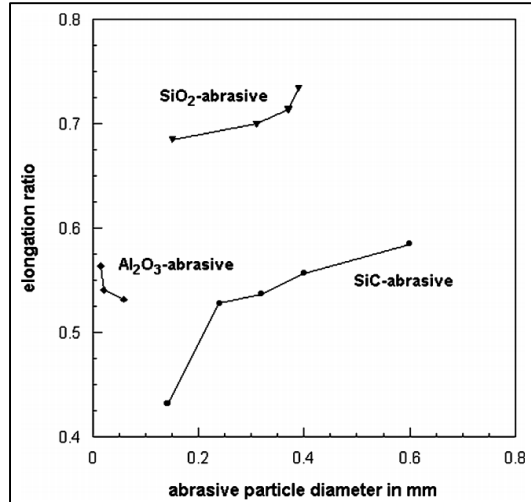


Figure 2.5 Shape, size, and type relationships. Momber A. *Blast Cleaning Technology: Chapter 2: Abrasive Materials*, 2008. p. 20. http://link.springer.com/chapter/10.1007%2F978-3-540-73645-5_2 (accessed March 31, 2013) Used with permission from Copyright Clearance Center, 2014.

2.2.2 Grit, Shot and Cylindrical

“The term grit characterizes grains with predominantly angular shape and they exhibit sharp edges and broken sections” [14]. Grit is typically classified by the shape parameters mentioned previously. A particle can be classified as grit if the shape factor, F_0 , is under 0.8 and has a sphericity above 0.6 and roundness above 0 or a roundness from 0 to 0.25 and sphericity of 0.4 as shown in Figure 2.4b. Figure 2.6 shows an image that compares grit media (top) and shot media (bottom) [15].

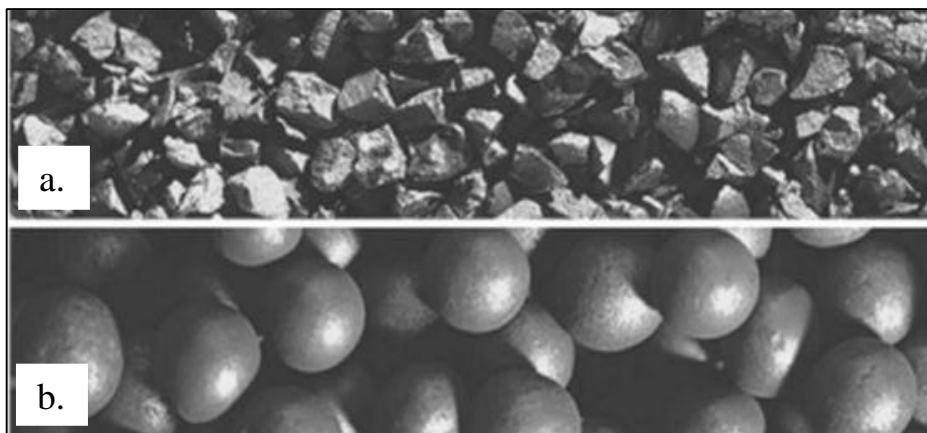


Figure 2.6 a. Grit image and b. shot image. Momber A. *Blast Cleaning Technology: Chapter 2: Abrasive Materials*, 2008. p. 18. http://link.springer.com/chapter/10.1007%2F978-3-540-73645-5_2 (accessed March 31, 2013) Used with permission from Copyright Clearance Center, 2014.

Because of its angular shape, grit media is used for several purposes.

- Surface roughening - roughen for polymeric coatings that need adhesion to substrates.

- Material Removal - remove rust, scale, or any unwanted debris to clean a substrate. Grit can also be utilized to remove mass from a product to reduce its weight for various applications.
- Texturing - grit media is used to create a certain luster or aesthetic appearance [16].
- Detailing- micromachining or micro blasting to create intricate details or machine uniquely shaped substrates.

Another shape designation is known as shot media, which generally is used in the shot peening process. “The term shot characterizes grains with a predominantly spherical shape. Their length-to-diameter is < 2 , and they do not exhibit sharp edges or broken sections” [14]. The shape factor for shot media is $F_0 > 0.8$. As the four geometrical form shape parameters approach unity, the shot media becomes more spherical. Shot media is typically used to generate a compressive stress layer on the substrate. Upon shot peening of the machined part, a continuous compressive stress layer covers the surface. “The compressive layer stops the fatigue cracks and stress corrosion that typically start at the surface of the part” [17].

The last media shape used for blasting is known as cylindrical media. “The term cylindrical denotes grains that are manufactured by a cutting process and their length-to-diameter ratio is ~ 1 ” [14]. A simple example of a cylindrical shaped particle is corn cob media.

2.2.3 Abrasive Size & Size Distribution

The size of the abrasive grits is another factor that determines the effect of the blasting process. “Coarse grains are measured in inches or millimeters, fine particles in terms of screen size, and very fine particles are measured in micrometers or nanometers” [14]. These descriptions are based on the average particle diameters for a certain size distribution of particles, which can be determined through several calculations. One example for calculating the size distribution of media is shown as follows [14]:

$$M_0(d_p) = f\left(\frac{d_p}{d^*}\right)^{n_M} \quad (7)$$

M_0 is the particle size distribution function, where the particle diameter is defined as (d_p) , average particle diameter (d^*) , and measure of the particle size spread (n_M) . “The higher the value for n_M , the more homogeneous is the grain size structure of the sample. For $n_M \rightarrow \infty$, the sample consists of grains with equal diameters” [14]. To generate a uniform and repeatable blasted surface, the size distribution needs to be small.

SSPC-AB standards and SAE standards define the size distribution from a percentage of weights from specific sets of sieves. In the sieve analysis method, the particles are displaced on the top of the sieve system, which has different sieve meshes stacked vertically. The screen openings of each sieve become smaller as the media approaches the bottom sieves. Each sieve is then emptied out and weighed to calculate the amount of particles in each section, which will be the different sizes of the particles. Figure 2.7 shows the size distribution of alumina 700 and Metagrit 65 after using this sieving method. The alumina particles have a bell-curve shaped size distribution and the Metagrit has a skewed bell-curve distribution.

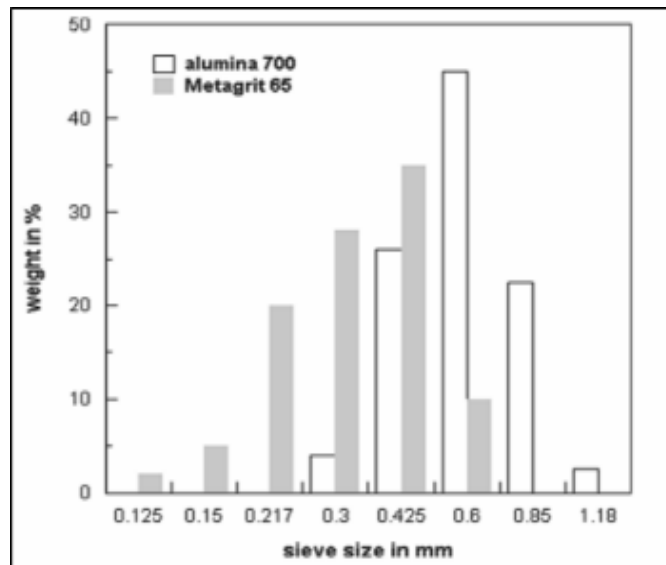


Figure 2.7 Distribution of sieve analysis. Momber A. *Blast Cleaning Technology: Chapter 2: Abrasive Materials*, 2008. p. 26. http://link.springer.com/chapter/10.1007%2F978-3-540-73645-5_2 (accessed March 31, 2013) Used with permission from Copyright Clearance Center, 2014.

Four methods used to define media size are:

- Particle diameter - the average particle size diameter is calculated for a known particle size distribution.
- Sieve size - designates the particles into the different size sieves or mesh sizes. Sigma-Aldrich displays this relationship of the mesh designation and nominal sieve openings in table format [19].
- Mesh size - the mesh number increases, the particle size and sieve openings decrease and is correlated with the meshes present in the sieving process. The following equation can be used to calculate average particle size from the mesh size [20]:

$$d_p = 17,479 \cdot mesh^{-1.0315} \quad (8)$$

- Grit size -Sometimes media are categorized based on grit size, instead of meshes, which means “the number of standardized holes that fit within the standard dimensional sized sieve, i.e., 200 holes equals 200 grit” [21]. Newport Glass Works, LTD shows the correlation between grit size designation and the average, maximum, and minimum particle sizes in another table. Additionally, Media Blast & Abrasive, Inc. has similar information, with the addition of the USS mesh sizes [22].

The particle size will have a tangible effect on the blasting performance. Smaller grit particles tend to yield rougher surfaces and less surface contamination and higher surface roughness, while medium particles result in the most surface contamination as shown in Figure 2.8.

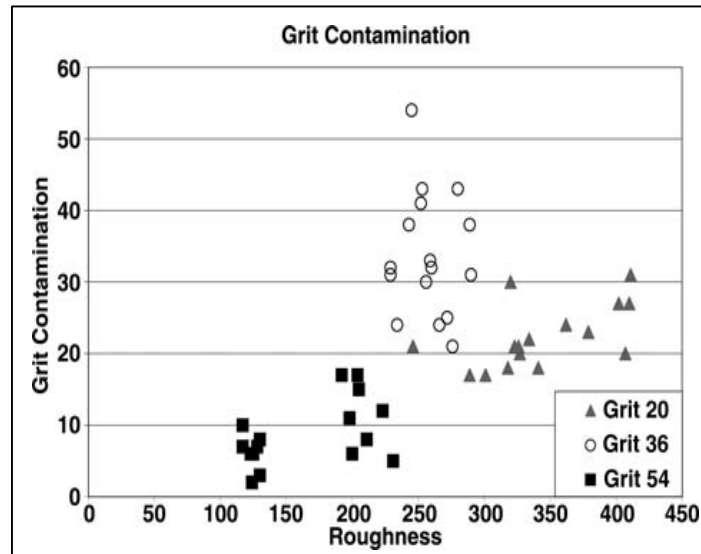


Figure 2.8 Grit contamination vs. roughness. Day, James; Huang, Xiao; and Richards, N.L. “Examination of a Grit-Blasting Process for Thermal Spraying Using Statistical Methods.” *Journal of Thermal Spray Technology*, 2005/Vol. 14, p. 477. <http://link.springer.com/article/10.1361%2F105996305X76469> (accessed November 2012) Used with permission from Copyright Clearance Center, 2014.

In another study, white alumina particles were blasted onto cold-rolled carbon steel. As the grit size increases, the residual grit weight increases exponentially and the penetration depth increases linearly. These findings are shown graphically in Figure 2.9. A separate study found a correlation between grit size and substrate surface energy. The surface energy imparted onto the substrate has been shown to have an inverse relationship with the grit size [25].

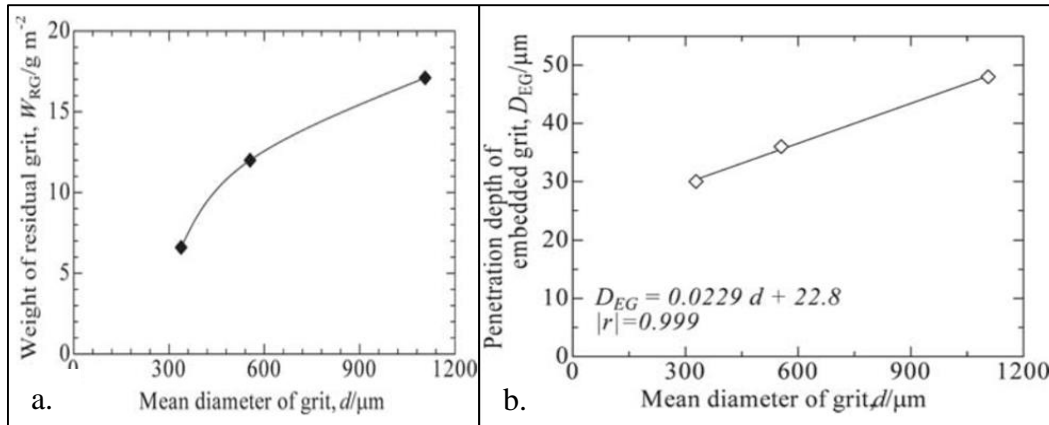


Figure 2.9 Grit diameter vs. a. residual grit and b. penetration depth. Maruyama T, Akagi K, Kobayashi T. "Effects of Blasting Parameters on Removability of Residual Grit." *Journal of Thermal Spray Technology*. 2006/Vol. 15, no. 4. p. 820. <http://link.springer.com/article/10.1361%2F105996306X147018> (accessed November 2, 2012) Used with permission from Copyright Clearance Center; letter attached.

2.2.4 Abrasive Hardness

The hardness of the abrasive media is one of the main determining factors of which type of media is selected for the abrasive blasting process. Material hardness can be defined as “the property of matter described as the resistances of a substrate to being scratched by another substance” [26]. When the media is significantly softer than the substrate, the surface will not be properly smoothed, roughened, or cleaned. Conversely, media may inadvertently damage the substrate when the substrate is much softer than the media.

Three common types of hardness testing methods for materials are scratching, indentation, and penetration. The Mohs hardness scale is utilized for the scratching test and is shown in Table 2-2.

Table 2-2 Mohs hardness scale. Momber A. *Blast Cleaning Technology: Chapter 2: Abrasive Materials*, 2008. p. 14. http://link.springer.com/chapter/10.1007%2F978-3-540-73645-5_2 (accessed April 1, 2013) Used with permission from Copyright Clearance Center, 2014.

Material	Mohs Hardness
Talc	1
Gypsum	2
Calcite	3
Fluorite	4
Apatite	5
Orthoclase (Feldspar)	6
Quartz	7
Topaz	8
Corundum	9
Diamond	10

For media hardness, the material is scratched by different materials shown in the table until it cannot be scratched anymore. As an example, if topaz does not scratch the material, but corundum scratches it, then the media would have a Mohs hardness of 8.5 [27].

Indentation hardness is often determined by the Vickers and/or Brinell hardness tests. A ball indenter is utilized for Brinell tests, while the Vickers test uses a pyramidal shaped indenter as shown in the following equations [14].

$$H_B = \frac{F}{\frac{\pi}{2}D \cdot [D - (D^2 - d^2)^{0.5}]} \quad (9)$$

$$H_V = \frac{2 \cdot F \cdot \sin(136^\circ/2)}{d^2} \quad (10)$$

With Brinell hardness, the measurement is made by determining the diameter of the indentation in the x and y directions, which are specified as d_1 and d_2 . The indenter size, D , and the indentation size is the average of the two actual indentations (d_1 and d_2). The indentation force, F , is applied by the machine unto the material. Brinell hardness, H_B , can be calculated after knowing values for these variables. To calculate Vickers hardness, H_V , the same d and F values are used with a pyramidal indenter.

Knoop hardness and Rockwell hardness measurements fall under the penetration testing method. Penetration tests focus on the depth of penetration for hardness calculations, whereas the indentation methods use the diameter of the indentation. The Knoop hardness is described as “the relative hardness of a material (as a metal) that is determined by the depth to which the bluntly pointed diamond pyramid of a special instrument can penetrate it” [28]. Rockwell hardness values are generated with the penetration depth of the indenter as well. This test is based on an inverse relationship to the measurement of the additional depth to which the indenter is forced by a heavy total (major) load beyond the depth resulting from a previously applied preliminary (minor) load [29].

The properties of the materials of interest will dictate the method by which the hardness values will be determined, since not all materials can be measured with the same hardness measurement technique. For instance, the Knoop, Vickers, and Mohs hardness measurements cover the hardest materials. For example, a rating of 10 for diamond on the Mohs scale correlates to 7000 Knoop hardness and titanium nitride of 9 with 1800 Knoop hardness, as shown by Ted Pella, Inc. [30]. Rockwell A and C hardness values cover the harder materials measured by the

Vickers method and Brinell hardness covers the soft to medium hardness materials. The Vickers hardness measurement range is the most applicable, since it umbrellas the entire spectrum of the other hardness measurement types. More hardness value conversions can be seen in a table created by NDT Resource Center [31].

Media selection will be based on the application and the substrate to be blasted. Equation 13 below shows the relationship of the media hardness to substrate hardness [32, 33].

$$\frac{H_M}{H_P} \rightarrow 1.0 \text{ to } 1.5 \quad (11)$$

H_M is the substrate hardness and H_P is the hardness of the particle. An increase in abrasive specific mass loss occurred with a ratio of $H_M/H_P = 0.9$ or lower as shown in Figure 2.10. For all three substrate/media combinations, mass loss amounts increased with the increasing media hardness levels. However when the ratio of 2.4 occurs, the function exhibited a steep decrease, so the media hardness becomes obsolete at very high hardness values. Appendix A contains hardness values for various media types [35].

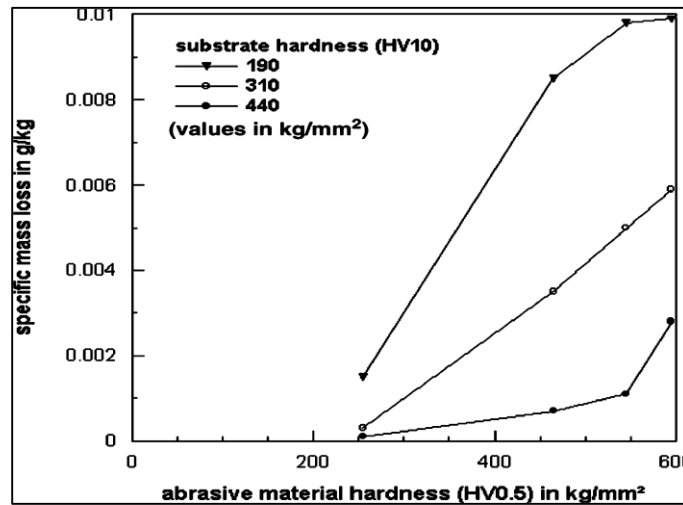


Figure 2.10 Abrasive hardness effect on specific mass loss. Momber A. *Blast Cleaning Technology: Chapter 2: Abrasive Materials*, 2008. p. 11, 12. http://link.springer.com/chapter/10.1007%2F978-3-540-73645-5_2 (accessed March 31, 2013) Used with permission from Copyright Clearance Center, 2014.

2.2.5 Abrasive Density

Particle density can be important in terms of blasting pressure and media flow rates. Particles with less porosity (higher density) affect the surface more than highly porous particles. The apparent density (ρ_p) is shown below in Equation 14 where particle mass (m_p) is related to particle volume (v_p) in terms of the particle diameter (d_p) [14].

$$\rho_P = \frac{m_P}{V_P} = \frac{6 \cdot m_P}{\pi \cdot d_P^3} \quad (12)$$

This density parameter includes flaws, pores, and cracks [14]. The highly dense materials generally have lower vacancies, while a material of low density would have many pores, cracks, or flaws, which lower the particle mass. The particle density and apparent density terms are synonymous, since they include material mass and the mass of void space in the particles. Bulk density would refer to the mass of the media in relation to its volume, only including the amount of the material, excluding effects of pores, flaws, and cracks.

2.2.6 Type (Metallic vs. Non-Metallic)

Blasting media can also be categorized into metallic and non-metallic abrasives. Cost, substrate type, and environmental effects play a role in which type of media is chosen for a particular application as well. Some common metal abrasives are iron grit, copper slag, and steel grit/shot. The difference in steel grit and shot is that the grit would remove more substrate mass, whereas the shot would justpeen the surface more. Figure 2.11 displays images of steel shot and steel grit on the left and brown corundum and demetalized steel slag on the right [36].

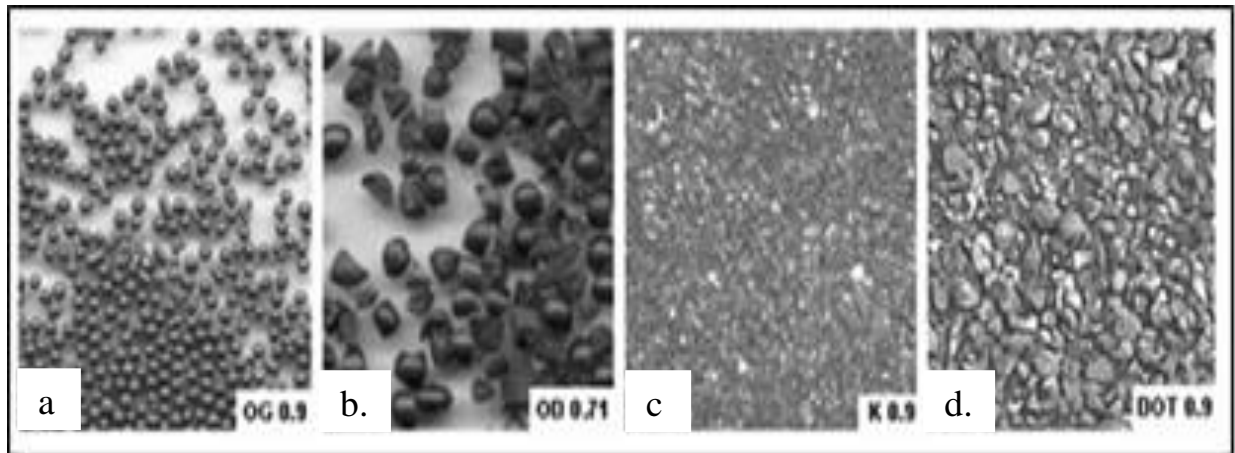


Figure 2.11 a. Steel shot, b. steel grit, c. brown corundum, & d. demetalized steel slag. Makova, I., Sopko, M. "Effect of Blasting Material on Surface Morphology of Steel Sheets." *Acta Metallurgica Slovaca*. 2010/ Vol. 16, no. 2, p. 111. (accessed March 07, 2013) Used with permission from Acta Metallurgica Slovaca, 2014.

Non-metallic materials encompass many different types of elements, compounds, or composites, but ceramic media is most commonly found in the grit blasting industry. White, pink, and brown alumina, garnet, coal slag, silica sand, quartz, and corundum are some non-metallic media used in industry, while glass beads and plastic falling under the shot category as shown in Appendix A. Ceramic bead media might be selected for applications which require high life cycles

(60-100) and low dust debris, and cost is not the primary factor. Coal slag is often utilized because of its low cost, but it has a life cycle of one use and high amounts of dust debris. Garnet has low dust accumulation, medium cost, and 3-4 uses before it becomes ineffective and aluminum oxide has low dust debris, 6-8 cycles, and a relatively high cost. Media types (including silica) that generate a high amount of dust should be blasted in a contained environment and breathing equipment should be used by operators.

2.2.7 Fracture Strength

Fracture strength is “the minimum tensile stress that will cause fracture” [37]. This tensile stress is of force (tension) applied to a cross-sectional area of a given material. Typically, the media fractures due to wear over repeated recycling during the blasting process. In some cases, media replacement is necessary other times the media breaks down due to manufacturing defects “such as micro-cracks, interfaces, inclusions, or voids” [14]. Huang applied the Weibull distribution to abrasive materials. Equation 13 shows a simple equation for particle fracture strength (σ_F), and its relationship with particle volume (V_p), defect distribution strength parameter (σ^*), and Weibull modulus (m_w) [38].

$$F(\sigma_F) = 1 - \exp \left[-V_p \cdot \left(\frac{\sigma_F}{\sigma^*} \right)^{m_w} \right] \quad (13)$$

For this equation, m_w determines if the variability of particle strength among a given set of particles is high or low. When m_w is low, the variability in particle strength of those particles would be high. Figure 2.12a shows the Weibull modulus plotted against the particle strength and the deviation from the trend line represents variation. Figure 2.12b shows the fracture strength decreases as corundum particles increase in size. Based on these two graphs, scatter in strength of abrasive particles is shown to be wider for larger particles [14].

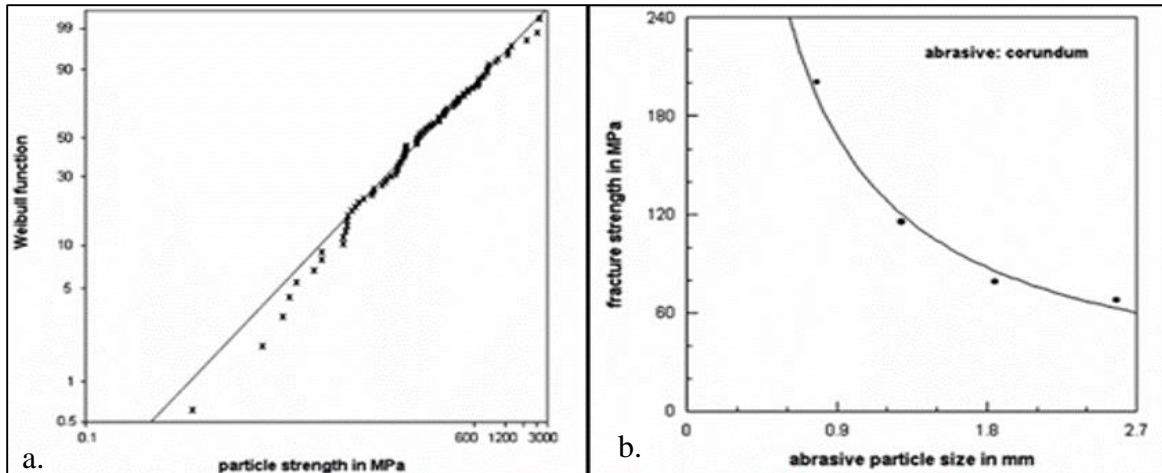


Figure 2.12 Particle strength vs. a. Weibull function & b. vs. fracture strength. Momber A. *Blast Cleaning Technology: Chapter 2: Abrasive Materials*, 2008. p. 11, 12. http://link.springer.com/chapter/10.1007%2F978-3-540-73645-5_2 (accessed March 31, 2013) Used with permission from Copyright Clearance Center, 2014].

The quality of the grit is important to the surface quality of when blasting the substrate. For instance, ISO 11124/2-4 is one example that sets maximum limits for the following particle properties by %: particle shape change, number of voids, shrinkage defects, cracks, and total defect % for chilled iron grit, high-carbon cast steel shot and grit, and low-carbon cast steel shot [40].

2.2.8 Impurities

The probability of the incorporation of impurities into the blasting media is relatively difficult to predict, but contamination can originate from the substrate, blast cabinet, and work environment. Solid and liquid impurities such as dust, lead, water soluble contaminants, and oil can be present in a media storage container. Accidental mixing of different media can occur when switching out media between blasting operations. Some solid foreign particles can be detected via magnetization or visual inspection. Impurity limitations can be set for recycled media and may include non-abrasive residue, lead content, water soluble contaminants, and oil content [41]. Conductivity testing and/or chemical analyses are other methods used to detect soluble foreign matter.

2.3 Substrates

For the abrasive blasting process, the substrate can be a deciding factor in which process parameters, media selection, and blasting machines are used to create a desired surface roughness, texture, thickness or mass removal amount. Some typical properties of substrates that are taken into consideration are substrate hardness, thickness, strength, and initial surface roughness. Other

properties such as substrate shape, pre-blasting strains and/or stresses, and cleanliness are important as well.

2.3.1 Substrate Material

Three generic types of substrates are blasted: metals, polymers, or ceramics. These substrate material are generally based on application, thus media selection occurs based on desired substrate surface modification.

Metals are classified as materials that are composed of one or more metallic elements (such as iron, aluminum, copper, titanium, gold, etc.) and nonmetallic elements (carbon, nitrogen, oxygen, etc.) in relatively small amounts [42]. Metals have a higher density than other materials, including composites, and have the highest tensile strengths as well. Metals are very stiff and have superb fracture toughness values. For ductile metals, sodium bicarbonate, plastic media, and walnut shells are commonly used to remove substrate mass. Media that are not spherical should be utilized on metals that need to be roughened and aluminum oxide is often used for removing mass and roughening harder, brittle substrates.

Polymer substrates are difficult to blast due to their unique properties. These materials consist of carbon backbones with hydrogen, oxygen, nitrogen, and silicon forming organic compounds with large molecular structures. Polymers have lower densities, tensile strengths, and fracture toughness values than metals and ceramics. As mentioned previously, beads or shot are optimum media to use based on polymers being very flexible and not hard. One drawback of polymer substrates is the need to keep the substrate in a narrow temperature range to reduce changes of degradation. With this in mind, polymers need to be blasted under conditions that would roughen the surface or remove mass, not destroy the entire substrate or melt the substrate due to over blasting.

Ceramic materials mainly consist of oxides, nitrides, and carbides [42]. Ceramic substrates are extremely hard, brittle, and can withstand higher temperatures than polymers and metals. High tensile strengths, high stiffness, and low fracture toughness values are given for ceramics. Due to the brittle nature of ceramics, very hard media needs to be applied when blasting ceramic substrates, given that the substrates are thick enough not to be blasted through easily. Typically, ceramic materials are used as media in the blasting operations, but in some cases, ceramics can be the substrate due to customer specifications.

2.3.2 Substrate Hardness

Substrate hardness can determine which type of media is best to use based on “hardness interactions” as shown in Equation 11. Substrate or stock hardness can indicate how much abrasive velocity is required to clean or roughen the surface and how much stock is removed from blasting. Softer materials might absorb the media energy and burn the substrate if the wrong blasting parameters or wrong type of media are used while blasting. Harder substrates are easier to blast without the worry of media energy/heat absorption, however an increase in media velocity is needed to roughen, clean, or remove mass from those substrates. Typically, blasting angle is varied for substrates based on their different hardness too.

2.3.3 Substrate Thickness

The specimen thickness can play various roles in the effectiveness of the grit blasting process. Thick substrates are less likely to deform due to the amount of bulk substrate material, whereas thinner substrates could break or bend due to blasting at the high pressures or close distances from the substrate. Figure 13 found in “Residual Stress on the Grit Blasted Surface” by Tosha and Iida shows that thinner substrates have more susceptibility to surface residual stresses and once a thickness of 4 mm is reached, the surface residual stress value becomes constant at -200 MPa for grit blasting [43]. Shot peening created more residual surface stresses as expected and peaked out at 6 mm thickness. Tosha and Iida also suggested that when the work hardened layer and substrate thickness overlap, the surface residual stress is zero [43].

2.3.4 Substrate Shape

Pre-blasted substrate shape can have an effect on the blasting process used. For instance a pyramid, cube, or cylinder substrates would have to be blasted in different patterns. As one would expect, a cube is simple to blast, just making sure to spend the same amount of time blasting on each face of the cube. A pyramid shaped substrate would have to be blasted in a similar fashion, with more consideration of the blast radius, traverse rate, and step sizes, which will be discussed under the process parameters section. Any of these substrate shapes, especially the sphere or cylindrical shape, could be blasted by having a rotating platform that keeps the substrates spinning around the z-axis, while the nozzle just moves in the x or y and z directions. The shape of the substrate can also effect the angle at which the substrate needs to be blasted and for unique not

geometrical substrates, problems like over-blasting, heat generation, and coverage would be primary issues to be considered before blasting.

2.3.5 Initial Surface Roughness

One purpose of surface roughness altering is “extending the surface area of the substrate allowing an adhesive or coating to flow in or on them” [44]. The initial roughness of the substrate can be defined as a smooth or rough surface in terms of numerous roughness qualities. Although it takes more time to blast a smooth surface, it tends to have less residual grit and grit reflection can be more controlled. The blast zone is harder to predict on a rough surface so grit reflection and surface uniformity would be harder to control.

A simple understanding of some of the many roughness parameters gives insight to what roughness actually means quantitatively. ISO reports surface structure under three different categories: primary profile (P), roughness profile (R), and waviness (W). R_a is the arithmetic-mean deviation of the assessed profile [45]. Some other parameters in Bacova and Draganovska’s study were R_q , R_t , R_v , R_z , R_c , S_{Sm} , and R_{Pc} . R_q is the root-mean square, R_t is described as the total height of the profile over a given length, R_p is the maximum peak height and R_v is the maximum peak depth. R_{pc} is the density of peaks for a profile, which corresponds to the number of peaks per profile unit length [45]. R_z is the maximum height or highest peak, of the profile, the mean height of the profile peaks is termed R_c , and R_{Sm} is used to describe the mean peak width for a given profile. R_{sk} is the profile skewness, while R_{ku} is the roughness kurtosis, and R_z represents the ten point height testing method. Equations for R_a , R_q , R_z , R_t , R_{sk} , and R_{ku} are shown below [46].

$$R_a = \frac{1}{n} \sum_{i=1}^n S_i \quad (14)$$

$$R_q = \sqrt{\frac{1}{n} \sum_{i=1}^n S_i^2} \quad (15)$$

$$R_z = \frac{\sum_{i=1}^s s_{pi} - \sum_{i=1}^s s_{vi}}{s} \quad (16)$$

$$R_t = \max_i s_i - \min_i s_i \quad (17)$$

$$R_{sk} = \frac{1}{nR_q^3} \sum_{i=1}^n S_i^3 \quad (18)$$

$$R_{ku} = \frac{1}{nR_q^4} \sum_{i=1}^n S_i^4 \quad (19)$$

2.3.6 Pre-Blasting Strains and Stresses

Normally, it is assumed that substrates for the abrasive blasting operation are under negligible strain (especially if the substrate isn't attached or part of a load-bearing application). The effects of the blasting media and parameters will contribute to the stress and strain changes. In real world applications, pre-strained substrates would be expected if a substrate was part of a machine or structure and was blasted in an open environment while being pre-strained during or prior to blasting.

A study by Tosha and Iida looked at the effects of pre-strain on 304 austenitic stainless steel substrates [47]. Pre-strain occurred at 0%, 10%, 20%, and 35% prior to blasting and the effect of work-softening occurred on the substrates. Generally, when grit blasting a work-hardened layer would be present after blasting. Due to the pre-strain that occurred prior to blasting, the opposite, work softening was noticed for all substrates with the pre-strain applied before blasting. One set of experiments used steel shot, while the other used steel grit. The effects of the grit blasting softening effect on the pre-strained substrates was more pronounced with a maximum softening ratio of 8.3% from blasting [47].

2.3.7 Cleanliness

Contamination evaluation must occur based on the type of contaminant, amount of contaminant, depth of contamination layer, and friability of contaminant. Common examples of surface contamination are excess oil, lubricants, dust, water, organic, and inorganic materials. External contaminants are materials or debris that appear on the substrate due to the surrounding environment or finishing part processes. Examples of human sources are finger prints, cigarette smoke, drink residues, and mucous, while non-human error environmental contaminants are lubricating oils and silicone greases.

Different types of contamination effect the surface properties of the substrates as shown in the *Handbook on Adhesion Technology*. In most cases, adhesive strength is evaluated for purposes of future coatings, however, in blasting operations, adhesives are also used as masking materials to protect parts of the substrate from being blasted. Thus, knowing how contamination effects adhesion to a substrate before and after blasting is relevant. Smith and Crane performed a study on the influence of contamination levels on adhesive strength of aluminum alloy adherents, with lubricating oil and silicon grease being contamination sources [48]. An increase in water contact

angle to 100° occurred when high levels of lubricating oil were added to a surface, while small levels, 3.5 to 20 nm, of silicone grease led to increases in the water contact angle and a huge reduction in failure load [44]. Another study, by Minford, demonstrated the effect of emulsified lubricants on 2036 T4 aluminum [49]. The joint strength of the aluminum lap-shear joint regions began to decrease at 0.82 mg/cm^2 of oil and after 0.95 mg/cm^2 of oil, the strength decreased from 10 to 6 MPa, and the level of cohesiveness decreased as well.

A few methods of degreasing metal adherents or substrates are simple immersion, wiping techniques, vapor degreasing, ultrasonic cleaning, etching, grit blasting, and surface temperature treatments. Environmentally safe alternatives are detergent degreasing and alkaline cleaners. Recommended methods for polymer contamination removal are flame treatment, corona discharge treatment, and plasma treatment [44]. For composites, the two best surface contamination reduction methods are peel plies, which are sacrificial external surface layers, and the use of surface abrasion (grit blasting) to eliminate the contaminated layer. Contamination lowers surface energy, which is related to the surface roughness and adhesion strength of substrates.

2.4 Blasting Environment

During the blasting process, both cabinet temperature and humidity can play a role in the outcomes seen from blasting [50]. The temperature of the blasting process is generally ambient or room temperature, but can vary based on the different blasting operations/locations. Humidity is generally location specific, but results will vary if blasting on a factory floor versus outside in ship hull blasting. “Little research has been done on the effect of temperature on erosion damage, while research on the influence of humidity on erosion could hardly be found in the literature” [50].

2.4.1 Temperature

Fang and Chuang showed that as substrate temperature increases, erosion loss or stock removal decrease for aluminum, stainless steel, and a titanium alloy [50]. Another one of their studies suggests that erosion damage might be varied with change in blast (attack) angle. Figure 2.13 displays these results for SS41 steel temperature and blast angle effects on volume loss, worn area, and mean penetration depth.

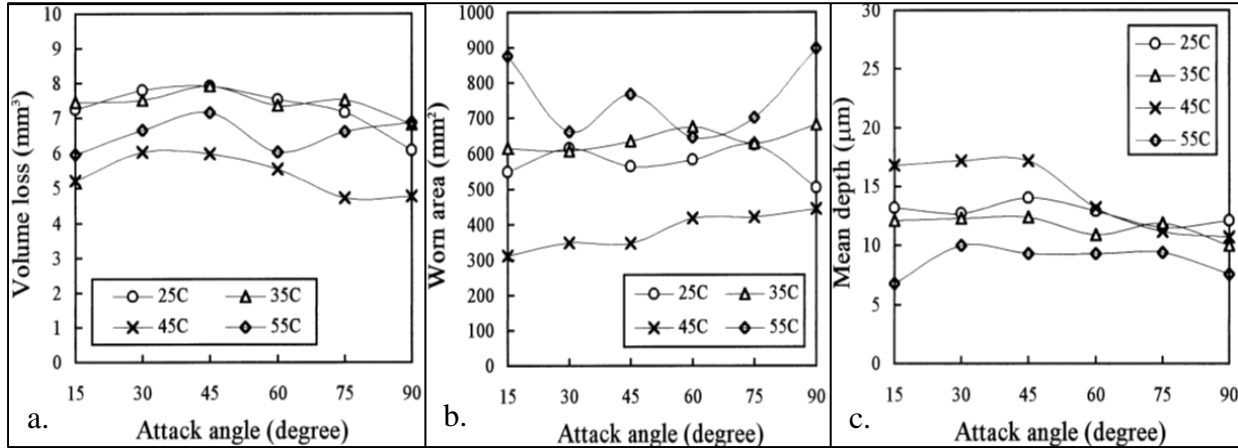


Figure 2.13 Temperature effects from blasting. Fang, C.K., Chuang, T.H. "Erosion of SS41 Steel by Sand Blasting." *Metallurgical and Materials Transactions A*. 1999/Vol. 30A, p. 944. (accessed January 11, 2013) Used with permission from Copyright Clearance Center, 2014.

The blast temperature of 45°C led to the least amount of volume loss/stock removal, smallest amount of worn area, and largest scar depth. For volume loss, lower temperatures led to more volume loss, suggesting that an elevated temperature might help save substrate stock in surface texturing applications. Certain substrate temperatures lead to a minimizing effect on mean depth of scars. Blast angle had an effect on these results as well.

2.4.2 Humidity

The effects of humid blasting environments have been of little discussion by research groups, although Fang and Chuang also studied blasting angle variation with four different humidity levels. Figure 2.14 displays the results of their studies with emphasis on 50, 65, 80, and 95% relative humidity.

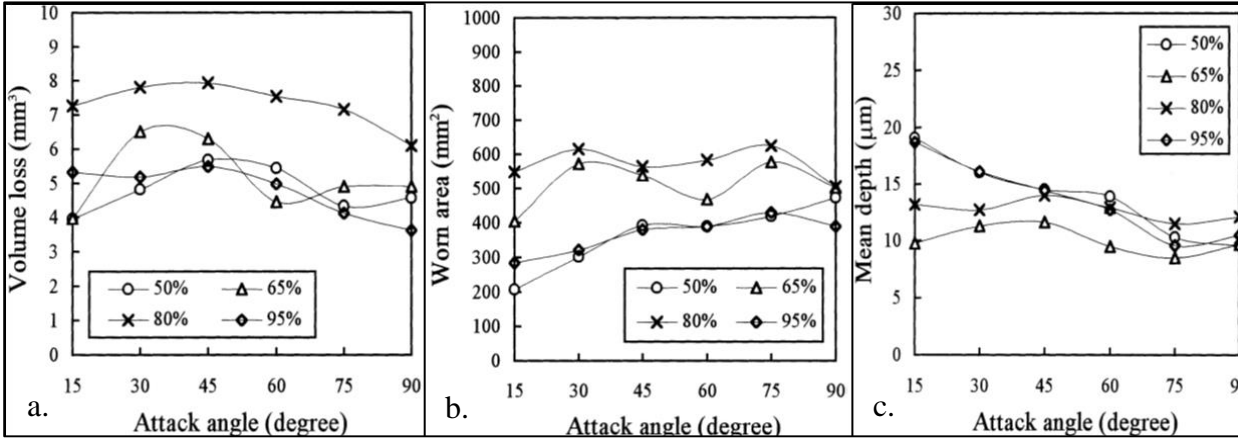


Figure 2.14 Effect of humidity during blasting. Fang, C.K., Chuang, T.H. "Erosion of SS41 Steel by Sand Blasting." *Metallurgical and Materials Transactions A*. 1999/Vol. 30A, p. 944. (accessed January 11, 2013) Used with permission from Copyright Clearance Center, 2014.

Some effects are noticeable regardless of blasting angle, which are that 80% RH led to the most volume loss and worn area, while 65% RH generated the smallest mean scar depths. Most of the data shown suggests that attack angle and humidity have a combination effect on surfaces, except that when attack angle increases, the mean depth decreases in most cases.

2.5 Blasting Process Parameters

There are many important factors that lead to changes in surface modification from grit blasting. Some of these process factors are: blasting pressure, stand-off distance, attack angle, blast time, coverage, media size degradation over time, media flow rate, media velocity, media impact energy, etc. The blasting pressure effects the media flow rate, media and air velocity, and to a certain extent the blast pattern generated. Assuming that the media flow is completely straight (no curvature due to low flow rate), the blast angle is the angle between the substrate and the media stream exiting the nozzle or the nozzle itself. . Stand-off distance is the direct distance from nozzle exit (possibly nozzle throat) to the substrate during blasting. Media flow or mass flow rate is effected by the amount and size of media, blasting (air) pressure, air velocity/volume, and blasting hose dimensions.

2.5.1 Blasting Pressure and Media Flow Rate

In any kind of dry abrasive blasting system, compressed air or gas is used to propel the media through a nozzle and unto the substrate. The amount of media leaving the nozzle and hitting the substrate (media flow/mass flow rate) and particle velocity are affected by the compressed air pressure. When the blast nozzle geometry stays constant and the hose and media flow regulator are not obstructed by various objects, the increasing blast pressure leads to higher abrasive flow and abrasive velocities. Figure 2.15 shows the effect of blasting pressure on grit blast rate (kg/min). As the blasting pressure increases, the grit flow rate increased regardless of grit size. A similar effect can be noted if the nozzle opening becomes smaller and the same blast pressure is used.

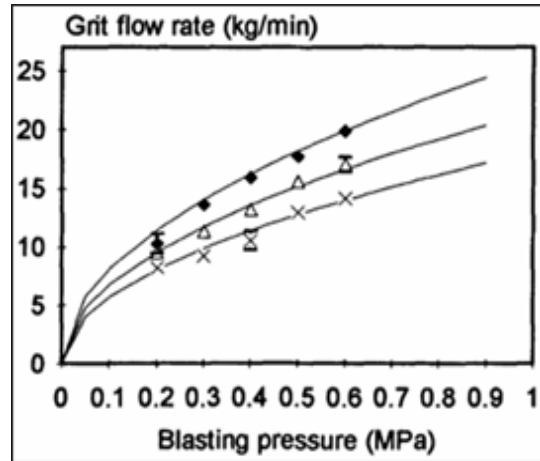


Figure 2.15 Blasting pressure vs. grit flow rate. Mellalia, M., Grimaud, A., Leger, A.C., Fauchais, P., and Lu, J. “Alumina Grit Blasting Parameters for Surface Preparation in the Plasma Spraying Operation.” *Journal of Thermal Spray Technology*. 1997/Vol. 6. No. 2. p 219. (accessed October 22, 2012) Used with permission from Copyright Clearance Center, 2014.

Roughness, adhesion strength, and residual stress are found to be related to pressure changes. Another study by Tosha and Iida shows that both grit and shot on stainless steel and titanium substrates generate higher R_{max} values, with grit roughening the surface more than shot, as expected [52]. The magnitude of residual stresses generated from blasting low carbon steel with alumina grit are shown in Figure 2.16. An increase in blast angle led to more compressive residual stresses, as did an increase in blast pressures for all three angles.

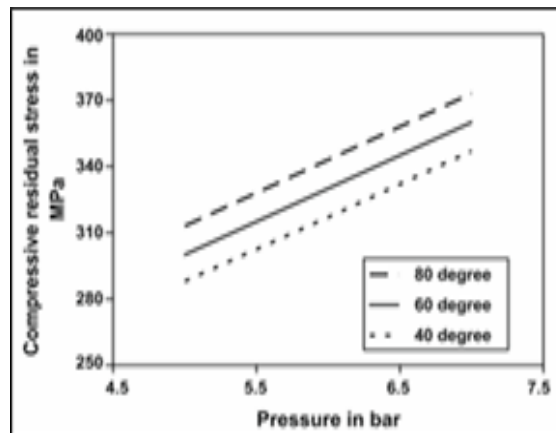


Figure 2.16 Blast pressure vs. compressive residual stress. Chander, K. Poorna, Vashita, M., Sabiruddin, Kazi, Paul, S., Bandyopadhyay, P.P. “Effects of Grit Blasting on Surface Properties of Steel Substrates.” *Materials and Design*. 2009. p. 2901. (accessed November 2012) Used with permission from Copyright Clearance Center, 2014.

2.5.2 Stand-off Distance

Blasting or standoff distance is the exact distance between the blasting nozzle and the substrate specimen and is usually listed in units of centimeters (cm), millimeters (mm), or inches

(in). If the distance is very small, then blasting might roughen the surface too much in localized zones, but if the distance is too far, media velocity would decrease and the substrate would barely be eroded, scarred, or grazed, if at all. Figure 2.17 displays a similar effect when alumina was blasted on steel substrates at different distances. At a blast distance of 100 mm, the maximum roughness was obtained and distances shorter or further seemed to create smaller increases in surface roughness.

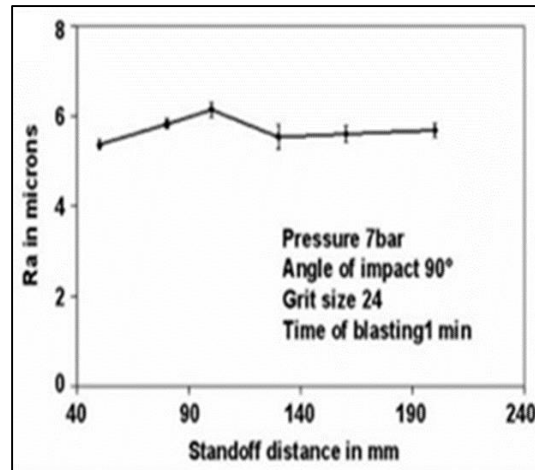


Figure 2.17 Surface roughness distance. Chander, K. Poorna, Vashita, M., Sabiruddin, Kazi, Paul, S., Bandyopadhyay, P.P. “Effects of Grit Blasting on Surface Properties of Steel Substrates.” *Materials and Design*. 2009. p. 2899. (accessed November 2012) Used with permission from Copyright Clearance Center, 2014.

Figure 2.18 links blast distance, grit size, and substrate type into one set of results. This figure shows “that, for a given material, R_a increases with the blasting distance, d , up to 100 mm, remains almost constant up to 150 mm, and then decreases again for higher values of d ” [51]. However, each substrate had different roughness values at the various blasting distances. The aluminum was roughened the most up to this 100 mm distance, with FT25 being next, and 100C6 being roughened the least for all three media sizes, due to the hardness of these substrates. This group reported that velocity decreased as distance became larger and that “when d is too short, the rebounding particles reduce the number and/or the efficiency of impacting grit particles they collide with in flight” [51].

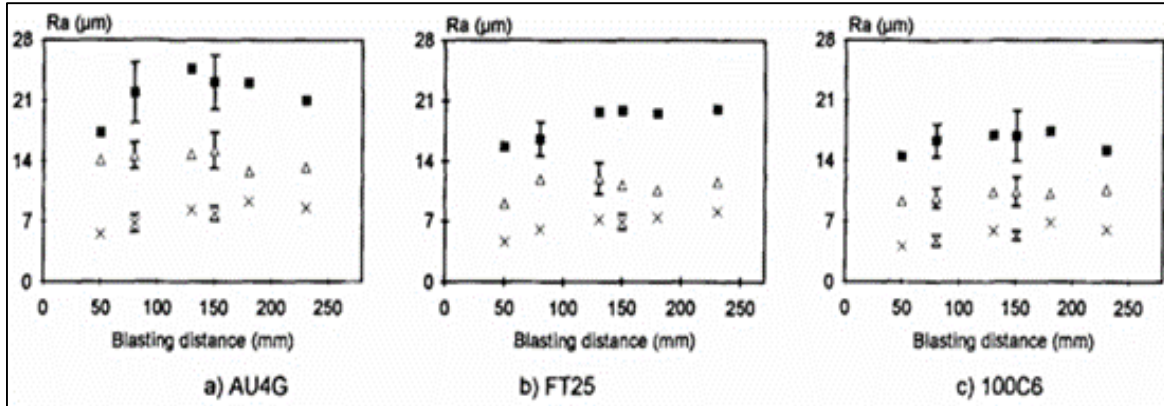


Figure 2.18 Surface roughness vs. blasting distance/substrate type. Mellalia, M., Grimaud, A., Leger, A.C., Fauchais, P., and Lu, J. "Alumina Grit Blasting Parameters for Surface Preparation in the Plasma Spraying Operation." *Journal of Thermal Spray Technology*. 1997/Vol 6. No. 2. p 221. (accessed October 22, 2012) Used with permission from Copyright Clearance Center, 2014.

2.5.3 Blast Angle

Depending on the application and substrate shape, the angle can be held constant or varied to generate certain mass erosion zones or surface roughness values. Figure 2.19a displays the effects of various blast angles of 45° , 60° , 75° , and 90° . Those same angles are displayed in Figure 2.19b, and show that the maximum roughness occurred at 70° , while similar roughness values were there for 75° and 90° [54].

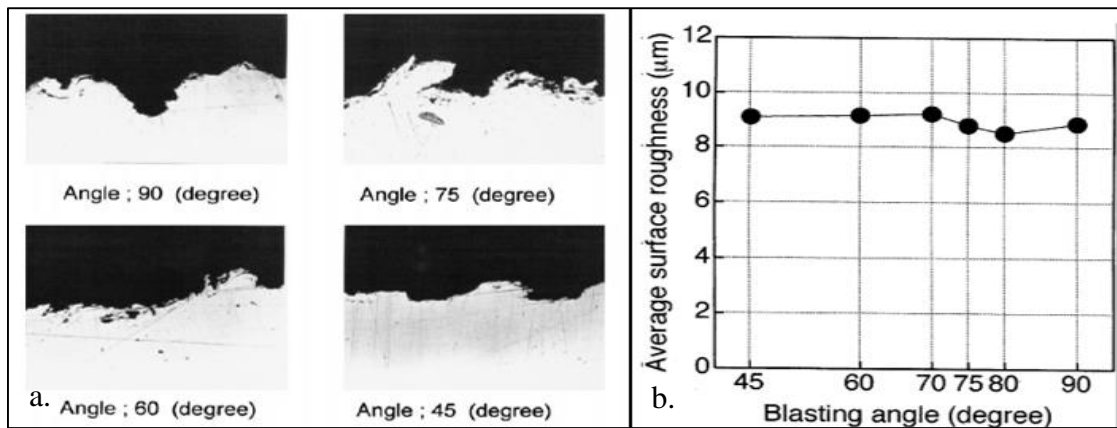


Figure 2.19 a. Cross-sectional photographs & b. Angle vs. Ra. Amada, Shigeyasu, Hirose, Tohru. "Influence of grit blasting pre-treatment on the adhesion strength of plasma sprayed coatings: fractal analysis of roughness." *Surface and Coatings Technology*. 1998/Vol. 102. p. 134. [http://dx.doi.org/10.1016/S0257-8972\(97\)00628-2](http://dx.doi.org/10.1016/S0257-8972(97)00628-2) (accessed October 29, 2012) Used with permission from Copyright Clearance Center, 2014.

Figure 2.20 shows the effect of incident blasting angle (angle from being perpendicular with the surface) for alumina grit blasting of copper substrates. At about 73° (17° from 90°) with the substrate, the maximum erosion rate occurred, which is close to the 75° maximum roughening of other substrate types. It is also seen that at angles of 0 to 10° , erosion rates stayed constant.

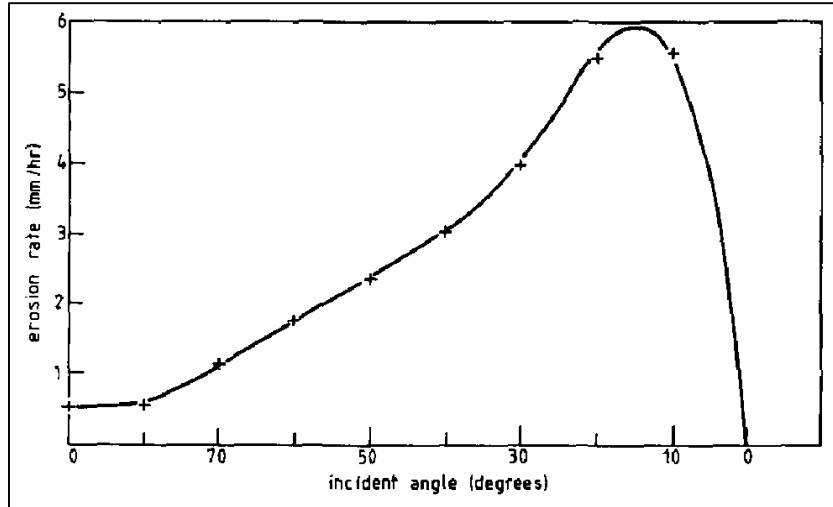


Figure 2.20 Erosion rate vs. incident angle. Carter, G., Bevan I.J., Katardjiev I.V., Nobes, M.J. "The Erosion of Copper by Reflected Sandblasting Grains." *Materials Science Engineering*. 1991/Vol. A. no. 132. P. 232. (accessed October 22, 2012) Used with permission from Copyright Clearance Center, 2014.

2.5.4 Blast Time

Blasting time can be defined with relation to total number of passes, traverse rate across the surface, and step size between blasts. Coverage area during the blasting process can simply be defined as the total area that the substrate is blasted. This usually correlates to a coverage area number, for instances, 100% coverage means that the exposed or pre-defined section of the substrate was blasted completely and evenly 1 time. This means that 200% coverage means the same spot was blasted over 2 complete times and so on. The various effects of blast time will be explained with examples in the following section. Tosha found that a lower traverse rate led to longer blasting time and longer time to reach 100% area coverage [43].

As a substrate is blasted, there is an optimum time of surface roughening or a maximum roughness generated from blasting "x" number of seconds or minutes, when this time is passed, the surface becomes smoother with excessive blasting time, as shown in Figure 2.21 for alumina blasting of stainless steel. Figure 13 by Khorasaizadeh from "The Effect of Shot and Grit Blasting Process Parameters on Steel Pipes Coating Adhesion" shows similar effects for a different steel alloy substrate with metallic grit, over-blasting occurred at 15 seconds, decreased from 15 to 25 seconds, roughness stayed constant after 25 seconds [57]. One study displayed displays the over-blasting effect on surface showing an overall lowering of the parameter Ra for blasting on plain carbon steel [58].

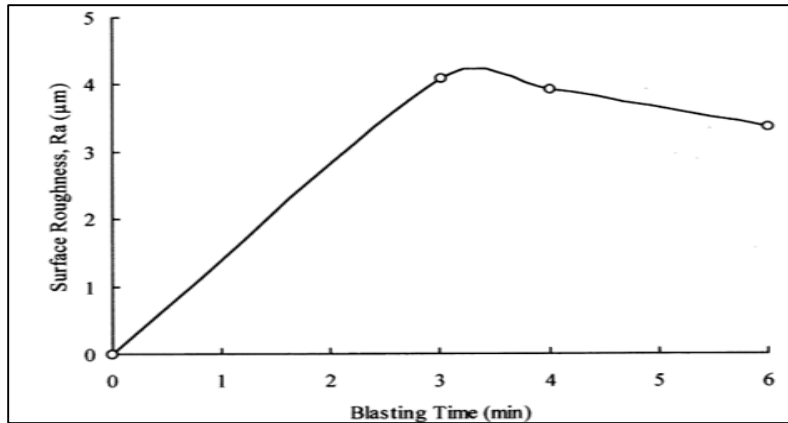


Figure 2.21 Time vs. roughness for Al₂O₃ against stainless steel. Celik, E., Demirkiran, A.S., Avci, E. "Effect of Grit Blasting of Substrate on the Corrosion Behaviour of Plasma-Sprayed Al₂O₃ Coatings." *Surface and Coatings Technology*. 1999/Vol 116-119. p. 1062. (accessed October 29, 2012) Used with permission from Copyright Clearance Center, 2014.

Results pertaining to blast time with effects on surface hardness, stock removal, residual surface stresses, and grit residue amounts were generated by various research groups as well. Khorasanizadeh showed in one study that steel substrate hardness increases with longer blast times [57]. Another study by Tosha and Iida demonstrates effects of blast time with grit and shot media blasted against annealed carbon steel, showing how stock removal increases with more blast time for grit media, while removed stock is almost 0 or constant for shot media [43].

Tosha and Iida demonstrated the effect of blasting a titanium substrate with cast steel at two angles (normal to & 30° with substrate surface) [52]. Blasting at an angle of 90°, the substrate generated an increase in residual stress up to 5 seconds of blasting, followed by a stress relief zone until the end of blasting. The same effect occurred at a shallow angle, with the stress relief zone being longer, but having less intensity. Figure 2.22 displays information from blasting at 45° and 90° angles with blasting times included. The shallow angle blasting and normal angle blasting both showed the over-blasting effects on surface roughness and saw increases in grit residue % over time. Grit blasting substrates at a 90° blast angle generated more residual grit (30%) in a shorter time than 45° angle blasting.

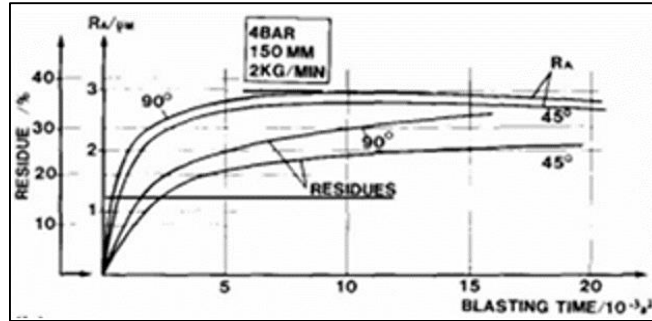


Figure 2.22 Blast time vs. grit residue. Wigren, Jan. "Technical Note: Grit Blasting as Surface Preparation Before Plasma Spraying." *Surface and Coatings Technology*. 1988/Vol 34. p. 107. (accessed January 15, 2013) Used with permission from Copyright Clearance Center, 2014.

2.5.5 Media Degradation/Fragmentation

Blasting media is very hard and has high fracture toughness values, thus media can be recycled through a system and used for “x” number of times, until the media begins to wear down into different size and shapes that originally planned. Once of the media breaks down, expected effects on surface roughness and mass erosion are no longer known. This media failure can occur due to blasting media for too many cycles, thus passing a certain failure limit, media reflection during blasting, cracks in media prior to blasting, unknown defects in media, and stresses from blasting on the media (not just the substrates). Gommel introduced a shatterability parameter, which is based upon substrate hardness and impact velocity, “which quantifies the particle fragmentation during the impingement on a substrate” [14].

Fracture due to impact with the substrate is shown below in Figure 2.23. Based on this diagram, a primary fracture zone is created by impact stresses, which create waves that travel through the particle and partially stop. The secondary fracture zone (coarse fragments) is created from these waves and appear on the rear side of the particle opposite of the impact zone.

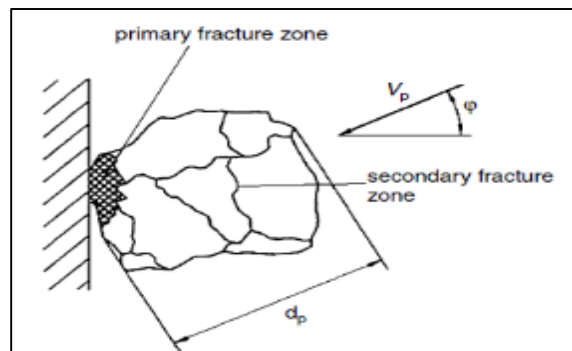


Figure 2.23 Fracture mechanisms. Momber A. *Blast Cleaning Technology: Chapter 2: Abrasive Materials*, 2008. p. 38. http://link.springer.com/chapter/10.1007%2F978-3-540-73645-5_2 (accessed March 31, 2013) Used with permission from Copyright Clearance Center, 2014.

Studies have shown that for glass bead blasting, low impact velocities lead to cracks in the media, whereas higher velocities lead to fragment and powder formations [14]. Another media/surface interaction was classified by Ohlsen as a disintegration number. Equation 20 displays the simple formula for disintegration number calculation [61].

$$\Phi_D = 1 = \frac{d_{p_{out}}}{d_{p_{in}}} \quad (20)$$

As the diameter after blasting changes, so does the disintegration number. When the particles do not vary in size from blasting then the disintegration number will stay low as well. Figure 2.24a and Figure 2.24b displays the correlation between number of blasting cycles and disintegration number.

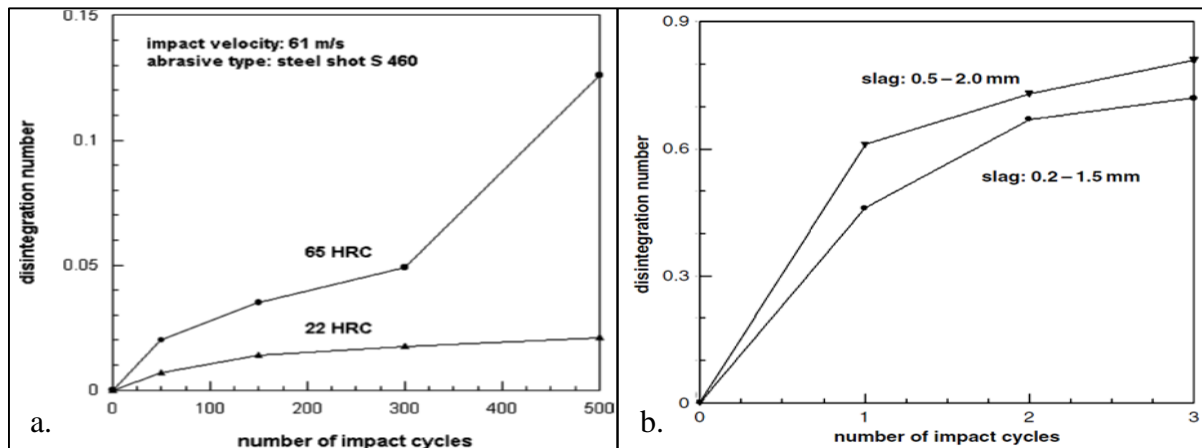


Figure 2.24 Number of cycles vs. disintegration #, a. substrate hardness & b. slag size. Momber A. *Blast Cleaning Technology: Chapter 2: Abrasive Materials*, 2008. p. 47, 48. http://link.springer.com/chapter/10.1007%2F978-3-540-73645-5_2 (accessed March 31, 2013) Used with permission from Copyright Clearance Center, 2014.

Figure 2.24a shows that for a softer substrate, the disintegration number remains low, which means less particle size change or fragmentation from blasting and the harder substrate led to a larger change in particles shape and size. Figure 2.24b details the effect of particle size on impact cycles for slag media. As particle sizes get bigger, so do the disintegration numbers and the likelihood of media shape/size alterations occurring increases likewise.

2.5.6 Nozzle Type

Based on the type of blasting media, nozzle materials can be made of tungsten carbide, boron carbide, or silicon carbide due to high hardness values and lower wear rates than other materials. The type of nozzle material, along with the nozzle shape designs can affect the substrate.

Appendix B displays images of five different nozzle designs: straight, flat straight Venturi, smooth throat Venturi, double Venturi, and wide throat nozzle.

The first image is the straight bore nozzle, which is used in smaller spot blasting jobs due to a smaller blast generated blast pattern. A reduction in the amount of media consumption can occur from Venturi nozzles also [63]. The Venturi nozzles shown in the second and third images of Appendix B, generate a wide blast pattern and can increase the abrasive jet velocity more than 100% for a given pressure. The double Venturi nozzle and the wide throat nozzles are enhancements from the Venturi nozzles. The gap in the double Venturi nozzle allows for extra air to enter the nozzle and along with a wider opening, the size of the blast pattern and help minimize abrasive velocity losses [63]. The wide throat nozzle helps increase the blast pattern size compared to smaller throat nozzle as well.

It is important to understand the wear of the nozzles over time from the abrasive wearing away at the nozzle throat as this affects the blast pattern and velocity. Due to this abrasive wear, the nozzle throat becomes more similar to a straight bore nozzle, along with a larger throat developing over time. A throat gauge can be used at regular intervals to monitor the nozzle wear and nozzles are to be replaced when the throat size increases to the size of the throat size of the next larger nozzle size. Replacing these worn nozzles is critical to ensure efficient blasting. Along with nozzle wear, the length, entrance and exit nozzle diameters and converging and diverging nozzle angles are critical to controlled blast pattern size.

2.6 Characterization Techniques

2.6.1 Mechanical Profilometry

With mechanical profilometry, a given surface (blasted or non-blasted) can be measured with a linear trace from the stylus probe for various roughness parameters. The stylus has a very small tip radius (between micrometers to nanometers) and uses a small measuring force that the presses the stylus tip as it skids across the surface. Figure 2.25 displays an image of a simple mechanical profilometer and illustrates how the stylus measures a given surface.

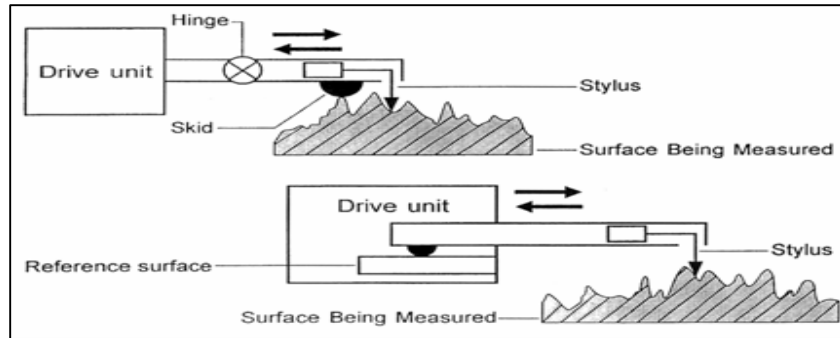


Figure 2.25 Mechanical profilometry. Tabenkin, Alex. "The Basics of Surface Finish Measurement." *Quality Magazine*. 2014. http://www.deterco.com/products/Mahr%20Federal/newsletter/finish_measure_10_19_04.htm (accessed May 14, 2014) Used with permission from Mahr Federal Inc., 2014.

Different roughness standards can be used with the profilometer, along with settings for the profile assessment, evaluation parameters, cut-off lengths, sample lengths, number of samplings, digital filters, and analysis graphs. Some of these standards are from various organizations such as the JIS, ISO, and ANSI. The profiles measured can be primary, roughness, DF, and roughness profile-Motif. The cut-off length is used to eliminate profile data when a certain resolution is needed. A large cut-off length, λ_c , will show more of the primary profile, whereas a small cut-off length will lead to a smoothing of the evaluation parameter measured. The sampling length, λ_s , is how much of the surface is measured during a surface measurement, with N being the number of sampling lengths. Olympus Corporation showed the effect of decreasing the cut-off length size on a given primary profile [65]. As the cut-off length decreases, a smaller range of roughness peaks and valleys is gathered, thus creating a smoother surface, thus a larger cut-off length leads to more accurate results.

The evaluation parameters refer to any parameter of the given profile assessments and graphs (like a bearing area curve (BAC) and amplitude distribution curve (ADC)) that can be obtained through profilometry. Figure 2.26 contains another representation of average roughness parameter R_a . The types digital filters used can affect the measured data and can reduce noise and extra data when utilized correctly.

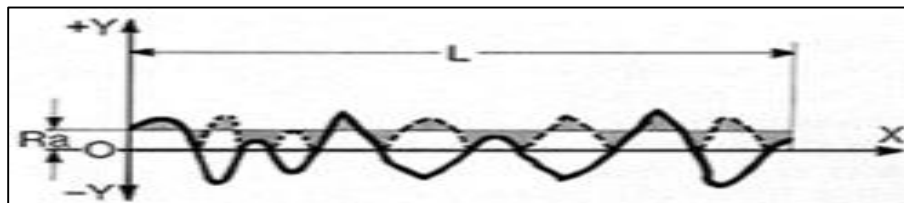


Figure 2.26 Average roughness, R_a image. Pickrell, G., Homa, D, Mills, R. "Abrasive Blasting Deliverable No.3." CCAM. 2014. (accessed April 2, 2014) Used with permission from Robert Mills, 2014.

2.6.2 Optical Profilometry/Microscopy

Non-contact profilometry is used to avoid substrate scratching from the stylus and to obtain evaluation parameters that are 3-D which would be S_a values. Figure 2.27 shows a surface for S_a , the 3-D equivalent arithmetic average roughness parameter and an image of the surface in which the S_a would be measured [57]. S_a is measured in both x and y directions of a surface over the z-direction (height of profile changes) and is averaged over the entire surface.

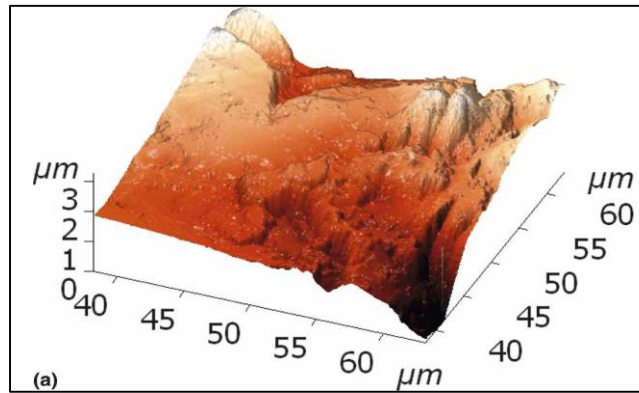


Figure 2.27 Surface roughness for S_a . Sosale, G., Hackling S.A., and Vengallatore, S. "Topography Analysis of Grit-Blasted and Grit-Blasted-Acid Etched Titanium Implant Surfaces Using Multi-scale Measurements and Multi-Parameter Statistics." *Journal of Materials Research*. 2011/Vol 23, Issue 10. p. 2709. (accessed June 6, 2014) Used with permission from Copyright Clearance Center; letter attached.

Optical profilometry is a non-contact characterization method which utilized image slices from an optical microscope taken from a blasted surface. The microscope is set to view a certain portion of the surface (the whole surface if the substrate is very small) and images are taken until the whole surface can be reconstructed. The images gathered from different focal planes of the surface can be stacked together, created a 3-D image similar to surface shown in Figure 2.27. With the help of other mathematics software (like Matlab or Mathematica), the S_a value can be obtained. Some settings that need to be pre-determined before carrying out surface roughness measurements through optical microscopy and profilometry are the magnification of the microscope and the distance the lens is away from the focal plane.

3 Experimental Methods

Two sets of experiments were conducted and the experimental procedures for these are explained in depth in this section. One set focusing on cleaning, blasting, and measuring surface roughness of 304 Stainless Steel substrates. The other set of experiments was focused on blasting and measuring temperature changes in-situ blasting for 304 Stainless Steel and thin stainless steel substrates.

3.1 Roughness Experimental Procedure

The experiments performed for the purposes of surface roughness measurements were similar, with the exception of the process parameters chosen for each experiment. First, the media and substrates were down-selected as a good match for the grit blasting process. The two cabinets were inspected and prepared for blasting. Substrates were then cleaned with acetone and dried, then labeled and placed in individual bags. Next, each set of process parameters was designated, and one set of 10 substrates were blasted for each different type of experiment. Once blasted, the substrates were cleaned again via compressed air and placed back in their labeled bags.

The surface roughness was measured via three different methods: mechanical profilometry, optical microscopy, and optical profilometry. These were carried out with the Mitutoyo SJ-210 Profilometer, HIROX Optical Microscope, and the UVA ROST Tool. A brief explanation of each of these steps for the blasting and surface roughness measurements will be discussed in the following sections.

3.1.1 Media, Substrate, and Parameter Selections

Based on the literature review and funding form CCAM (Commonwealth Center for Advanced Manufacturing), it was decided that stainless steel would be a good substrate material, along with brown alumina as the blast media, and variations of the blast angle, distance, and pressure. Selected specifications of the abrasive media and substrate information are shown in Table 3-1. It is important to use the correct size and amount of grit for a given blasting system. If the media is too hard or too large, the system will not work correctly and possible equipment damage and injuries may occur. It is also important that the substrates are of small enough size to gather roughness data from them, because large substrates could lead to injuries due to the

bulkiness of the substrates. The media hardness and substrate hardness were taken into consideration before blasting as well.

Table 3-1 Media and substrate properties.


Media Specifications [68]		Substrate Specifications [69]	
Type	Sulzer Metco VF Grit	Type	304 SS
Density	1.74 g/cm ³	Pressure	8 g/cm ³
Hardness	9 Mohs	Hardness	129 Vickers
Composition	94 Al ₂ O ₃ , 3.5 TiO ₂ , 2.5 other	Yield Strength	215 MPa
Size	350 μm	Size	3" x 3" x 3/16"

The set of process parameters chosen were based on the literature review as well with the following settings: angle at 90°, pressure between 20-80 psi, distance 3" to 18", and total blast time of 18 to 20 seconds (one pass or 100% coverage between 8 to 10 seconds).

3.1.2 Cabinet Information

Prior to any experimentation, the blast cabinet(s) must be set up and inspected for safety. The two types of cabinets used in the roughness experiments were the Commonwealth Center for Advanced Manufacturing (CCAM) EMPIRE Pro-Former 3642 and VT EMPIRE Pro-Finish 4848 blast cabinets. Table 3-2 contains a table of information about each cabinet with some of these safety and maintenance issues addressed during the experimentation process. Prior to experimentation it was important to check for any leaks or damage to the equipment.

Table 3-2 Cabinet specifications for roughness testing.

Process Detail	CCAM	VT
Blast Cabinet	Pro-Former 3642	Pro-Finish 4848
Nozzle	3/16" Venturi	3/16" Venturi, 5/16" Straight
Media Pulsation	Minimum	None, Minimum
Pulsation Elimination	No	Yes
Measurement System	Laser Level	Laser Level (2)
Media Replacement	None	Once
Cabinet Maintenance	Yes	Yes
Dust Collection Inspection	Yes	Yes
Orifice Cleaned	No	Yes
Laser System		

Once the equipment safety was insured, the following issues needed to be resolved before experiments: media pulsation, laser leveling, and media replacement. One issue was the problem of media pulsation, which will reduce the effect of the blasting operation and possible damage the equipment. The two methods for reducing the media pulsation are shown in Appendix C. The

media pulsation was reduced (or eliminated), to best achieve optimum blasting was achieved. In order to have a better understanding of nozzle location, each blast nozzle had a laser level attached. The laser was set so that if the laser read 6” on the back wall of the cabinet, then the nozzle was actually around 4” away from the substrate during experiments. Media replacement needed to occur based on the number of cycles the media was used as well. Even with a small number of experiments, issues with both broken down media and pulsating media flow were present and will be discussed in the Results section. It was found that cleaning the orifice of the media flow regulator eliminated or significantly reduced the media pulsation issue.

3.1.3 Substrate Preparation

The stainless steel substrates were 3” x 3” x 3/16”. For each experiment, the substrates were first deburred for ease of handling in the lab environment and then cleaned of any contaminants. Acetone was applied to each substrate and then wiped off with paper towels to remove any visible contamination such as oil, dirt, or machining artifacts. A substrate before and after blasting can be seen in Figure 3.1.

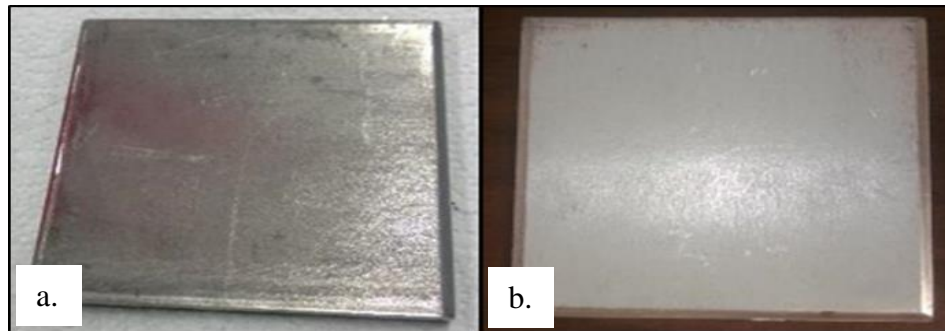


Figure 3.1 a. unclean substrate & b. clean substrate.

Once the acetone had air dried, the substrates were each labeled by experiment set number, and sample number of that experiment. Figure 3.2 displays an image of a substrate after the labeling process had occurred.

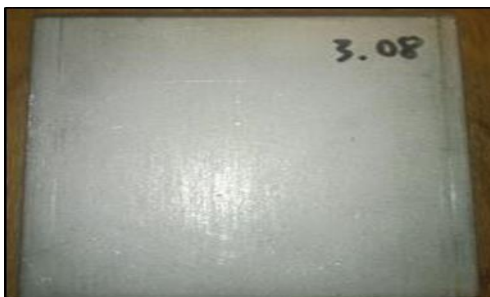


Figure 3.2 Example of sample labeling (experiment # followed by sample #).

Information about each experiment was recorded in a log in Microsoft Excel, with emphasis on process parameters, which cabinet the blasting occurred on, and times (time per pass and total blast time) are shown in Table 3-3.

Table 3-3 Blasting information during one experiment.

Logistics		Blasting Parameters	
Batch	3	Angle	90
Date	8/5/2013	Pressure	42?
Blaster	Robert	Time (Pass #1)	Goal of 9 seconds
Time Recorder	Venkat	Time (Pass #2)	Goal of 18 seconds
Machine	EMPIRE PF 3642	Blast Height	Constant, 7-9 inches
Recorded Stopwatch Times			
Sample #	Time (Pass #1)	Time (Pass #2)	Total Time
1	10.54	10.37	20.91
2	10.45	10.11	20.56
3	7.74	10.07	17.81
4	11.01	11.3	22.31
5	9.81	10.81	20.62
6	12.96	12.35	25.31
7	9.93	11.51	21.44
8	10.61	10.84	21.45
9	10.9	11.42	22.32
10	9.17	11.33	20.5

3.1.4 Cabinet Preparation and Substrate Blasting

A total of 18 sets of substrates were deburred, cleaned, labeled, blasted, and packaged. The process parameters including the blast pressure, distance, nozzle, angle, cabinet, and operator are shown below in Table 3-4. The first four sets of experiments occurred on the CCAM PF-3642, while the remainder of the experiments occurred by blasting with the VT PF-4848. Experiments were performed to quantify process parameter changes, along with differences in different operators on the same cabinet, different cabinets with the same operator, and blasting under the same conditions on different dates.

Table 3-4 Experimental design sets for roughness testing.

Sample	Pressure	Height	Nozzle	Angle	Extra
1	42	4	3/16" Venturi	90	Repeatability -CCAM
2	42	6	3/16" Venturi	90	Distance
3	42	10	3/16" Venturi	90	Distance

4	60	6	3/16" Venturi	90	Pressure
5	42	4	5/16" Straight	90	Repeatability - VT
6	42	6	5/16" Straight	90	Distance
7	42	10	5/16" Straight	90	Distance
8	60	6	5/16" Straight	90	Pressure
9	42	6	3/16" Venturi	90	Reproducibility
10	60	6	3/16" Venturi	90	Reproducibility
11	42	4	3/16" Venturi	90	Operator Variability (RM-DH)
12	42	10	3/16" Venturi	90	Operator Variability (RM-DH)
13	42	6	3/16" Venturi	90	Repeatability (day) - RM
14	60	6	3/16" Venturi	90	Repeatability (day) - RM
15	42	4	3/16" Venturi	90	Operator Variability (RM)
16	42	10	3/16" Venturi	90	Operator Variability (RM)
17	42	4	3/16" Venturi	90	RM
18	42	6	3/16" Venturi	90	RM

Once the preliminary deburring, cleaning, and labeling of substrates was completed, the blast cabinet was activated and set up for each set of experiments. For every experiment, the compressed air line valve was set to open, followed by the opening of the ball choke valve was opened as well. An image of the compressed air valve and ball choke valve in the open positions is shown in Figure 3.3.

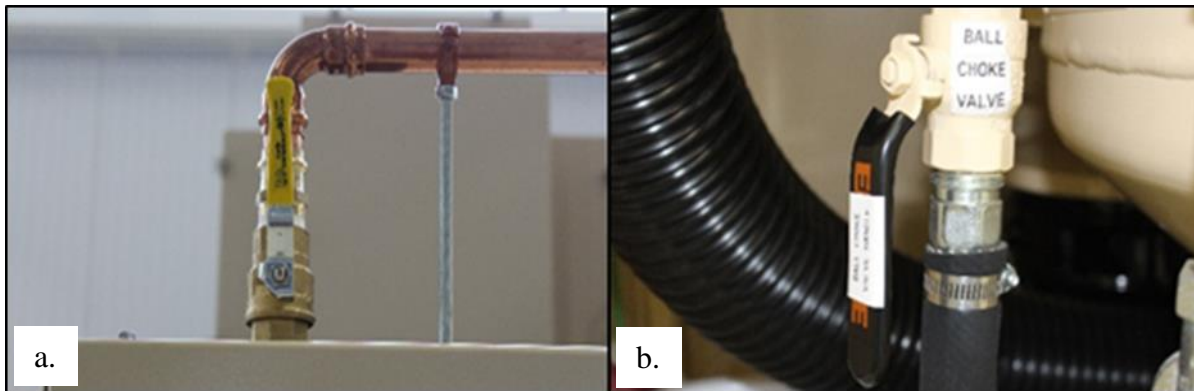


Figure 3.3 a. Compressed air valve open & b. ball choke valve open.

The dust collection system was automatically activated once the machine was turned on for the CCAM cabinet, but needed to be plugged in before blasting with the VT cabinet. The blast pressure was then adjusted with the air pressure regulator located at the bottom of each cabinet. Figure 3.4a shows an image of the blast pressure gage along with the pressure regulator knob. Once the pressure was set, the media flow must be set correctly (number of turns determines how

much the orifice is open below the pressure pot). Figure 3.4b displays the media flow regulation handle as well and when set correctly, along with a clean orifice, the media flow is constant, non-pulsating, and barely visible by eye.

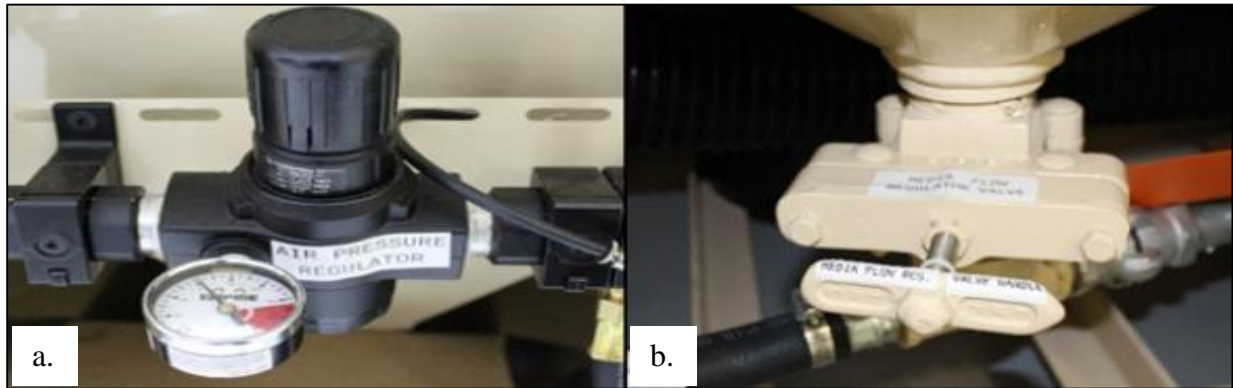


Figure 3.4 a. Blast pressure regulator knob/gage & b. media flow regulator/handle.

The last steps of blasting preparation were loading the desired number of samples (usually three or four) to the cabinet and to have another person assist the blast operator with a stopwatch. The actual blasting time for each set of experiments ranged from about 18 to 20 seconds per sample and only was slowed down by the irregular media flow before blasting samples. In order to hasten the experiments, the blast nozzle was placed flush with the blast cabinet wall, while the blast pressure was activated from the foot treadle. After a few seconds, no sound was heard from the nozzle, which meant that the pressure reached equilibrium due to the plunger sealing the pressure pot and the media falling correctly into the blast hose. Next, the blast stream was inspected visually and by listening to ensure constant media flow, then substrates were blasted according to Table 3-4.

The substrates were individually blasted, with 200% coverage, meaning that each substrate was blasted a total of 2 times or 4 traverse passes. Each set of 4 passes (100% coverage of the substrate) occurred in 8 to 10 seconds time frame. The first time the substrate was blasted, an S-shaped blast pattern was used, which consisted of 4 traverses of the substrate and the second time a reverse S-shaped blasting pattern occurred. The blast angle was kept close to a constant 90° and the distance was controlled manually as well at three heights of 4", 6" and 8", but monitored via the laser level system shown in Table 3-2. The blast cabinet and type of nozzle were pre-determined per set of experiments.

3.2 Post-Process Characterization

Three post-process characterization techniques were utilized to measure the surface roughness, either R_a , or S_a for different sets of blasted substrates. The following instruments were used to measure roughness on the blasted substrates: Mitutoyo SJ-210 Mechanical Profilometer, HIROX Optical Microscope, and UVA Optical Stacking Tool (for roughness measurements, designated as ROST). The settings and methods of each of these measurements will be discussed in the following sections. The number of samples and number of total measurements are shown below in Table 3-5.

Table 3-5 Measurement information for roughness testing.

Detail	Tool/Value	# of Samples	# of Measurements
Mechanical Profilometry	Mitutoyo SJ-210	190	>2400
Optical Microscopy	Hirox	2	30
Optical Microscopy	UVA Portable Tool	16	150

3.2.1 Mitutoyo SurfTest SJ-210 Mechanical Profilometer

The SJ-210 profilometer was used to measure roughness parameter, R_a , along with other roughness parameters. Table 3-6 lays out the measurement settings used in the SJ-210 [70].

Table 3-6 SJ-210 measurement settings.

Setting	Setting Value	Setting	Setting Value
Standard	ISO 1997	Cut-off Length, λ_c	0.8 mm
Profile	R	Sampling Length	2.5 μm
Stylus Force	4mN	Number of Sampling, N	8
Measuring Speed	0.25 mm/s	Digital Filter	Gaussian
Z Axis Range/Resolution	360 μm / 0.02 μm	Evaluation Parameter	R_a

As shown previously in Table 3-4, 18 different experiments were performed with ten substrates blasted under the same conditions. Each substrate (for a given blasting condition) was then measured ten times after blasting, which yielded 100 measurements per blasting condition. Figure 3.5 displays an image of the measurement technique use for the 10 surface measurements of each substrate. The measurements denoted as “V” when the SJ-210 did a linear trace perpendicular to the traverse rate of the blasting process and by an “H” when the trace was parallel with the traverse rate. A total of 5 measurements in each direction, led to 10 measurements per substrate. Appendix C contains a sample output from the SJ-210 for 20 different roughness parameters including R_a .

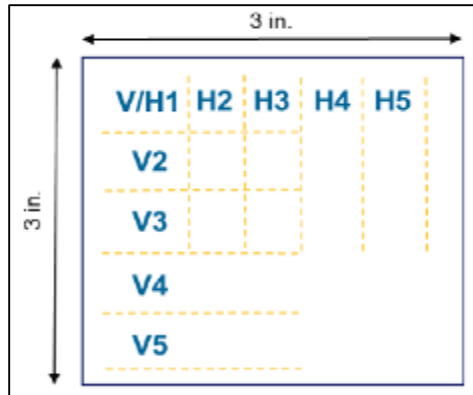


Figure 3.5 SJ-210 surface measurement technique.

The last step of each set of experiments was to compare the R_a values, and the following standard deviation (σ) values: measurement, average R_a , and process + measurements. The measurement σ was the standard deviation of the each of the 10 samples per set (standard deviation of 10 standard deviations). The average R_a σ was the standard deviation of the average R_a values (standard deviation of 10 average R_a values) and the process + measurements σ was the standard deviation for the 100 roughness measurements taken per experiment set. Figure C.3 contains an example of these mentioned calculations for experiment #2 in Appendix C. Those values can be seen, along with all of the other measured values of Average R_a , and calculated standard deviations in Figure 4.1 in the Results Section.

3.2.2 HIROX Optical Microscopy

Another set of characterization data came from using the HIROX optical microscope at UVA. For this device, magnification of 350X and 700X were used, along with focal distances of 2m and 4m. An 800 micron bandpass was used and an area of 20 x 27 points was analyzed, with 33.54 μm (350X) and 16.962 μm (700X) between each measurement. Only two substrates were analyzed with this method, due to the large amount of measurement time (3-4 hours for 15 measurements per sample) and those substrates were 2.10 and 3.10. Figure C.4 contains a portion of these 15 measurements per sample at different focal distances of 2m and 4m at 350X for Sample # 2.10 in Appendix C. Figure 4.2 contains the values for all of the S_a measurements with the HIROX optical microscope.

3.2.3 UVA ROST Optical Profilometry

The last set of surface roughness measurements was obtained via optical profilometry. The UVA Roughness Optical Stacking Tool (ROST) was the device used for these measurements. For

this device, 40 slices were taken per substrate measured and the step size of these image slices was $2\mu\text{m}$. A total of 16 substrates were measured with this tool, taking about an hour per set of 10 measurements per substrate. Figure C.5 contains some of the measurements taken per substrate (blasting condition) along with S_a and measurement σ in Appendix C. Figure 4.3 contains the S_a and measurement σ for all of the substrates measured with the ROST device in the following Results sections.

3.3 Substrate Temperature Experimental Procedure

The following sections are related to the substrate temperature experiments of the 304 stainless steel and thin stainless steel substrates. Initial testing was used to help set up accurate temperature measurement in the blast cabinet different light sources in the cabinet and the last set of experiments occurred on the actual blasting of substrates that had temperature sensors or probes attached to opposite sides of the given substrates.

3.3.1 Optical Fiber Splicing, Adaptors, and Connectors

Initially when setting up the optical fiber sensing rig in the blast cabinet, it was determined that the optical fiber needed to be robust enough to withstand the effects of accidentally blasting the coated fibers. Splicing and using adaptors was the best option to create a single long fiber strand that was connected from the interrogator to the substrates, with less issues of fiber damage from blasting. With this in mind, the fiber strand went through a small opening already present in the cabinet. The fiber was duct taped in various locations throughout the cabinet to keep the fiber out of the blasting range and to keep the fiber from being moved around or accidentally broken.

In order to splice two fibers together, the outer coatings were removed first with fiber strippers. Next, the unprotected fiber had to be cut almost perfectly to create a flat surface for splicing. Figure D.1 shows the device used to cleave/cut the ends of the optical fibers in Appendix D. Following the fiber coating stripping and the fiber end cutting, the fiber was cleaned with alcohol and was locked into the fusion splicer and the fiber in which it was to be fused was prepared in the same fashion. Figure 3.6a shows the two cleaved fibers before fusion occurs, while Figure 3.6b shows the fused fiber, with the amount of signal loss of 0.04 dB from the fusion. In order to ensure high quality sensor data, the amount of signal loss should be minimal.

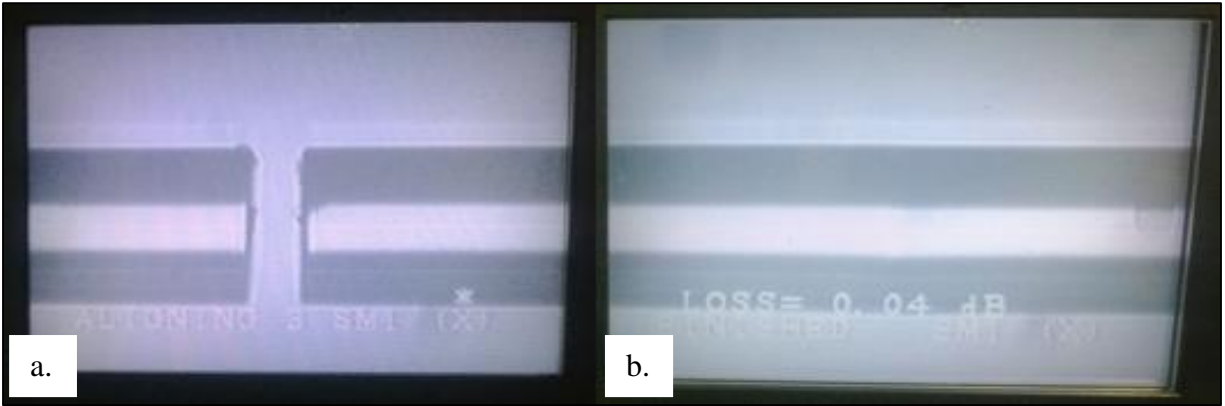


Figure 3.6 a. Fibers before & b. after fusion splicing.

The type of fiber adaptors and number of connections used will also lead to a decrease in the signal through the fiber system. Different types of adaptors were used with the optical fibers, angled and straight. Figure 3.7a shows three images of the adaptor types; blue and yellow are straight, while green are angled adaptors can be used with the interrogator directly or along with other fibers with connection pieces as shown in Figure 3.7b and Figure 3.7c. Only straight adaptors were used in all tests.

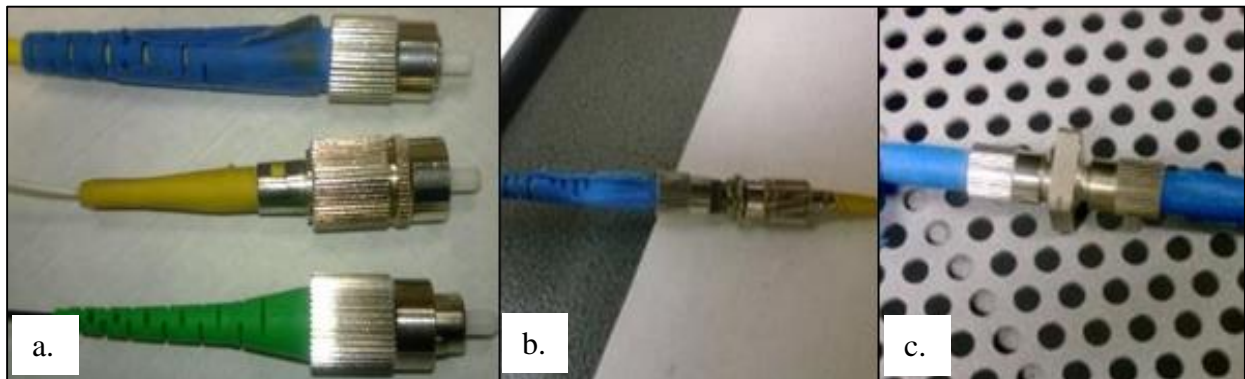


Figure 3.7 a. Fiber connectors, b. connector for blue-yellow adaptors, & c. blue-blue connection.

3.3.2 Optical Fiber Connection Cleanliness

The importance of clean fiber connections is similar to the effect of not having a clean fiber before the splicing process. When a fiber is unclean, damaged, or uneven in the splicing process, faulty splices occur leading a fused fiber that breaks easily or has a huge signal loss from the bad splice. Before screwing an adaptor into a connection piece, the adaptor end must be visually inspected and cleaned, if not signal loss will occur. Figure 3.8 shows an image of the end face

cleaner used for the adaptors. It is recommended that the end faces are wiped off with the cloth and only used on six different end faces before using a new cloth.



Figure 3.8 F1-7020C connector end face cleaner.

3.3.3 Micron Optics SM125 Optical Sensing Interrogator

Once all of the fibers were spliced or connected correctly on the single strand of fibers, the temperature sensor or temperature probe fiber strand was then connected to the SM125 Optical Sensing Interrogator. Figure 3.9 shows an image of the correct sensor set-up with the interrogator unit. The adaptor piece between the blue and yellow connectors is seen on the left, the middle shows the junction of the optical fibers coming from the SM 125 Interrogator, and the right side of the picture shows the two yellow connections to the device. With the use of this junction fiber, the signal can leave the interrogator through one port and be read as the wavelength changes come back down the fiber into the second port.



Figure 3.9 Optical fibers connected to the SM125 Interrogator.

3.3.4 Temperature Sensor and Probe

One type of optical fiber sensor that can be used is a temperature sensor. The sensor works in a simple fashion, light is sent from an interrogator device through an optical fiber to the temperature sensor and a wavelength change occurs in the sensor due to a temperature change from blasting, which can be detected in-situ during the blasting process. The goal is for the

propelled media impacting against the substrate (opposite substrate side of sensor location), to cause a temperature change in the substrate, which will be captured by the sensor. Equation 21 shows an example of how the temperature data can be determined via a change in wavelength of the light traveling through the optical fiber [72].

$$\Delta T = (1 \times 10^3)(\Delta \lambda / S_T) \quad (21)$$

For the given equation, as the temperature (T) changes, the wavelength will change accordingly. S_T is the pre-determined or constant temperature sensitivity of the sensor in units of pm/°C. This Fiber Bragg grating (FBG) sensor can be used to calculate the thermal expansion of the substrate. The index of refraction changes in the FBG can be monitored for the thermally induced strains as well [72]. The thermal expansion and the change in refractive index lead to the change in wavelength of the sensor on a given substrate.

A temperature probe, which is an FBG, was also used to monitor the live temperature change in an environment or the substrate. During the blasting process, the temperature probe was placed on the substrate, similar to the location of the temperature sensor. The goal here is to monitor and record temperature of the substrate before, during, and after blasting. The temperature probe will work as a partner of the temperature sensor and will show similar temperature changes due to particle impingement of the substrate. Equation 22 shows the calculation of temperature based on the changing wavelength due to temperature changes in the substrate [73].

$$T = C_3(\lambda + \lambda_{OS})^3 + C_2(\lambda + \lambda_{OS})^2 + C_1(\lambda + \lambda_{OS}) + C_0 \quad (22)$$

Values for C_0 , C_1 , C_2 , and C_3 are constant calibration coefficients and vary with each individual temperature probe. The wavelength offset, λ_{OS} , is a constant value along with the S_T value which is at a lower value than the temperature sensor, thus a higher accuracy in temperature change can be obtained.

These FBG fibers work with the optical fiber interrogator; a change in wavelength is detected by the interrogator and accompanying software. The advantage of the FBGs is a large temperature range can be measured, so damage is less likely to occur in these fibers versus non-FBG fibers when working in robust environments like grit blasting [74].

3.3.5 Micron Optics Enlight Software

The last stage for the optical fiber experiment design is to use the correct settings in the Micron Optics Enlight Software. First, the Ethernet cord from the SM125 must be connected to a

computer. The following windows were important for the small set of temperature tests performed in the VT PF-4848: “Acquisition”, “Sensors”, “Chart”, and “Save”. The threshold (dBm), relative threshold (dB), width (nm), and width (dB) values can be altered manually and must be selected so that the peak detection of the optical sensor is clear. An image of the “Acquisitions” window and those settings for peak detection are given in Figure D.2.

The “Sensors” window is very important as well, allowing the user to identify the optical fibers that are being detected by the interrogator and thus creating the sensor criterion (based on manufacturing specifications) in the Enlight software for a given temperature probe or temperature sensor. Figure D.3 shows an image of this window, with the temperature probe hooked into the interrogator. The current wavelength of the probe is shown in the upper left of the window, with the current temperature appearing next to the sensor labeled “TempProbe2”.

The following two sensors were created in the Enlight software: “TempSens2” and “TempProbe2”.

The “TempSens2” utilized the “os4100-1555-1FC-1UT” Temperature Compensation Sensor, which had a nominal wavelength (λ_0) of 1555.2 nm at 25°C and accuracy of +/- 0.75 °C [75]. Figure D.4 shows an image of this sensor information in the Enlight software, with an adaptation of starting the temperature measurement closer to room temperature by adding the room temperature (T_r) value of 21°C to the Expression option, which contains Equation 21. Figure D.5 shows the similar Edit tab feature of the “TempProbe2” or “os4210-1528-1UT-S-SR” sensor with Equation 22 and values for all of the constants appear generating a near room temperature value for the os-4120 temperature probe. The accuracy of the temperature probe used is 0.2 °C and a λ_0 of 1528.038 nm was given for this probe [76]. The temperature probe and sensor can be used in one simple fiber strand if deemed necessary.

The “Charts” window allows the Enlight software operator to view up to four different outputs at one time. These could be all from one channel with four fibers connected in series or from various fibers on various channels. For purpose of substrate temperature measurements, only one optical sensor was used at a time only one set of data was monitored live when blasting substrates. Figure D.6 showed an image of the live temperature data. The “Save” window is important since it allows the software operator to select which sensor or sensors are to be recorded into a text file with an accuracy of data collected per second of any given test. Figure D.7 shows some of the options under the “Edit Sensors Data Saving” tab in the “Save” window. For all data

gathered for different temperature tests, the data time and amounts were unbound, continual acquisition occurred and the all FBG added into the Enlight program were selected based on using the temperature probe or temperature sensor for testing.

3.3.6 Sensor Attachment to Substrates

Two methods for substrate/sensor attachment were utilized for aluminum and stainless steel substrates. Initial testing occurred with obtained various data for an Al 3003 substrate with both a temperature sensor and strain gage attached via epoxy resin and epoxy hardener to the substrate. The temperature sensor “os4100-1559-1FC-1UT” or “TempSens1” and strain gage “os3120-1528-1FC-1yy” or “OptStrainGagePlusTemp1” are shown in Figure 3.10 after the epoxy mixture cured.



Figure 3.10 Epoxied temperature sensor and strain gage on Al 3003 substrate.

The temperature sensor is shown at the top of the substrate, with the strain gage appearing at the bottom. The purpose of this step was to adhere the sensor and strain gage to the substrate directly on the back side of the substrate to ensure data collection distortion from vibrations generated from blasting the substrates was reduced. A mixture ratio of 5:1 Epoxycure resin (20-8130-032) and Epoxycure Hardener (20-8132-008) was used to adhere the sensors to the back of an aluminum substrate. The epoxy needed to sit for roughly 6 hours to cure and ensure successfully adherence to one of the Al 3003 substrates. The aluminum substrate with the epoxied sensors was used for various small-scale tests in the cabinet used to show effects from number of adaptors used and heat generated from light sources in the blast cabinet.

The 304 stainless steel and thin stainless steel substrates had the “TempProbe2” sensor attached with a method of duct taping the sensor to each substrate whenever that substrate was to be blasted in the cabinet. Figure 3.11a shows the 304 stainless steel substrate with the duct taped temperature probe. Figure 3.11b shows where the stainless steel substrates were set upon prior to

blasting. Measurement artifacts can occur based on this attachment method due to heat being trapped by the duct tape, which would cause the wavelength to change, thus affecting temperature results and leading to measurement error. The goal was simply to see large substrate temperature changes, as well as negate artifacts that would arise from using epoxy on each substrate for instance.

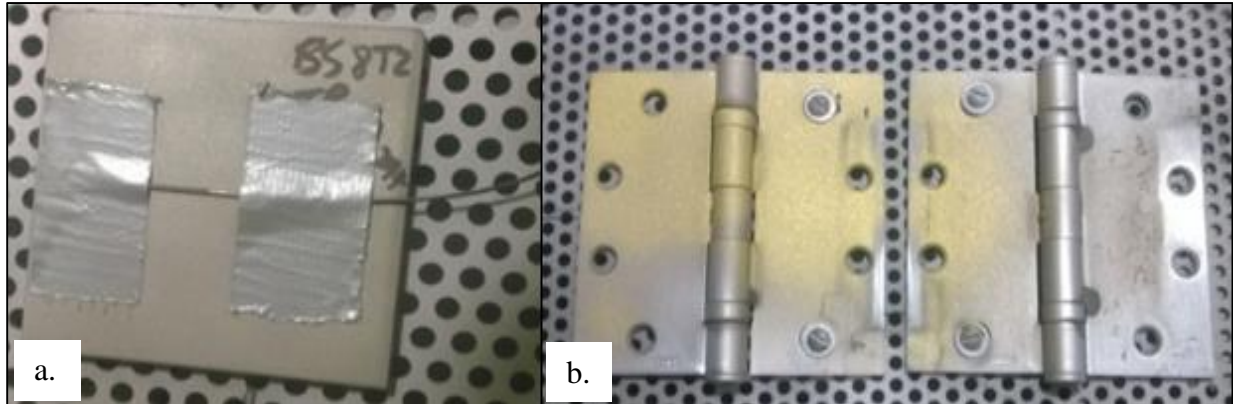


Figure 3.11 a. “TempProb2” attached to 304 SS substrate & b. blast platform pre-blasting.

A raised platform with a gap for the temperature probe fiber was used in the 304 stainless steel and thin stainless blasting, to ensure similar blast conditions and allow for cooling from air between each blast. Figure D.8 displays an image of the thin stainless steel substrate prior to blasting and appears in Appendix D. Figure 3.12a displays the layout of the 304 stainless for the temperature blasting effects at different parameters after blasting, during the substrate cool down phase. It should be noted that a strand of duct tape is required on the optical fiber portion under the substrate down the side of the protruding fiber to ensure no accidental blaster of the fiber. Figure 3.12b shows a similar layout of the thin stainless steel substrate for temperature blasting during the cool down phase as well.

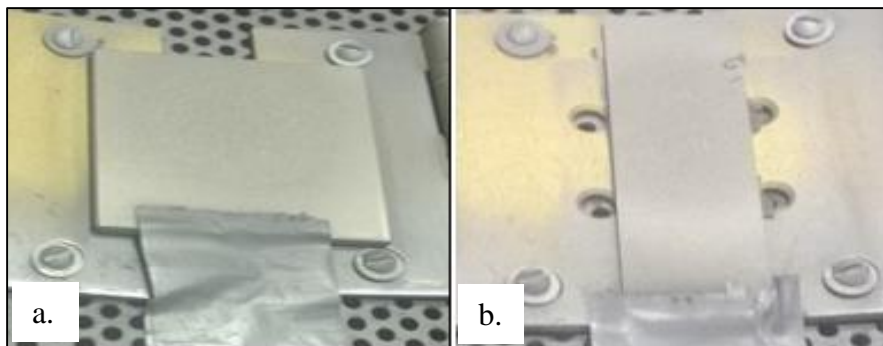


Figure 3.12 a. 304 SS & b. Thin SS substrates during experiments.

3.3.7 Temperature Blast Conditions

Similar to the blasting of the 304 stainless steel substrate for roughness measurements, a pre-determined set of experimental conditions was designed before experimentation. Table 3-7 displays the information for each of the 10 temperature experiments. Six experiments were performed on 304 SS substrates while 4 were performed on thin SS substrates. Three pressures, three distances, and two angles were used in these experiments, along with 5 blasting condition repetition per experiment and a constant blast time of 20 seconds per repetition.

Table 3-7 Experimental design sets for temperature testing.

Experiment #	Substrate	Pressure (psi)	Distance (in)	Angle (°)
1	SS 304	40	8	90
2	SS 304	40	6	90
3	SS 304	40	6	45
4	SS 304	40	4	90
5	SS Thin	40	8	90
6	SS Thin	40	6	90
7	SS Thin	40	6	90
8	SS Thin	60	6	90
9	SS 304	60	6	90
10	SS 304	50	6	90

A stopwatch program was used to record time data within a second accuracy, matching the Enlight software. For each set of tests shown in Table 3-7, one minute of data recording was followed by a 20 second blast of the substrate. The substrates were allowed to cool after this initial blast for two minutes, upon which the second blast repetition occurred. This was repeated 5 times for each experiment condition, to ensure mean calculations could be generated post blasting. With the use of the stopwatch and careful data recording, the start time of each blast was known and thus a set of 5 temperature curves and data was observed graphically in Microsoft Excel. It was then determined that a 35 second time frame included the temperature increase and cool down of each blast repetition

3.4 Statistical Analysis of Roughness and Temperature Data

F-tests and t-tests were performed on roughness and temperature data sets to validate differences in variances and significance of data means. Equations 23 and 24 show the null and alternative hypothesis used for both sets of tests.

$$\text{Null:} \quad H_0: \mu_1 = \mu_2 \quad (23)$$

$$\text{Alternative:} \quad H_0: \mu_1 \neq \mu_2 \quad (24)$$

For roughness data, 10 R_a values were generated for each experiment set F_{calc} values were created based on Equation 25, where Var_A and Var_B are the variances for set A and set B.

$$F_{calc} = \frac{Var_A}{Var_B} \quad (25)$$

Next F_{crit} is selected from an F table, based on degrees of freedom for the roughness testing which was 18 and 8 degrees of freedom for temperature F-tests. Two conclusions are made from the F-test values, one assumption is that $F_{calc} < F_{crit}$, thus the variance of means is equal. The other assumption is that from $F_{calc} > F_{crit}$ meaning that variances are not equal. These assumptions are shown as Equations 23 and 24 above. All comparisons made were at CI of 95% or $\alpha = 0.05$. Under optimum process scenarios, low spread of data or low variance from the mean is expected. When variances are equal, 18 degrees of freedom for R_a comparisons and 8 degrees of freedom for temperature comparison are used in the t-test calculations. When variances are not equal from the F-test calculations, then different degrees of freedom are used in the t-tests, thus a different t_{crit} is compared to each t_{calc} value from two-tailed t-tests.

Two-tailed t-tests were performed to determine if the means of each data set comparison were significant. When $t_{calc} < t_{crit}$, with a $p_{calc} > 0.05$, then the means of each data set are not different, thus no difference in blasting conditions is seen for that specific comparison. Alternatively, when $p_{calc} < 0.05$ (high confidence) and $t_{calc} > t_{crit}$, then there is significance in two means from two difference blasting conditions for roughness and temperature testing. Equation 26 shows the t_{calc} value based on equal variances in data. \bar{X} is the mean value for a data set, n is the number of experiments in each set of data, and S is the standard deviation of each data set.

$$t_{calc} = \frac{\bar{x}_A - \bar{x}_B}{\sqrt{\left[\frac{(n_A - 1) \cdot S_A^2 + (n_B - 1) \cdot S_B^2}{(n_A + n_B - 2)} \right] \cdot \left[\frac{n_A + n_B}{n_A \cdot n_B} \right]}} \quad (26)$$

A sample F-test and t-test calculation are shown in Appendix E. The calculated F value (F_{calc}) was less than the table F value (F_{crit}), so variances were equal. When a two-tailed t-test was performed with this set of data, the assumption of equal variances was used, which gives a t_{crit} at 18 degrees of freedom. The $t_{calc} > t_{crit}$, so there was a significance in means is present, thus the blasting conditions affected the surface roughness parameter R_a for example.

4 Results and Discussion

4.1 Roughness Characterization Results

Surface roughness measurements occurred by using the SJ-210 Mechanical Profilometer, HIROX optical microscope, and UVA ROST. Table 4-1 contains data obtained from characterizing all 18 sets of blasting conditions with the SJ-210 mechanical profilometer. R_a , along with values for other roughness parameters were gathered through mechanical profilometry and average R_a , along with standard deviations for: measurements, average R_a , and process plus measurements.

Table 4-1 SJ-210 R_a results with three types of standard deviation.

Sample	Avg. R_a (μm)	σ_M	$\sigma_{\text{Avg.}R_a}$	σ_{P+M}
1	3.89	0.26	0.23	0.34
2	3.67	0.18	0.15	0.22
3	3.45	0.19	0.14	0.23
4	3.36	0.27	0.10	0.25
5	4.47	0.31	0.19	0.35
6	4.24	0.23	0.11	0.26
7	4.08	0.27	0.18	0.31
8	3.98	0.29	0.31	0.41
9	5.01	0.34	0.24	0.40
10	4.67	0.33	0.20	0.38
11	4.50	0.35	0.27	0.43
12	4.68	0.39	0.22	0.44
13	4.70	0.34	0.24	0.41
14	4.18	0.28	0.42	0.49
15	4.23	0.46	0.40	0.63
16	4.47	0.36	0.23	0.42
17	4.35	0.36	0.24	0.42
18	4.23	0.30	0.24	0.37

Average R_a varied from a minimum of 3.45 μm for Experiment #3 to a maximum of 5.01 μm for Experiment #9. Experiment #2 had the smallest σ_M and σ_{P+M} between samples blasted under the same condition, while Experiment #15 had the largest σ_M and #4 had the largest σ_{P+M} . Experiment #6 had the lowest $\sigma_{\text{Avg.}R_a}$ value, while Experiment #4 had the largest of these values. The reason #4 had large values of standard deviation was due to sample 4.05 being rougher from running out of media during blasting on the second pass.

Table 4-2 contains results of the HIROX data for substrate 2.10 and 3.10. The influence of magnification and focal distances are shown for average S_a and σ_M . Using a smaller focal distance, along with lower magnification led to smaller σ values. However, at higher magnification, a large focal distance led to larger σ values. Based on these HIROX characterization methods, the S_a results were more accurate for lower focal distances and lower magnification.

Table 4-2 Hirox measurements for S_a & σ calculations of samples 2.10 and 3.10.

Measurement	Sample	Magnification	Focal Distance	Avg. S_a	σ_M
A.	2.10	350X	2m	3.858	0.240
B.	2.10	350X	4m	3.854	0.248
C.	2.10	700X	4m	4.189	0.395
D.	2.10	700X	2m	4.180	0.403
E.	3.10	350X	2m	3.377	0.221
F.	3.10	350X	4m	3.368	0.227
G.	3.10	700X	4m	4.133	0.340
H.	3.10	700X	2m	4.144	0.338

The last characterization utilized for roughness characterization was the optical profilometry method via the UVA ROST. Only samples from four different blasting conditions were measured and the results of average S_a and σ_M are shown below in Table 4-3. According to this set of data, sample 2.10 had the largest S_a value 4.46 μm and sample 4.06 had the lowest S_a value of 3.44 μm . Sample 3.09 had the smallest σ_M , while sample 4.08 had the largest σ_M .

Table 4-3 ROST Avg. S_a and measurement σ values.

Sample #	Avg. S_a	σ_M
1.03	4.358	0.508
2.05	4.062	0.488
2.06	3.860	0.524
2.07	4.422	0.254
2.08	4.300	0.264
2.09	4.236	0.412
2.10	4.458	0.422
3.08	3.827	0.338
3.07	3.894	0.540
3.09	3.827	0.248
3.10	3.863	0.450
4.06	3.442	0.662
4.07	3.602	0.460
4.08	3.534	0.729
4.09	3.824	0.411

4.10	4.173	0.702
------	-------	-------

Table 4-4 contains results from the three characterization techniques used to obtain average roughness parameters R_a and S_a . It can be noted that for each sample set (blasting condition), the SJ-210 took ten measurements per substrate, for ten substrates. The UVA ROST used ten measurements per blasting condition, however only a few of the samples from each of the four blasting conditions were tested, thus standard deviation values were high. The HIROX microscope was utilized to calculate R_a for only two substrates. The Hirox measurement σ values were lower due to the measurement accuracy from fifteen measurements taken per substrate. Based on the low σ values, relative quickness of data collection, and device availability, the SJ-210 mechanical profilometer was utilized as the main roughness characterization device in the following sections.

Table 4-4 Comparison of R_a and σ_M for characterization techniques.

Sample Set	Mitutoyo SJ210 Profilometer		UVA ROST		UVA Hirox	
	R_a (μm)	σ_M	R_a (μm)	σ_M	R_a (μm)	σ_M
1	3.89	0.26	4.358	0.508	-	-
2	3.67	0.18	4.223	0.394	3.854	0.240
3	3.45	0.19	3.853	0.394	3.377	0.221
4	3.36	0.27	3.798	0.593	-	-

4.2 Effect of Process Parameters on Surface Roughness

As shown in Table 3-4, the surface roughness experiments differed based upon blast height, blast pressure, nozzle type, blasting operator, and blasting on different days under the same conditions. With the use of JMP statistical analysis software, data was gathered from the various 18 blasting conditions to generate Figure 4.1. Figure 4.1 showed that a shorter blast distance 4'' led to rougher surface than the higher blast distance of 6''. These results were statistically compared with 95% confidence under an F-test, which showed that the variance of each set of data were equal. Once the F value was calculated, a two-tailed t-test was performed with an alternative hypothesis that distance changes would affect roughness values. A t_{calc} value of 2.52, with probability ($p_{\text{calc}} = 0.022 < p_{\text{crit}} = 0.05$) was larger than t_{crit} of 2.10 with the calculation of degrees of freedom = 18. With the t-test results under 95% confidence, it is proven that a shorter blast distance (4'') lead to a rougher surface than larger distance (6'') by 0.22 μm , as R_a changed from 3.89 $\mu\text{m} \pm 0.07 \mu\text{m}$ to 3.67 $\mu\text{m} \pm 0.05 \mu\text{m}$. Appendix F contains results from Microsoft Excel

for these F-tests and t-tests under these blasting conditions, as well as all other statistical results for roughness data.

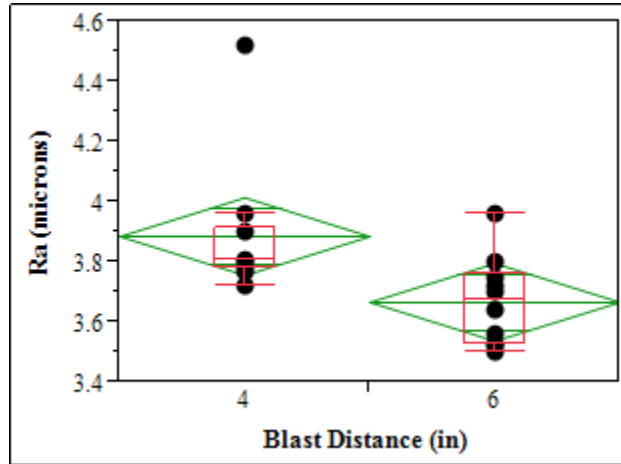


Figure 4.1 Blast distances effects on Ra for 4” and 6” blasting.

A similar comparison was made between blast distances of 6” and 8” to show the same effect on surface roughness and is shown in Figure 4.2. The F value was calculated to be 1.15, which was smaller than F_{crit} of 3.18 with p_{crit} being $0.42 > 0.05$, thus the variances of the means were equal. Next a two-tailed t-test was performed with the same alternative hypothesis that a distance change would affect surface roughness values. The t_{calc} value was calculated as 3.49, while t_{crit} is 2.10 and p_{calc} is 0.0026. With 95% confidence, blasting at 6” led to a higher Ra than 8” blasting by a difference of $0.22 \mu\text{m}$ from $3.67 \mu\text{m} \pm 0.05 \mu\text{m}$ to $3.45 \mu\text{m} \pm 0.04 \mu\text{m}$.

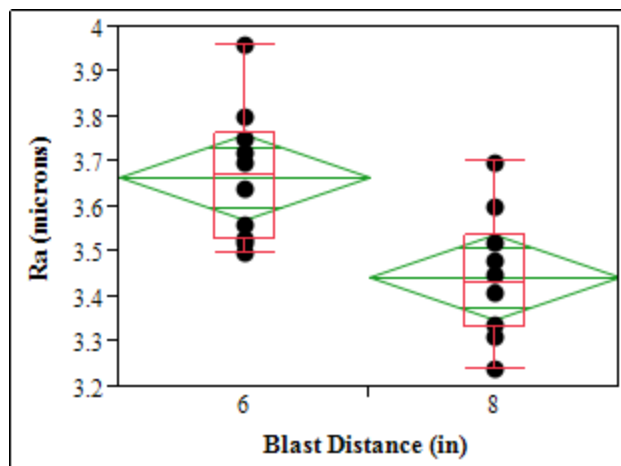


Figure 4.2 Blast distance effects on Ra for 6” and 8” blasting.

When blasting stainless steel substrates with alumina grit, an increase in surface roughness with increasing blasting pressure is expected, according to studies of other research groups [23].

Figure 4.3 suggests the opposite trend, so this comparison between 42 psi and 60 blasting was then compared with F-test and t-test to see if lower pressure actually lead to rougher surfaces than higher pressure. $F_{\text{calc}} = 1.39$ and $p_{\text{calc}} = 0.32$ led to the use of a two-tailed t-test with the assumption of equal variances between means. The two-tailed t-test gave $t_{\text{calc}} = 3.42$, with $p_{\text{calc}} = 0.0031$, thus with 95% confidence, it was proved that blasting at 42 psi led a rougher surface by $0.33 \mu\text{m}$ difference from 60 psi blasting or change from $5.01 \mu\text{m} \pm 0.08 \mu\text{m}$ to $4.68 \mu\text{m} \pm 0.06 \mu\text{m}$.

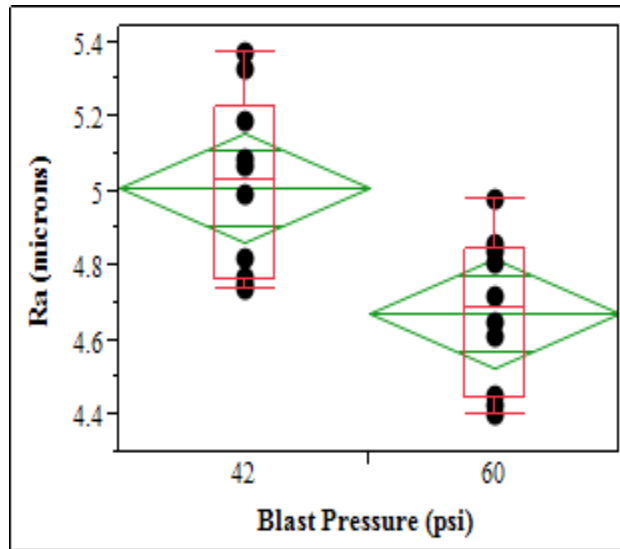


Figure 4.3 Blast pressure effect on Ra for 42 psi and 60 psi blasting.

The nozzle type, whether 3/16" Venturi or 5/16" straight was expected to affect the surface roughness differently. Based on nozzles of the same throat dimensions, it is assumed that Venturi nozzles would create higher roughness values than straight nozzles. Figure 4.4 displays the effects of 5/16" straight nozzle and the 3/16" Venturi nozzle of surface roughness, with the use of as received media. First an F-test was performed to once again see if the variances between means for the 5/16" straight and 3/16" Venturi nozzles were actually different. $F_{\text{calc}} = 4.7 > F_{\text{crit}} = 3.18$, with $p_{\text{calc}} = 0.015$, thus the null hypothesis of the variances being equal was false. Next a two-tail t test was performed with the assumption of unequal variances. The $t_{\text{calc}} = 0.072$, with $p_{\text{calc}} = 0.94$, so with 95% confidence the null hypothesis of the 5/16" straight nozzle creating a higher roughness than 3/16" Venturi by $0.01 \mu\text{m}$ was rejected. The reason for the higher surface roughness is due to the larger diameter throat of the 5/16" straight nozzle when compared to the 3/16" Venturi nozzle.

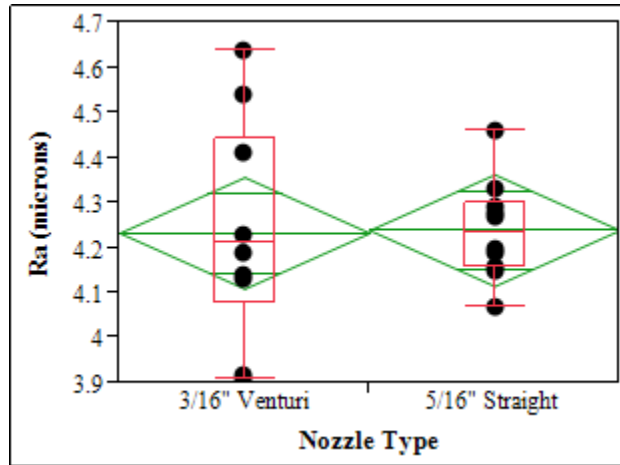


Figure 4.4 Nozzle type effect on Ra.

As mentioned previously, pulsating media or irregular media flow would lead to a difference in surface roughness modifications. As Figure 4.5 denotes, experiments performed with pulsating media flow created a lower surface roughness when compared to blasting where pulsation did not occur. The $F_{\text{calc}} = 2.64$ with $p_{\text{calc}} = 0.082$, thus it was determined the variances of means for non-pulsating and pulsating media flows were not equal. For the two-tailed t-test, $t_{\text{calc}} = 6.38$ with $p_{\text{calc}} = 5.3 \times 10^{-6}$, thus with 95% confidence it was concluded that pulsation will decrease the roughening effect of blasting by $0.56 \mu\text{m}$, going from $4.23 \mu\text{m} \pm 0.08 \mu\text{m}$ to $3.67 \mu\text{m} \pm 0.05 \mu\text{m}$.

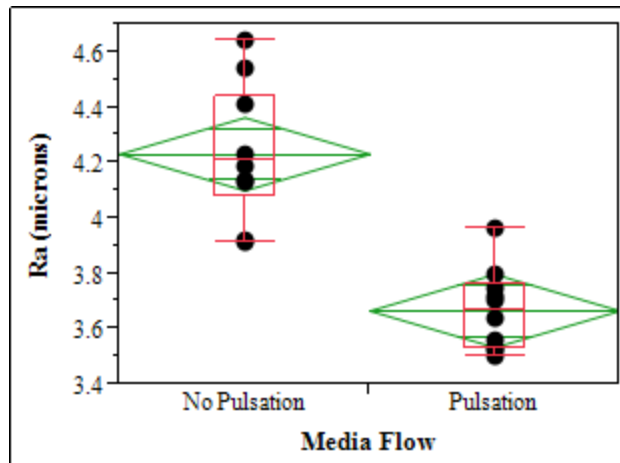


Figure 4.5 Media flow effect on Ra.

The effect of media break done or recycled media (age) is shown in Figure 4.6. An F-test of the data proved that variances were equal since $F_{\text{calc}} = 1.01$, with $p_{\text{calc}} = 0.49$. The alternative hypothesis was that broken down media would lead to a smoother surface than newer media.

However, due to $t_{\text{calc}} = 4.31$ and $p_{\text{calc}} = 4.18 \times 10^{-4}$, with 95% confidence the old media (smaller media) led to rougher surfaces than newer (larger) media by $0.47 \mu\text{m}$ as R_a increased from $4.23 \mu\text{m} \pm 0.08 \mu\text{m}$ to $4.70 \pm 0.08 \mu\text{m}$. The new media generated lower surface roughness values since the media velocity was lower and the blast pattern was less dense, but had larger particles eroding the substrate surface.

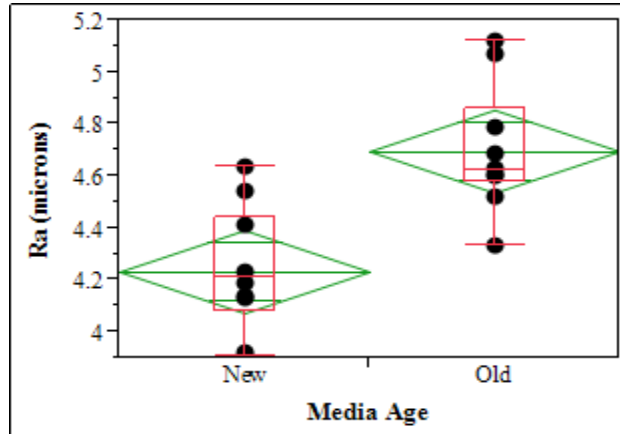


Figure 4.6 Media Recycling effect on Ra.

4.3 Repeatability and Reproducibility

Three areas that were investigated along with process parameter variation, were the use of two different cabinets, two blast operators, and one blast operator blasting under same conditions at different times. Figure 4.7 shows the Ra differences when blasting under the same conditions, with blasting occurring almost one week apart between “Day A” and “Day B”.

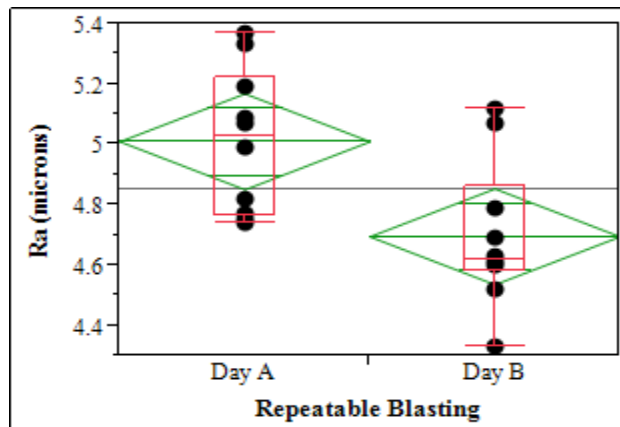


Figure 4.7 Repeatability of same blast conditions.

An F-test was performed, which gave $F_{\text{calc}} = 1.03$ at $p_{\text{calc}} = 0.049$, so the variance between means of “Day A” and “Day B” were equal. A two-tailed test was performed next since there was

no expected or hypothesized difference for blasting under the same conditions on different days. The $t_{\text{calc}} = 2.94$ at $p_{\text{calc}} = 0.0087$, thus it was shown with 95% confidence since the two-tailed $t_{\text{crit}} = 2.10$ ($df = 18$) that blasting under the same conditions on different days does effect surface roughness. There was a difference in R_a mean values (significance) due to shorter blast times on average from Day A to Day B and low R_a for one substrate on Day B, however there was no variance between the data sets.

Another area investigated was the difference in surface roughness from using two different blast cabinets: CCAM 3642 and VT 4848. Figure 4.8 shows the differences in R_a for the two different cabinets. The F-test gave $F_{\text{calc}} = 1.07$ with $p_{\text{calc}} = 0.46$, thus the variances of cabinet mean R_a values were equal. Another two-tailed t-test was performed with the null hypothesis that the different cabinets would not affect R_a . At 95% confidence, the $t_{\text{calc}} = 4.34$ and $p_{\text{calc}} = 3.98 \times 10^{-4}$, the null hypothesis was rejected. An increase in R_a of $0.46 \mu\text{m}$ was shown when switching from the CCAM cabinet to the VT cabinet as roughness increased from $3.89 \mu\text{m} \pm 0.07 \mu\text{m}$ to $4.35 \mu\text{m} \pm 0.08 \mu\text{m}$.

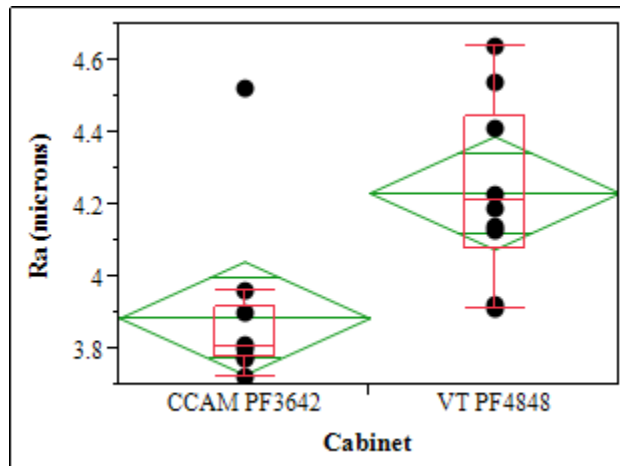


Figure 4.8 Cabinet type effect on R_a .

The last area of process variation occur when using two different operators to blast under the same conditions. Figure 4.9 contains R_a values gathered from two blast cabinet operators from the VT cabinet. The F-test gave $F_{\text{calc}} = 1.15$ with $p_{\text{calc}} = 0.42$, thus the variances between operator mean R_a were equal. The two tailed t-test was performed next, with the null hypothesis that the mean R_a values for different operators would be the same. At 95% confidence, $t_{\text{calc}} = 1.98$ with $p_{\text{calc}} = 0.064$, there was no statistical difference in the means of “Operator A” (novice) and “Operator B” (experienced).

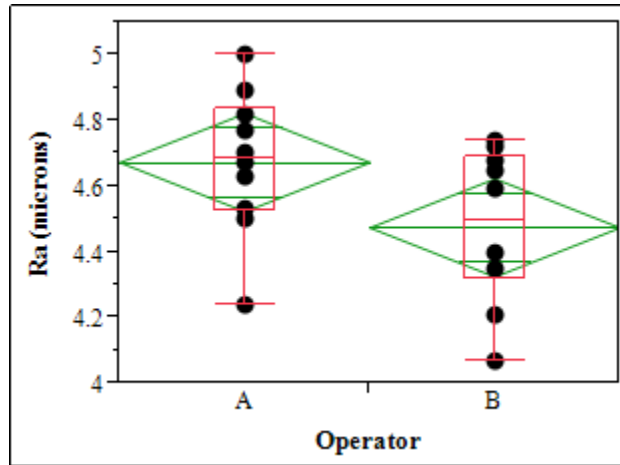


Figure 4.9 Operator effect on Ra.

Visual inspection showed distinct differences in surface texture between experienced and novice operators. This detectable difference is shown below in Figure 4.10 with a comparison of good (experienced operator) blasting coverage and bad (novice operator) blasting coverage. The novice blaster created blast lines on the surface, whereas the experienced operator generated more even coverage of the substrate.

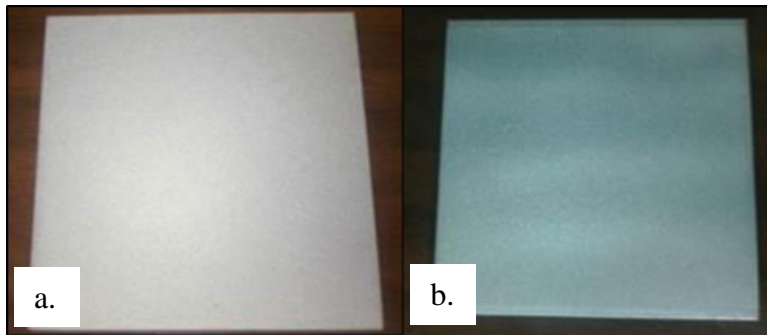


Figure 4.10 a. Good coverage & b. bad coverage.

4.4 Temperature Sensor Measurements

Some small-scale experiments were performed prior to the blasting of the stainless steel substrates with the attached temperature probe. One of these experiments showed the effect of adding additional adaptors to the fiber strand connected between the “TempSens1” on an aluminum substrate and the SM125 Interrogator. For this experiment, no blasting occurred, the cabinet doors were shut and the dust collection system was on. Figure 4.11 shows that when adding additional adaptors, an increase in temperature reading occurred with the addition of each adaptor, suggesting that signal loss would for this system show an increase in substrate temperature without

blasting occurring. There was clear distinction in the temperature readings as well, with no overlapping temperatures.

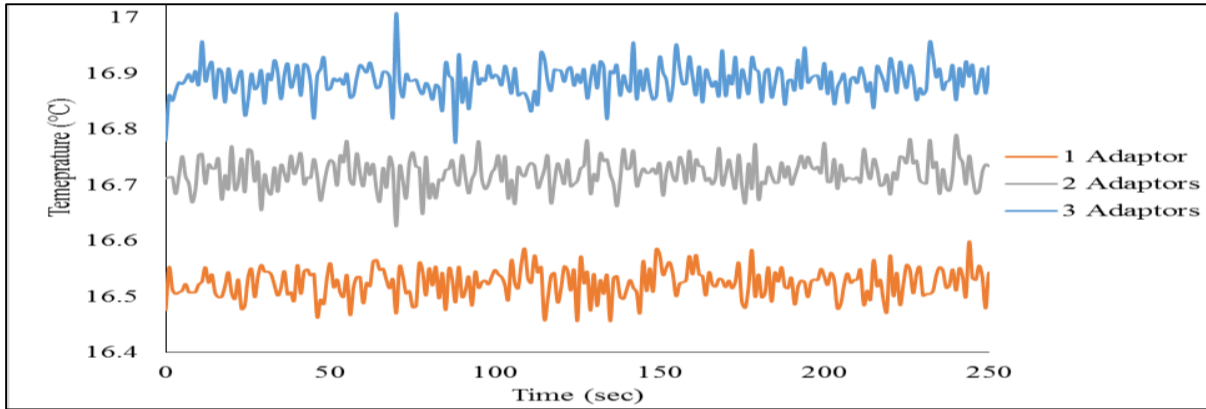


Figure 4.11 Adaptor effect on substrate temperature.

Another set of experiments performed prior to any blasting of the SS substrates monitoring the temperature of an aluminum substrate with different light sources. Another clear distinction was noticed when having the light source, either Halogen or LED turned on for three hours with no blasting occurring using the temperature sensor on the Al substrate to monitor substrate temperature as shown in Figure 4.12. The Halogen light showed an increase in temperature from 17°C to 30°C, over the three hour span. The halogen light was replaced with the LED light and the temperature change of the same substrate only saw an increase around 0.5 °C. For the purposes of understanding temperature in the blast cabinet and the substrate temperature, the LED light source was used to help eliminate any external temperature effects.

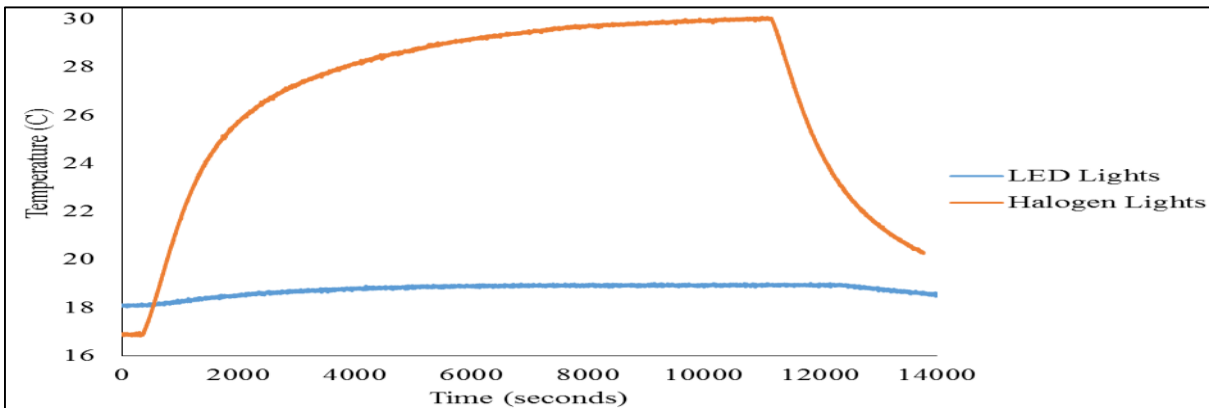


Figure 4.12 LED and halogen effect on substrate temperature.

The last set of experiments performed with temperature sensor were on five different stainless steel substrates to show the effect of temperature change from changing the blast distance

of each experiment. The experiments were performed in this order for the following distances: 8", 2", 6", 4" and 10" and mean data is shown in Figure 4.13.

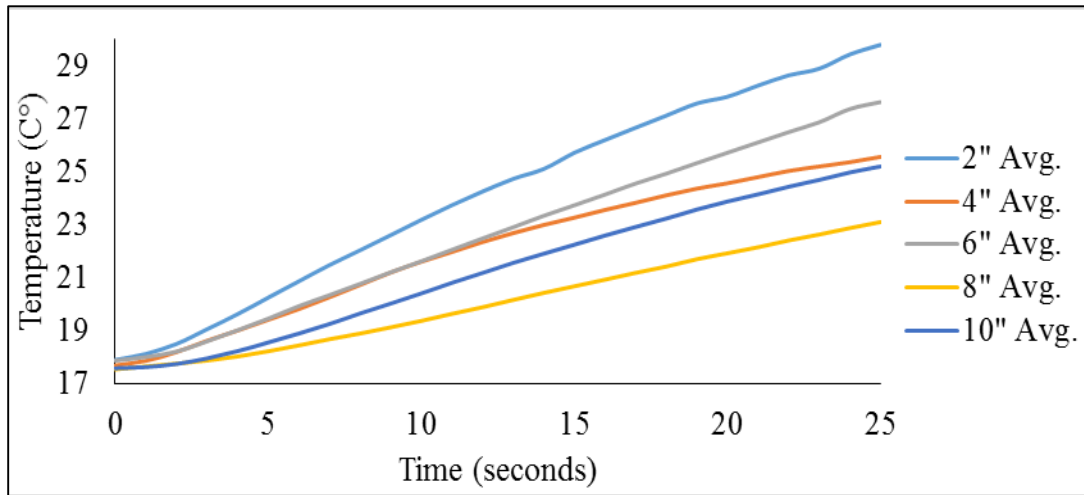


Figure 4.13 Blast height effect on substrate temperature with "TempSens2".

The first three tests showed as to be expected, decreasing the blast height would lead to higher temperature. The last two experiments with blast height of 4" and 10" did not follow this trend. The temperature changes are scattered, but the use of additional duct tape and media age were the reasons for the differences in the expected and unexpected results shown in Figure 4.7. With these results, it was decided that the temperature probe might give more valid temperature readings, as well as a higher accuracy when using the probe.

4.5 Temperature Probe Measurements

For this set of experiments, a total of 10 different blast conditions were utilized to show differences in effects of blasting pressure, angle, distance, and substrate shape. Each set of experiment was performed at least 5 times, so average data could be gathered from each individual experiment. Figure 4.14 shows an example of raw blasting data after the start of each blast time was zeroed out using the timestamps from the Enlight Software and the stopwatch data for Experiment #1.

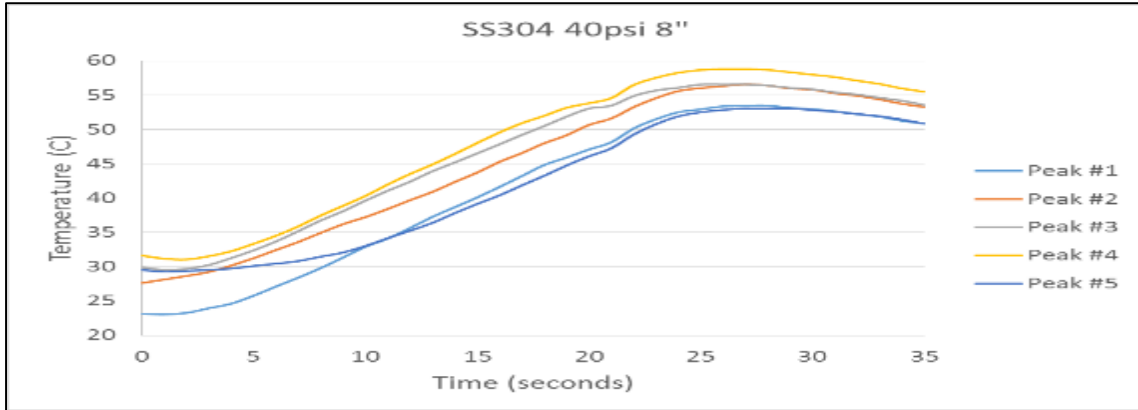


Figure 4.14 Experiment #1 data.

In order to compare data from these experiments, the data had to be zeroed out by subtracting the initial temperature value from each repetition curve of each experiment. Figure 4.15 contains a graphical representation of “zeroed” data from experiment #1. Once the data was zeroed, average curves of each experiment could be obtained for comparison of effects of blast angle, pressure, distance, and substrate type.

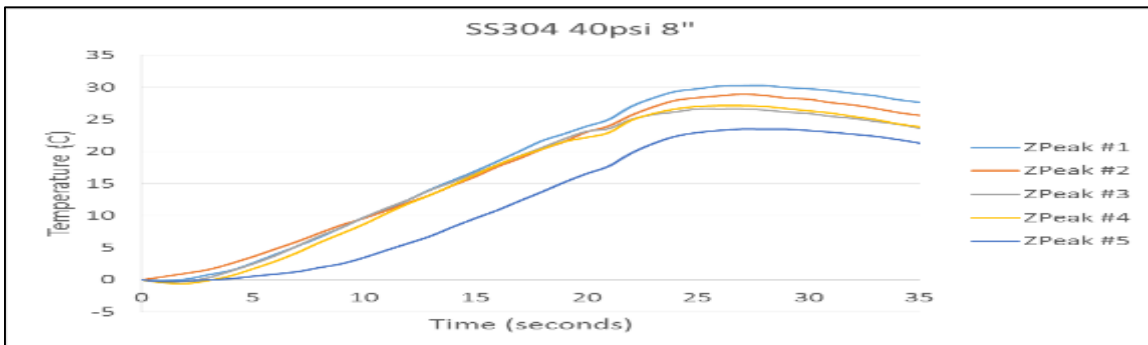


Figure 4.15 Zeroed temperature experiment #1 data.

Table 4-5 shows results of the “TempProb2” measurements on the 304 stainless steel substrates. One row contains the average of five temperature changes that occurred from blasting condition after 20 seconds of blasting had occurred, while the last two rows display the standard deviation and error of those values. Based on this table, the lowest temperature change occurred from blasting condition #3 (40 psi, 6” distance, and 45° angle) and the highest temperature change occurred at blasting condition #9 (60 psi and 6” distance). Experiments from Table 4-5 show that as blast distance decreases, substrate temperature from blasting saw a larger temperature increase. Higher blast pressures lead to higher temperature increases in 304 stainless steel substrates and angled blasting reduced the temperature increase of the substrates.

Table 4-5 304 Stainless steel substrate temperature results.

Experiment #	1	2	3	4	9	10
Pressure (psi)	40	40	40	40	60	50
Distance (inch)	8	6	6	4	6	6
Angle (°)	90	90	45	90	90	90
T (°C) at 20 sec	21.7	19.9	8.3	29.1	45.1	35.2
σ	3.0	3.5	0.9	4.1	4.9	2.6
Error	1.3	1.6	0.4	1.8	2.2	1.1

In order to justify these results, F-tests and t-tests were performed for validation. Appendix G contains the calculations for these tests for the blasting condition comparison of 4" and 6" distance blasting 304 SS for temperature effect differences. For this comparison, F_{crit} was found from the F table to be 6.39 and F_{calc} was 1.34 at $p_{calc} = 0.39$, so the variance of the means were equal. Performing a two-tailed t-test gave $t_{calc} = 3.79$ at $p_{calc} = 0.005$ when $t_{crit} = 2.31$, so at 95% CI a substrate ΔT occurred when blast distance changed from 6" to 4". For this case, $\Delta T = +9.2$ °C from the 6" T of 19.9 °C ± 1.6 °C to the 4" T of 29.1 °C ± 1.8 °C. Another distance test occurred when changing the blasting distance from 6" to 8", with an $F_{calc} = 1.40$ at $p_{calc} = 0.38$, so a two-tailed t-test was performed with an equal mean variances assumption. The t_{calc} was 0.89 and $p_{calc} = 0.41$, so with 95% confidence no distinction can be made between the 6" blasting and 8" blasting effects on 304 SS ΔT . F test and t test values are in Appendix G as well, Figure 4.16 shows a graphical representation of the temperature changes in 304 SS from different blast distances.

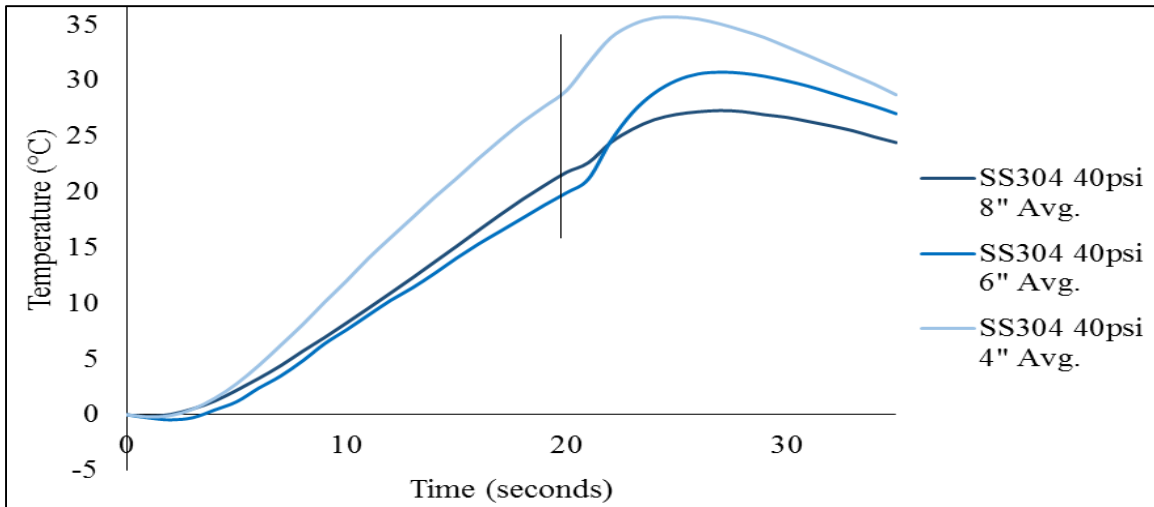


Figure 4.16 Blast distance effects on 304 SS temperature changes.

When comparing the pressure changes from 40 psi to 50 psi, $F_{\text{calc}} = 1.90$ and $p_{\text{calc}} = 0.27$, so variances were equal and thus a two-tailed t-test was performed assuming equal variances. The t_{calc} was 7.79 at $p_{\text{calc}} = 5.3 \times 10^{-5}$, so with 95% confidence $+\Delta T$ of 15.3 °C occurred when going from the lower pressure (40psi) $T = 19.9 \text{ °C} \pm 1.6 \text{ °C}$ to medium pressure (50 psi) $T = 35.2 \text{ °C} \pm 1.1 \text{ °C}$. Next a comparison of 50 psi and 60 psi blasting occurred, giving $F_{\text{calc}} = 3.60$ at $p_{\text{calc}} = 0.12$, so another assumption of equal variances was made when performing a two-tailed t-test. The $t_{\text{calc}} = 4.03$ with $p_{\text{calc}} = 0.0038$, so at 95% confidence, increasing the blasting pressure of 50 psi to 60 psi led to an 304 SS $+\Delta T$ of 9.9 °C from $T = 35.2 \text{ °C} \pm 1.1 \text{ °C}$ to $T = 45.1 \text{ °C} \pm 2.2 \text{ °C}$. Figure 4.17 displayed these effects of blasting pressures on 304 SS temperature. Higher pressures lead to higher particle impact speeds, thus more heat is generated with increasing pressure.

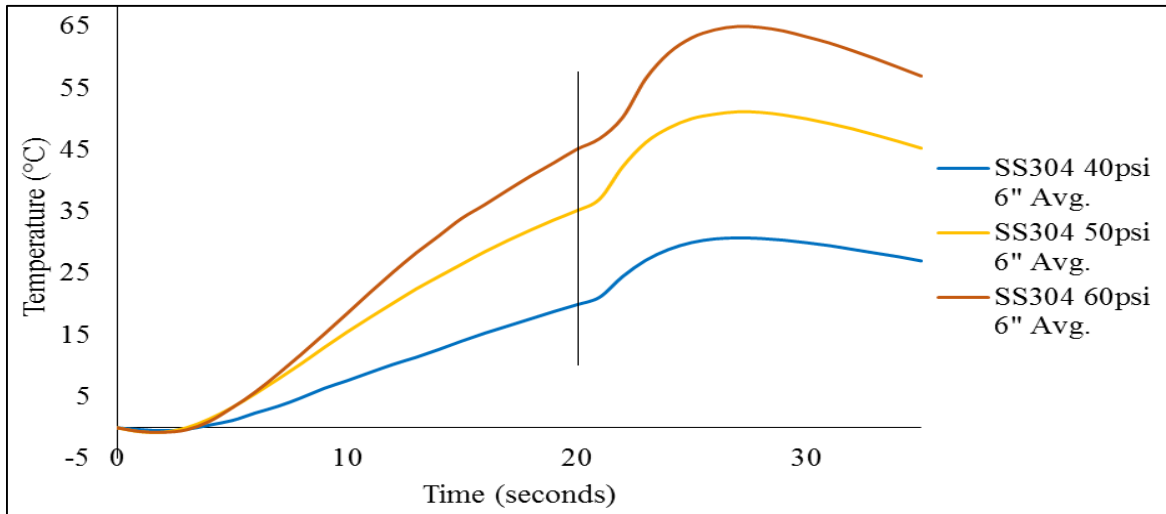


Figure 4.17 Pressure effect on 304 SS temperature.

The last set of temperature testing for 304 stainless steel substrates was changing the blast angle from 90° to 45°. An F-test was performed for variances, giving F_{calc} of 14.01 and $p_{\text{calc}} = 0.013$, so unequal variances were present between data means. The t_{calc} value of 7.09 and $p_{\text{calc}} 8.7 \times 10^{-4}$ under 95% confidence validated the significance in means through a two-tailed t-test with t_{crit} being 2.57 (degrees of freedom = 5). A $-\Delta T = 11.6 \text{ °C}$ was seen from the $19.92 \text{ °C} \pm 1.6 \text{ °C}$ for 90° blasting to $8.3 \text{ °C} \pm 0.4 \text{ °C}$ for 45° blasting. These results are shown graphically in Figure 4.18 for 20 seconds of blasting, showing that a lower angle leads to a lower increase in temperature. As the blast angle gets shallower, the blast pattern will get larger, leading to a lower temperature change in substrate temperature.

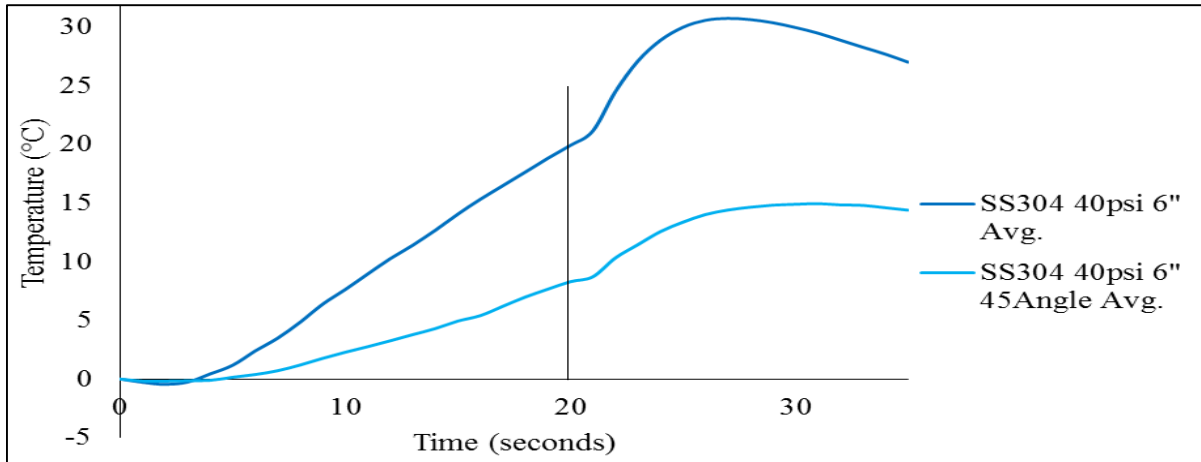


Figure 4.18 Angle effect on 304 SS temperature.

The thin stainless steel substrates were subjected to tests of blast distance, pressure, and angle effects as well. Table 4-6 shows temperature data for thin stainless steel substrates. Based on this data, the blast distance showed the same trend as the 304 SS of decreasing distance leading to a larger temperature change in thin SS substrate temperature. The values of experiments #6, #7, and #8 were very close in value, thus more F-tests and t-tests were performed.

Table 4-6 Thin stainless steel substrate temperature results.

Experiment #	5	6	7	8
Pressure (psi)	40	40	40	60
Distance (inch)	8	6	6	6
Angle (°)	90	90	45	90
T (°C) at 20 sec	14.3	24.1	23.5	24.9
σ	1.7	4.5	2.4	5.1
Error	0.8	2.0	1.1	2.3

Distances of 6\"/>

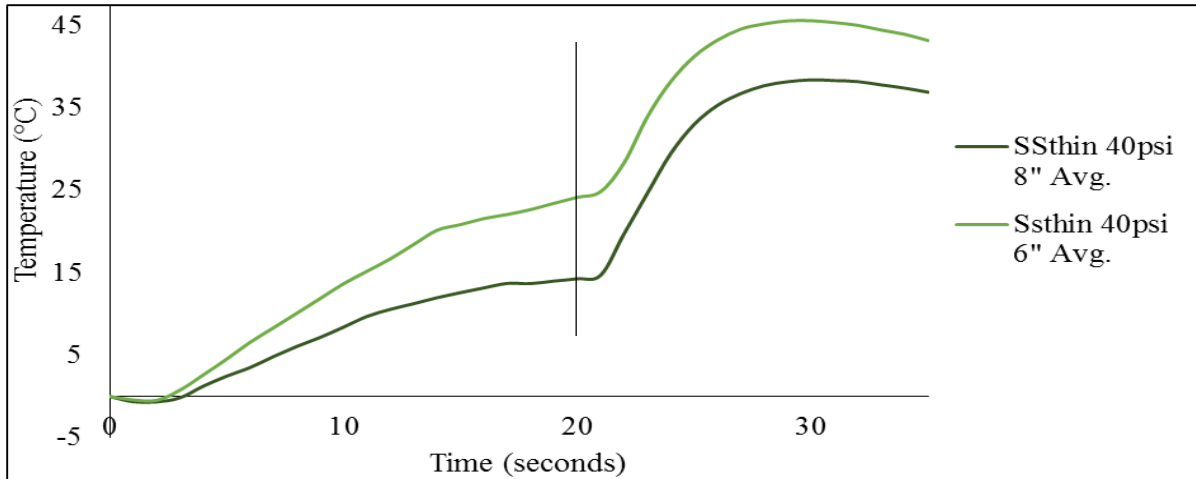


Figure 4.19 Blast distance effect on thin SS temperature.

Next the pressure effects on thin stainless steel substrates from blasting were analyzed and the results are shown in Figure 4.20. An F-test was performed between the T means for 40 psi and 60 psi data sets, giving $F_{\text{calc}} = 1.26$ and $p_{\text{calc}} = 0.41$, so equal variances were present. The alternative hypothesis through a two-tailed t-test was that different pressures would lead to different ΔT for thin SS when blasting, however due to t_{calc} being 0.26 and $p_{\text{calc}} = 0.80$ no distinction could be made at 95% confidence for this blast condition.

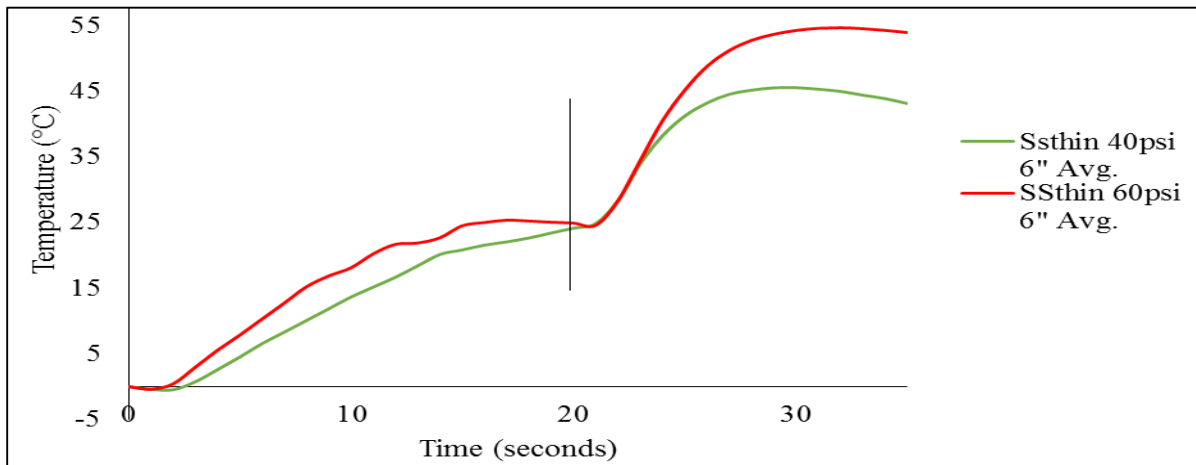


Figure 4.20 Blast pressure effect on thin SS temperature.

The last set of comparisons made for thin SS was changing the blast angle from 90° to 45° . Performing an F-test gave $F_{\text{calc}} = 3.65$ and $p_{\text{calc}} = 0.12$, so a two-tailed t test was performed assuming equal variances. The t_{calc} was 0.27 and $p_{\text{calc}} = 0.79$, so no distinction could be made between the angled and perpendicular blasting of the thin SS with 95% confidence. Figure 4.21 shows the graphical representation of the angle effect on temperature changes in thin SS substrates.

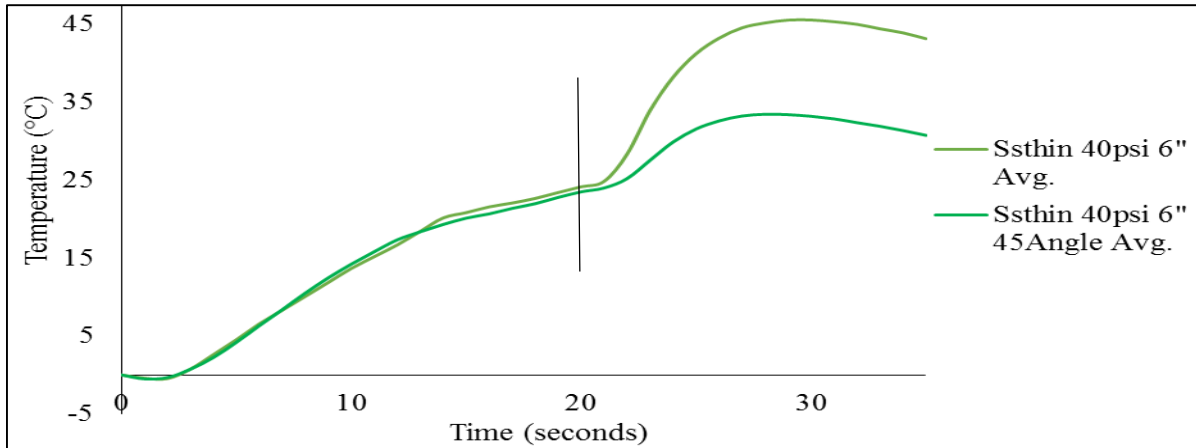


Figure 4.21 Blast angle effect on thin SS temperature.

The last set of comparisons to be validated through F-tests and t-tests were by comparing data from the 304 SS and thin SS blasting at the same conditions to view the importance of substrate thickness/shape. At 6" blast distance the F_{calc} was 1.63 and p_{calc} was 0.32, so equal variances were present between means of 304 SS and thin SS substrates. The t_{calc} was 1.64 and $p_{\text{calc}} = 0.14$, so no distinction could be made between substrate effect on temperature change at 6" blasting with 95% confidence. At 8" blast distance the F_{calc} was 3.18 and $p_{\text{calc}} = 0.15$, so variances were present again for the two-tailed t-test. The t_{calc} was 4.85 and p_{calc} was 0.0013, so with 95% confidence a substrate effect was detectable at 8" blasting. For this case, $+\Delta T$ of 7.4 °C occurred when going from a thin SS $T = 14.3 \text{ °C} \pm 0.8 \text{ °C}$ to thick SS $T = 21.7 \text{ °C} \pm 1.3 \text{ °C}$.

Blasting at 60 psi pressure and blasting at the 45° angle were compared between 304 SS and thin SS substrate temperature changes as well. For the 60 psi blasting condition, the F_{calc} was 1.09 and p_{calc} was 0.47, so a two-tailed t-test was performed assuming equal variances of means between 304 SS and thin SS data sets. The t_{calc} was 6.41 and $p_{\text{calc}} = 2.1 \times 10^{-4}$, so $+\Delta T$ was seen with 95% confidence. For this scenario $\Delta T = 20.2 \text{ °C}$ from the thin SS $T = 24.9 \text{ °C} \pm 2.3 \text{ °C}$ to thick SS $T = 45.1 \text{ °C} \pm 2.2 \text{ °C}$. The angled blasting F_{calc} was 6.27 and p_{calc} was 0.052, so variances were equal for the two-tailed t-test. The t_{calc} was 13.35 and p_{calc} was 9.5×10^{-7} , so with 95% confidence ΔT between substrate type/shape occurred at 45° blasting. That temperature $-\Delta T = 15.2 \text{ °C}$ from the thin SS $T = 8.3 \text{ °C} \pm 1.1 \text{ °C}$ to 304 SS $T = 23.5 \text{ °C} \pm 0.4 \text{ °C}$.

5 Conclusions

Blasting process parameters affect the surface roughness generated and the amount of temperature change in the substrate. Based on the surface roughness experiments, conclusions could be made based on: blast distance, pressure, angle, time, recycled media, media pulsation, nozzle type, operator experience, blast date, and blast cabinets. The results of the experiments proved that decreasing the blast distance led to higher surface roughness values due to the smaller blast pattern generated when being closer to the substrate with the blast nozzle. With 95% confidence, $\Delta R_a = 0.22 \mu\text{m}$ when going from 6" to 4" distances and a $\Delta R_a = + 0.22 \mu\text{m}$ when going from 8" to 6" distances. SJ-210 measurements proved that $\Delta R_a = -0.33 \mu\text{m}$ from 42 psi to 60 psi blast pressures. Blast angle was shown to have numerous effects on the substrate roughness. Generally, a decrease in the blast angle lead to a more erosive effect on the stainless steel substrate surface. Blast time can lead to an over blasting effect after a certain optimum blast time (maximum roughness was obtained). Based on these individual parameters, a combination of a shorter distance and lower blast pressure would generate the highest R_a values.

The type of nozzle will create differences in surface roughness when the inner throat diameter of the straight nozzle and Venturi nozzles are the same. When the throat sizes are the same, the Venturi nozzle would lead to a wider spread blast pattern and an increase in roughness would occur due to higher media velocities. However, a 3/16" Venturi and 5/16" straight nozzle were used in experiments, thus the throat sizes were not the same. At 95% confidence, the straight nozzle and Venturi nozzle created no significant difference in means. Media pulsation created an issue with surface roughness and it was shown through experiments that pulsating media led to a lower surface roughness change than non-pulsating or regular media flow rates by $\Delta R_a = -0.56 \mu\text{m}$. Recycled media through experimentation over different blast cycles under the same blasting conditions proved to lead to lower R_a values due to smaller particles creating a denser blast pattern by $0.47 \mu\text{m}$.

The same operator blasting under same conditions was investigated, showing that ΔR_a decreased in later experiments due to shorter average blast times and one substrate with low R_a , and equal variances were present. Using different cabinets under the same blast conditions generated ΔR_a , with the CCAM PF-3642 creating slightly smoother surfaces than the substrates

blasted with the VT PF-4848 $\Delta R_a = 0.46 \mu\text{m}$. Blasting with two different operators did not significantly affect ΔR_a .

Various tests occurred through changing the process parameters of blasting 304 SS and thin SS substrates for investigation of substrate ΔT from blasting. With 95% confidence, changing the blast distance from 6" to 4" led to a substrate $\Delta T = +9.2 \text{ }^\circ\text{C}$ for 304 SS substrates due to the blast pattern being more concentrated near the temperature probe. No statistical distinction could be made when blasting between 6" and 8". When blasting at different pressures, positive ΔT occurred with increasing pressure. When going from 40 psi to 50 psi, the $\Delta T = +15.3 \text{ }^\circ\text{C}$ and $\Delta T = +9.9 \text{ }^\circ\text{C}$ when pressure changed from 50 psi to 60 psi on 304 SS substrates due to higher impact velocities of grit particles. The blast angle affected the substrate temperature proportionally, when the lower blast angle to 45° was utilized $\Delta T = -11.6 \text{ }^\circ\text{C}$ from 90° blast angle. This effect can be attributed to the larger blast pattern generated at lower angles. Having a perpendicular blast angle, with higher pressure and low blast distances would lead to the largest 304 SS substrate ΔT .

For thin SS, process parameters were changed similar to the 304 SS temperature testing. As the blast height decreased from 8" to 6", the blast pattern radius increased, leading to $\Delta T = +9.8 \text{ }^\circ\text{C}$. The angled blasting and pressure blasting of the thin SS substrates generated higher temperatures than the 8" distance testing. However no distinction could be made with 95% confidence when changing the angle or pressure.

The other expected results were that the shape or thickness of the substrate would lead to different temperature changes when blasting. When blasting the thin SS and 304 SS substrates, no distinction could be made between the substrate temperatures at 6" distance. However, viewing the effect of substrate thickness or shape at 8" blast distance showed that a $\Delta T = +7.4 \text{ }^\circ\text{C}$ when switching from the thin SS to 304 SS. Similar effects were seen when blasting different substrates at the same 45° and another experiment at 60 psi. A $\Delta T = +20.2 \text{ }^\circ\text{C}$ occurred for the angled blasting and $\Delta T = -15.2 \text{ }^\circ\text{C}$ for the higher pressure blasting when switching from the thin SS to 304 SS substrates. Based on these results, with 95% confidence the substrate thickness or shape does play a role in the temperature generated from blasting under conditions of a larger standoff distance, 45° angle, and higher pressure.

6 Future Work

Based on the results of these experiments, further investigation is needed in the following areas for purposes of understanding surface roughness changes from process parameter variation. For any future testing, use new media for each set of experiments for different blast conditions, this would allow for more refined results. Another set of experiments would be to use different media types or sizes and follow up on other literature and add in experiments to better understand lacking areas for a given media/substrate combinations. Since blast time and blast angle were not varied for the roughness tests, other experiments could use three different blast angles and three different blast times to show more distinct changes in roughness values. A better understanding of the repeatable and reproducible experiments with different blast cabinets, blast operators, and same operator re-running experiments would be interesting to see how roughness would be altered if new media was used in all experiments. Future work for roughness data would also contain interactions of the various altered parameters, to optimize generating the highest R_a values possible.

For purposes of measuring ΔT from blasting, more temperature probes or sensors would help better illustrate the effects from different process parameters. If the media flow rate would be controlled with an automatic media flow regulator, media flow effects on temperature could be better understood. Using different size/type of media and different substrate materials, shapes, and sizes would be of interest to learn more about the thermal changes generated from blasting. Calculations of ΔT on the side of the substrate being blasted would be of interest as well. Strain gage testing on the substrates during blasting would be beneficial to understand the effects of the thermal strain and change in refractive index of the fibers.

Other areas of interest would be to combine the roughness and temperature testing into one set of experiments. Results would show the effects of roughness on the surface and various conclusions would be gathered from knowing how much the temperature change affects the quality of the substrate surface. These tests could be combined with strain testing, along with other types of characterization techniques for in-situ blasting and post blasting.

References

- [1] Tilghman, B.C. "Improvement in Cutting and Engraving Stone, Metal, Glass, etc. US States Patent 108,408." Copyright October 18, 1870.
- [2] No Author. "The Difference Between Surface Profile and Class of Blast." Blast One. Copyright 2014. Online: <http://www.blast-one.com/weekly-tips/the-difference-between-surface-profile-and-class-of-blast>
- [3] Rettermayer, Robert. "The History of Sandblasting". Gero Sandblasting. Copyright 2013. Online: <http://www.sand-blasting.co/the-history-of-sandblasting/>
- [4] No Author. "Progressive Surface History." Progressive Surface. Copyright 2014. Grand Rapids, Michigan. Date Accessed: January 22, 2014. Online: <http://www.progressivesurface.com/company.php>
- [5] Momber A. *Blast Cleaning Technology: Chapter 1: Introduction*. Springer. Copyright 2008. Berlin, Heidelberg. Pages 1-6. Online: http://link.springer.com/chapter/10.1007/978-3-540-73645-5_1
- [6] No Author. "Blast Cabinets." Norton Sandblasting Equipment. Chesapeake, VA. Copyright 2014. Online: <http://www.nortonsandblasting.com/nsbcontact.html>
- [7] No Author. "Abrasive Blast Equipment: Pressure versus Suction." Surface Preparation. Copyright 2014. Online: <http://www.surfacepreparation.com/abrasive-blast-equipment-pressure-versus-suction>
- [8] Heywood, H. "Numerical Definition of Particle Size and Shape." Chemical Ind. Copyright 1933. Volume 32. Pages 149-154.
- [9] Vasek, J., Martinec, P., Foldyna, J. "Influence of properties of garnet on AWJ Cutting Process". Proc. 7 Am. Water Jet Conference. Water Jet Technology Association. St. Louis, Missouri. Copyright 1993. Volume 1. Pages 365-387.
- [10] Wadell, H. "Sphericity and Roundness of Rock Particles." *J. Geol.* Copyright 1933. Volume. 41. Pages 316-331.
- [11] Hansink, J.D. "Economics of Abrasive Selection for Shipyard Use." Protective Coatings Europe. Copyright 1998. Volume 3. Issue 5. Pages 24-27.
- [12] Bohemia Garnet & Momber A. *Blast Cleaning Technology: Chapter 2: Abrasive Materials*. Springer. Copyright 2008. Berlin, Heidelberg. Page 21.
- [13] Bahadur, S., Badruddin, R. "Erodent Particle Characterization and the Effect of Particle Size and Shape on Erosion." *Wear*. 1990. Volume 138. Pages 189-208.
- [14] Momber A. *Blast Cleaning Technology: Chapter 2: Abrasive Materials*. Springer. Copyright 2008. Berlin, Heidelberg. Pages 7-53. Online: http://link.springer.com/chapter/10.1007%2F978-3-540-73645-5_2
- [15] Kuhmichel GmbH & Momber A. *Blast Cleaning Technology: Chapter 2: Abrasive Materials*. Springer. Copyright 2008. Berlin, Heidelberg. Page 18.
- [16] No Author. "What is Grit Blasting?" *Progressive Surface*. Grand Rapids, Michigan. Online: http://www.progressivesurface.com/gritblasting_process.php
- [17] No Author. "What is Shot Peening?" *Progressive Surface*. Grand Rapids, Michigan. Online: http://www.progressivesurface.com/shotpeening_process.php
- [18] Metabrasive Ltd. & Momber A. *Blast Cleaning Technology: Chapter 2: Abrasive Materials*. Springer. Copyright 2008. Berlin, Heidelberg. Page 18.
- [19] No Author. "Particle Size Conversion Table. Sigma-Aldrich Co. LLC. Copyright 2013. Online: <http://www.sigmaaldrich.com/chemistry/stockroom-reagents/learning-center/technical-library/particle-size-conversion.html>
- [20] Kelly, E.G., Spottiswood, D.J. *Introduction to Mineral Processing*. John Wiley & Son. Copyright 1982. New York. Pages 21-45. Date Accessed: March 31, 2013.
- [21] No Author. "Abrasives & Compounds." Newport Glass Works, LTD. Stanton, CA. Copyright 2013. Online: <http://www.newportglass.com/grit.htm>
- [22] No Author. "Grit Size Conversion Table." Media Blast & Abrasive, Inc. Copyright 2013. Online: <http://www.mediablast.com/grit-size-conversions.php>
- [23] Day, J., Huang, X., Richards, N.L. "Examination of a Grit-Blasting Process for Thermal Spraying Using Statistical Methods." *Journal of Thermal Spray Technology*. 2005. Volume 14. Pages 471-479.
- [24] Maruyama, T., Akagi, K., Kobayashi, T. "Effects of Blasting Parameters on Removability of Residual Grit." *Journal of Thermal Spray Technology*. 2006. Volume 15. Issue 4. Pages 817-821.

- [25] Boerio, F.J., Roby, B., Dillingham, R.G., Bossi, R.H., Crane, R.L. "Effect of Grit-Blasting on the Surface Energy of Graphite/Epoxy Composites." *The Journal of Adhesion*. 2006. Issue 82. Pages: 19-37.
- [26] No Author. "Hardness." The Free Dictionary. Farlex, Inc. Copyright 2013. Online: [http://encyclopedia2.thefreedictionary.com/Hardness+\(materials+science\)](http://encyclopedia2.thefreedictionary.com/Hardness+(materials+science))
- [27] Tabor, D. *The Hardness of Metals*. Claredon Press. Copyright 1951.
- [28] No Author. "Knoop Hardness." Merriam Webster Dictionary. Merriam-Webster, Incorporated. Copyright 2013. Online: <http://www.merriam-webster.com/dictionary/knoop%20hardness>
- [29] No Author. "Rockwell Testing." Wilson Hardness. Copyright 2013. Online: <http://www.wilson-hardness.com/Resources/RockwellTesting/tabid/80/language/en/Default.aspx>
- [30] No Author. "Hardness Tables." Ted Pella, Inc. Copyright 2013. Online: http://www.tedpella.com/company_html/hardness.htm
- [31] No Author. "Hardness Conversion Chart." NDT Resource Center. Online: <http://www.ndt-ed.org/GeneralResources/HardnessConv/HardnessConv.htm>
- [32] Wellinger, K., Uetz, H. Gleitverschleiß, Spülverschleiß, Strahlverschleiß unter der Wirkung von körnigen Stoffen. *VDI-Forschungshefte*, Copyright 1955. No. 449, 1–40.
- [33] Uetz, H. *Abrasion und Erosion*. Carl Hanser Verlag, München-Wien. Copyright 1986.
- [34] Wellinger, K., Uetz, H., Gommel, G. Gütekennwerte von Strahlmitteln und deren Veränderung während des Strahlvorganges. *Stahl Eisen*, Copyright 1962. Vol. 82, No. 21, 1436–1445.
- [35] No Author. "Abrasive-Blast Media Chart." Norton Sandblasting Equipment. Copyright Unknown. Online: <http://www.nortonsandblasting.com/nsbabrasives.html>
- [36] Makova, I., Sopko, M. "Effect of Blasting Material on Surface Morphology of Steel Sheets." *Acta Metallurgica Slovaca*. Copyright 2010. Volume 16. Issue 2. Pages 109-115.
- [37] No Author. "Fracture Stress." Answers Corporation. Copyright 2013. Online: <http://www.answers.com/topic/fracture-stress>
- [38] Huang, H., Zhu, X.H., Huang, Q.K. "Weibull strength distributions and fracture characteristics of abrasive materials." *Engineering Fracture Mechanics*. Copyright 1995. Volume 23, Pages 773-776.
- [39] Verspui, M.A., With, G., Dekkers, E.C. "A crusher for single particle testing." *Reviewed Scientific Instruments*. Copyright 1997. Volume 63. Issue 3. Pages 1553-1556.
- [40] No Author. ISO 11124/2-4. Preparation of steel substrates before application of paints and related products - Specifications for metallic blast-cleaning abrasives - Part 2: Chilled-iron grit. International Organization for Standardization. Geneva. Copyright Unknown.
- [41] SSPC-AB 2. Abrasive Specification No. 2: Cleanliness of Recycled Ferrous Metallic Abrasives. Revised version. The Society of Protective Coatings. New York. Copyright 2004.
- [42] Callister, Jr., W.D., Rethwisch, D.G. *Fundamentals of Materials Science and Engineering: An Integrated Approach*. John Wiley & Sons, Inc. Copyright 2008.
- [43] Tosha, K., Iida, K. "Residual Stress on the Grit Blasted Surface." *Metal Behaviour & Surface Engineering*. Copyright 1989. Pages 323-328.
- [44] Crithclow, G. Handbook of Adhesion Technology: Chapters 7 & 8. Loughborough, UK. Loughborough University. 2011: Pages 119-177. Online: http://link.springer.com/referencework/entry/10.1007/978-3-642-01169-6_7
- [45] Bacova, V., Draganovska, D. "Analyses of the Quality of Blasting Surfaces." *Materials Science*. 2004. Volume 40. Issue 1. Pages 125-131.
- [46] Acton, S., Agnew, S., Fitz-Gerald, J. CCAM Surface Characterization Interim Report. Charlottesville, VA. University of Virginia. Pages 1-24.
- [47] Tosha, K., Iida, K. "Crystal Transformation of Austenitic Stainless Steel by Shot Peening and Grit Blasting." International Conference on Shot Peening and Blast Cleaning. Pages 111-120.
- [48] Smith, T., Crane, R. Proceedings of the National SAMPE Symposium. Copyright 1980. Page: 25.
- [49] Minford, J. "Aluminum 57." Copyright 1981. Issue 10. Page: 657.

- [50] Fang, C.K., Chuang, T.H. "Erosion of SS41 Steel by Sand Blasting." *Metallurgical and Materials Transactions A*. 1999. Volume 30A. Pages 941-948.
- [51] Mellalia, M., Grimaud, A., Leger, A.C., Fauchais, P., Lu, J. "Alumina Grit Blasting Parameters for Surface Preparation in the Plasma Spraying Operation." *Journal of Thermal Spray Technology*. 1997. Volume 6. Issue 2. Pages 217-227.
- [52] Tosha, K., Iida, K. "Stock Removal and Surface Residual Stress of Grit Blasting Titanium." Meiji University. Kawasaki, Japan. Copyright 1990.
- [53] Chander, K. P., Vashita, M., Sabiruddin, K., Paul, S., Bandyopadhyay, P.P. "Effects of Grit Blasting on Surface Properties of Steel Substrates." West Bengal, India. *Materials and Design*. 2009. Pages: 2895-2902.
- [54] Amada, S., Hirose, T. "Influence of grit blasting pre-treatment on the adhesion strength of plasma sprayed coatings: fractal analysis of roughness." *Surface and Coatings Technology*. 1998. Volume 102. Pages 132-137. Online: [http://dx.doi.org/10.1016/S0257-8972\(97\)00628-2](http://dx.doi.org/10.1016/S0257-8972(97)00628-2) Article #5
- [55] Carter, G., Bevan I.J., Katardjiev I.V., Nobes, M.J. "The Erosion of Copper by Reflected Sandblasting Grains." *Materials Science Engineering*. 1991. Volume A. Issue 132. Pages: 231-236.
- [56] Celik, E., Demirkiran, A.S., Avci, E. "Effect of Grit Blasting of Substrate on the Corrosion Behaviour of Plasma-Sprayed Al₂O₃ Coatings." *Surface and Coatings Technology*. 1999. Volume 116-119. Pages: 1061-1064.
- [57] Khorasanizadeh, S. "The Effect of Shot and Grit Blasting Process Parameters on Steel Pipes Coating Adhesion." Ahvaz, Iran. World Academy of Science, Engineering and Technology. 2010. Pages 1290-1298.
- [58] Griffiths, B.J., Gawne, D.T., Dong, G.. "The erosion of steel surfaces by grit-blasting as a preparation for plasma spraying." *Wear*. 1995. Volume 194. Pages 95-102.
- [59] Wigren, J. "Technical Note: Grit Blasting as Surface Preparation Before Plasma Spraying." *Surface and Coatings Technology*. 1988. Volume 34. Pages 101-108.
- [60] Buhlmann, S. Ein stochastisches Modell der Prallzerkleinerung. Chemie-Ing.-Techn. Copyright 1970. Vol. 42, No. 5, 277–281.
- [61] Ohlsen, J. Recycling von Feststoffen beim Wasserabrasivstrahlverfahren. VDI Fortschritt-Berichte, Reihe Copyright 1997. 15, No. 175.
- [62] Hareux, D., Riach, B. "A comparative study of air blasting using different abrasives—parts 1+2". *Corros. Prot. Mater.* Copyright 1986. Vol. 5, No 1, 18–34.
- [63] No Author. "Abrasive Blast Nozzle Catalog." Kennametal Inc. Traverse City, MI. Copyright 2012. Online: http://www.kennametal.com/content/dam/kennametal/kennametal/common/Resources/Catalogs-Literature/Advanced%20Materials%20and%20Wear%20Components/B-12-02861_KMT_Blast_Nozzles_Catalog_EN.pdf
- [64] Tabenkin, A. "The Basics of Surface Finish Measurement." *Quality Magazine*. Mahr Federal Inc. Copyright 2014. Online: http://www.deterco.com/products/Mahr%20Federal/newsletter/finish_measure_10_19_04.htm
- [65] No Author. "Roughness Terminology." Olympus Corporation. Copyright 2014. Online: <http://www.olympus-ims.com/en/knowledge/metrology/roughness/dictionary/>
- [66] Pickrell, G., Homa, D., Mills, R. "Abrasive Blasting Deliverable No.3." CCAM. Copyright 2014.
- [67] Sosale, G., Hackling, S.A., Vengallatore, S. "Topography Analysis of Grit-Blasted and Grit-Blasted-Acid-Etched Titanium Implant Surfaces Using Multi-scale Measurements and Multi-Parameter Statistics." *Journal of Materials Research*. 2011. Volume 23, Issue 10. Pages 2704-2713. Online: <http://journals.cambridge.org/action/displayAbstract?fromPage=online&aid=7954744>
- [68] No Author. "Metcolite Grits." Sulzer Metco. Copyright 2014. Online: www.sulzer.com/cs/-/media/.../DSMTS_0028_2_Metcolite.pdf
- [69] No Author. "AISI Type 304 Stainless Steel." Aerospace Specification Metals, INC. Copyright 2014. Online: <http://asm.matweb.com/search/SpecificMaterial.asp?bassnum=MQ304A>
- [70] No Author. "Surfrest SJ-210 Series Brochure." Mitutoyo. Japan. Copyright 2014.
- [71] No Author. "Empire Pro-Former 3642 Manual." EMPIRE Abrasive Equipment. Langborne, PA. Copyright 2014.
- [72] No Author. "Os4100 Temperature Compensation Sensor: Sensor Equation Sheet." Micron Optics. Atlanta, GA. Copyright 2014.

- [73] No Author. "Os4200 Temperature Probe: Sensor Equation Sheet." Micron Optics. Atlanta, GA. Copyright 2014.
- [74] Paschotta, R. "Fiber-Optics Sensors." RP Photonics Consulting GmbH. Copyright 2014. Online: http://www.rp-photonics.com/fiber_optic_sensors.html
- [75] No Author. "Temperature Compensation Sensor: os4100." Micron Optics. Atlanta, GA. Copyright 2009. Date Accessed: June 6, 2014. Online: <http://www.moiag.com/Product/moiag-os4100.pdf>
- [76] No Author. "Temperature Probe: os4200." Micron Optics. Atlanta, GA. Copyright 2009. Online: <http://www.sengenia.com/pdfs/os4200.pdf>

Appendices

Appendix A Blast Media Chart

Table A-1 Blast media chart. No Author. "Blast Media Chart." Norton Sandblasting Equipment. 2014. <http://www.nortonsandblasting.com/nsbabrasives.html> (accessed June 9, 2014) Used with permission from Norton Sandblasting Equipment, 2014.

Abrasive	Mesh Sizes	Density (lbs/ft³)	Mohs Hardness	Cycles	Dust	Cost	Cost/Use	Metal Removal
Baking Soda	60-170	60	2.5	1	High	High	Med	None
Dry Ice	3 mm cylinders	98	NA	1	Low	High	Med	None
Sponge	16-320	9-33	2.5-8.0	5-20	Low	High	Med	None-High
Plastic	12-80	45-60	3.0-4.0	8-10	Low	High	Med	None
Glass Bead	30-325	100	5.5	8-10	Med	Med	Med	None-Low
Crushed Glass	30-400	100	5.5	1	Low To Med	Low	Low	Low- Med
Ceramic Bead	60-120	150	800-1000 Vickers	60-100	Low	High	Med	None-Low
Jetmag	16-150	84	6.5-7	3-4	Med	Low	Low	Med
Coal Slag	12-40	85-112	7.0-7.5	1	High	Low	Med	Med
Garnet	30-80	140-150	7.5	3-4	Low	Med	Med	Low
Aluminum Oxide	16-220	125	8.0-9.0	6-8	Low	High	Med	High
Steel Grit	12-50	230	8	200+	Low	High	Low	High
Steel Shot	10-80	280	8	200+	Low	High	Low	None

Appendix B Nozzle Design

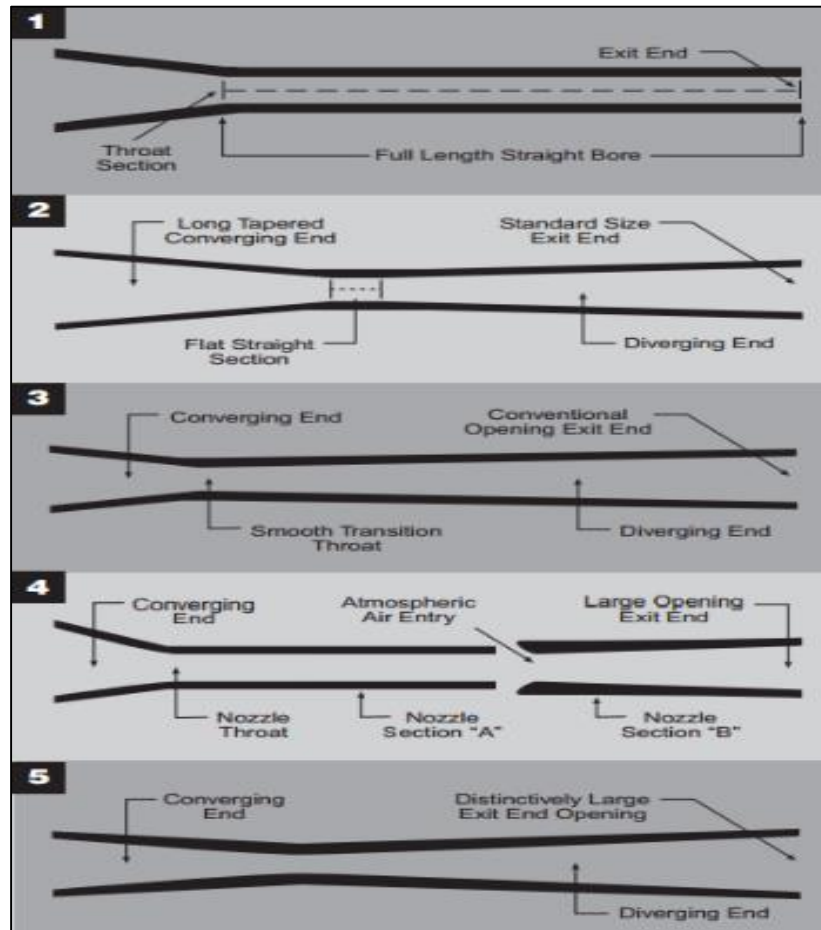


Figure B.1 Nozzle descriptions. No Author. "Abrasive Blast Nozzles." Kennametal Inc. 2012 page 9. http://www.kennametal.com/content/dam/kennametal/kennametal/common/Resources/Catalogs-Literature/Advanced%20Materials%20and%20Wear%20Components/B-12-02861_KMT_Blast_Nozzles_Catalog_EN.pdf (accessed June 9, 2014) Used with permission from Kennametal, Inc., 2014.

Appendix C Roughness Testing Information

Method 1

1. Turn the ball choke valve to the media off and take the nozzle off of the blasting hose.
2. Set the blasting pressure to 70-80 psi and blast for about 30 seconds.
3. This should clear up any debris trapped in the hose and hopefully in the orifice between the pressure vessel and the blast hose connection.
4. If this does not work, use the second method mentioned below.

Method 2

1. Remove the media from the blast system by turning the choke valve to closed, open the media flow regulator valve to fully open position, and blast all of the media into a bucket at a low pressure of 20-30 psi.
2. Once the media is removed from the system, bleed the air out of the machine, then close the compress air valve to the system, and lock-out (if possible).
3. Next the media flow regulator needs to be taken apart with a screwdriver and a socket wrench.
4. Once the regulator is apart, the rubber tube that is part of the regulation system needs to be taken out and inspected.
5. Once the rubber tube is wiped off for dust and debris, make sure the blast hose connection and pressure vessel is clear and clean of debris and rebuild the media flow regulator.
6. Once rebuilt, add media back into the system via protocol from the EMPIRE PF 4848 user manual and set the media flow regulator correctly until pulsating is gone.
7. The pulsating should be gone or reduced tremendously once the orifice is clear of debris.

Figure C.1 Pulsation elimination methods [71].

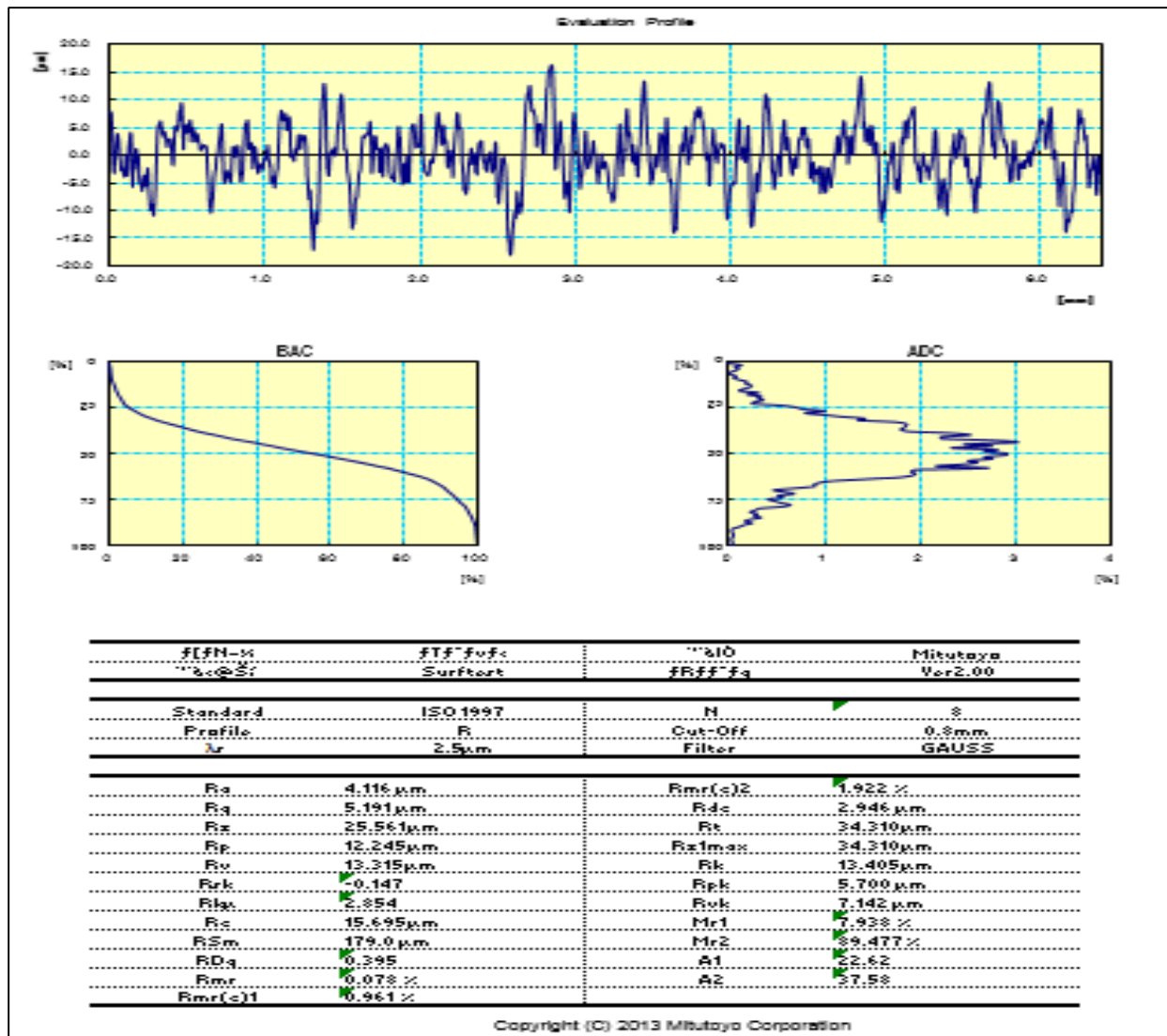


Figure C.2 SJ-210 Example sample results for SS304 7-01 V3 measurement.

Sample	Measurement ID						Average Ra	$\sigma_{\text{measurement}}$
	V1	V2	V3, V4, V5, H1, H2, H3	H4	H5	Units		
2-01	3.382	3.382	3.561	4.126	μ m	3.77	0.306
2-02	3.456	3.840	3.642	3.512	μ m	3.54	0.207
2-03	3.633	3.693	3.835	3.585	μ m	3.61	0.242
2-04	3.450	3.426	3.420	3.733	μ m	3.55	0.178
2-05	3.778	3.273	3.295	3.324	μ m	3.51	0.256
2-06	3.867	3.429	3.628	3.262	μ m	3.46	0.188
2-07	3.566	4.149	3.543	3.543	μ m	3.75	0.250
2-08	3.617	3.962	3.648	3.855	μ m	3.72	0.159
2-09	3.368	3.493	3.289	3.287	μ m	3.44	0.199
2-10	3.695	3.457	3.521	3.836	μ m	3.68	0.182

$\sigma_{\text{Process + Measurements}} = 0.239$

$\sigma_{\text{Average Ra}} = 0.119$

$\sigma_{\text{measurement}} = 0.217$

Figure C.3 Standard deviation calculations for experiment #2.

Magnification	350x	2m	800 micron bandpass					20 x 27 points		33.54 microns apart							Avg. Sa	M St. Dev.
Substrate	2.101	2.102	2.103	2.104	2.105	2.106	2.107	2.108	2.109	2.1010	2.1011	2.1012	2.1013	2.1014	2.1015			
Measurement #																		
Sa	3.712479	3.520431	3.778973	4.256505	4.115823	3.539105	3.909362	3.58639	3.761011	3.985614	3.663805	3.950103	4.111683	4.205235	3.774771	3.858086	0.240311977	
Unit	µm	µm	µm	µm	µm	µm	µm	µm	µm	µm	µm	µm	µm	µm	µm			

Magnification	350x	4m	800 micron bandpass					20 x 27 points		33.54 microns apart								
Substrate	2.101	2.102	2.103	2.104	2.105	2.106	2.107	2.108	2.109	2.1010	2.1011	2.1012	2.1013	2.1014	2.1015			
Measurement #																		
Sa	3.704367	3.538585	3.771903	4.253813	4.126819	3.505779	3.932906	3.566421	3.739208	3.996629	3.644812	3.953846	4.128036	4.192113	3.754118	3.854024	0.247707934	
Unit	µm	µm	µm	µm	µm	µm	µm	µm	µm	µm	µm	µm	µm	µm	µm			

Figure C.4 Hirox S_a and standard deviation measurements and calculations.

Sample:	Run #1:	Run #2:	Run #3:	Run #4:	Run #5:	Run #6:	Run #7:	Run #8:	Run #9:	Run #10:	Avg. Sa	M σ
1.03	3.7982	4.2582	4.6341	4.9864	3.7989	5.3186	4.5643	3.9955	4.1249	4.1009	4.3580	0.5082
2.05	3.6550	3.2944	4.1762	4.4645	3.7575	4.3363	4.7200	4.2177	4.5362	3.4592	4.0617	0.4880

Figure C.5 UVA ROST S_a and standard deviation measurements and calculations.

Appendix D Temperature Testing Information



Figure D.1 Optical fiber ready for fusion splicing.

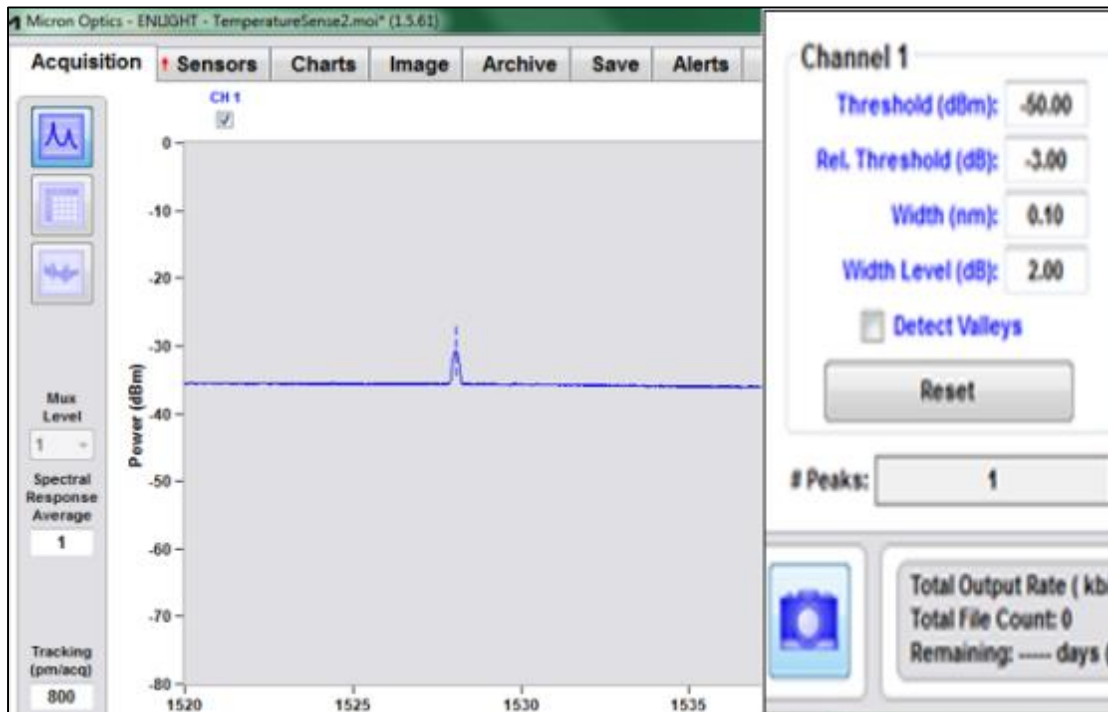


Figure D.2 “Acquisition” window of Enlight software.

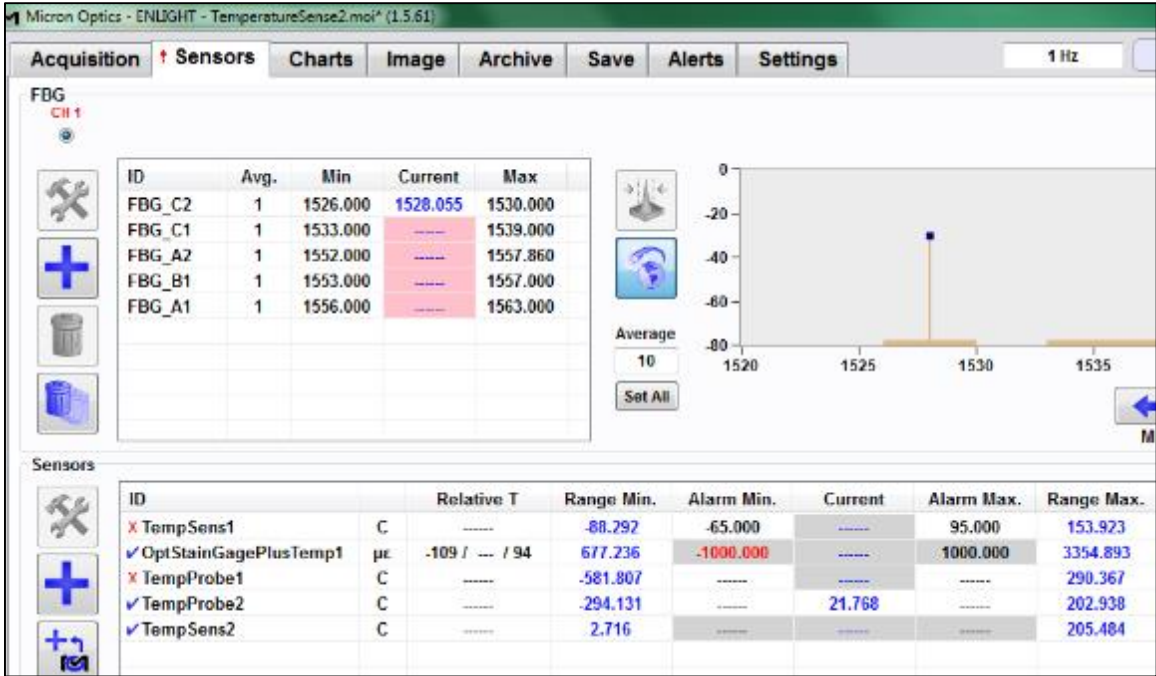


Figure D.3 “Sensors” window.

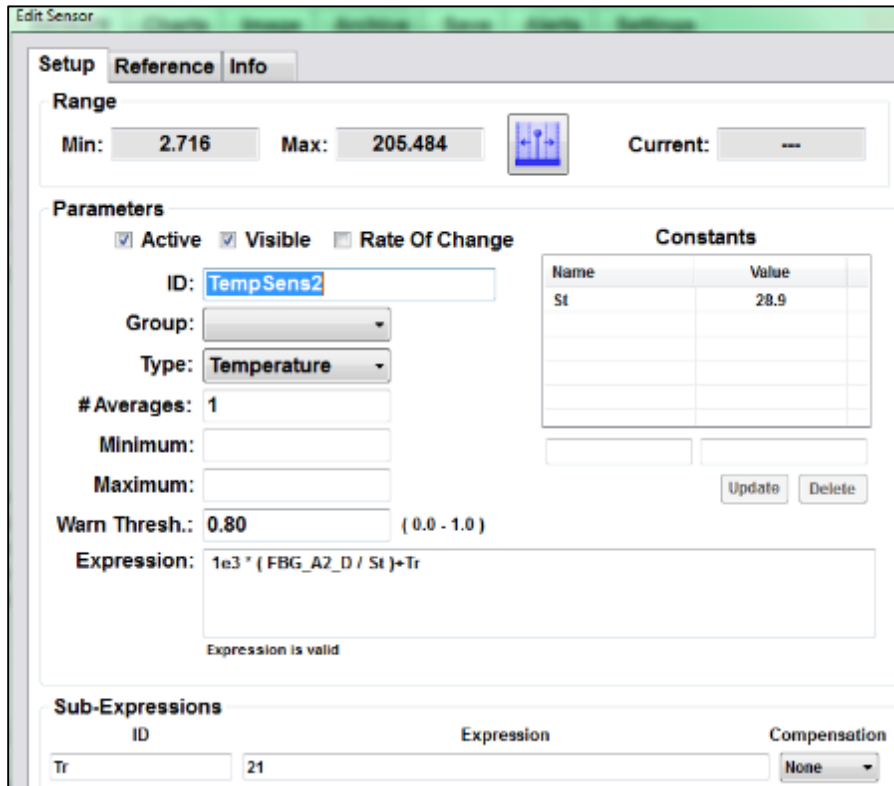


Figure D.4 “TempSens2” information.

Parameters

Active Visible Rate Of Change

ID:

Group:

Type:

Averages:

Minimum:

Maximum:

Warn Thresh.: (0.0 - 1.0)

Expression: $C3*(FBG_C2+Lambda0S)^3+C2*(FBG_C2+Lambda0S)^2+C1*(FBG_C2+Lambda0S)+C0$

Expression is valid

Constants

Name	Value
Lambda0S	-11.9934
C3	4.139809474771...
C2	-18843.3096330...
C1	28589996.82606...
C0	-14459428166.8...

Figure D.5 "TempProbe2" information.

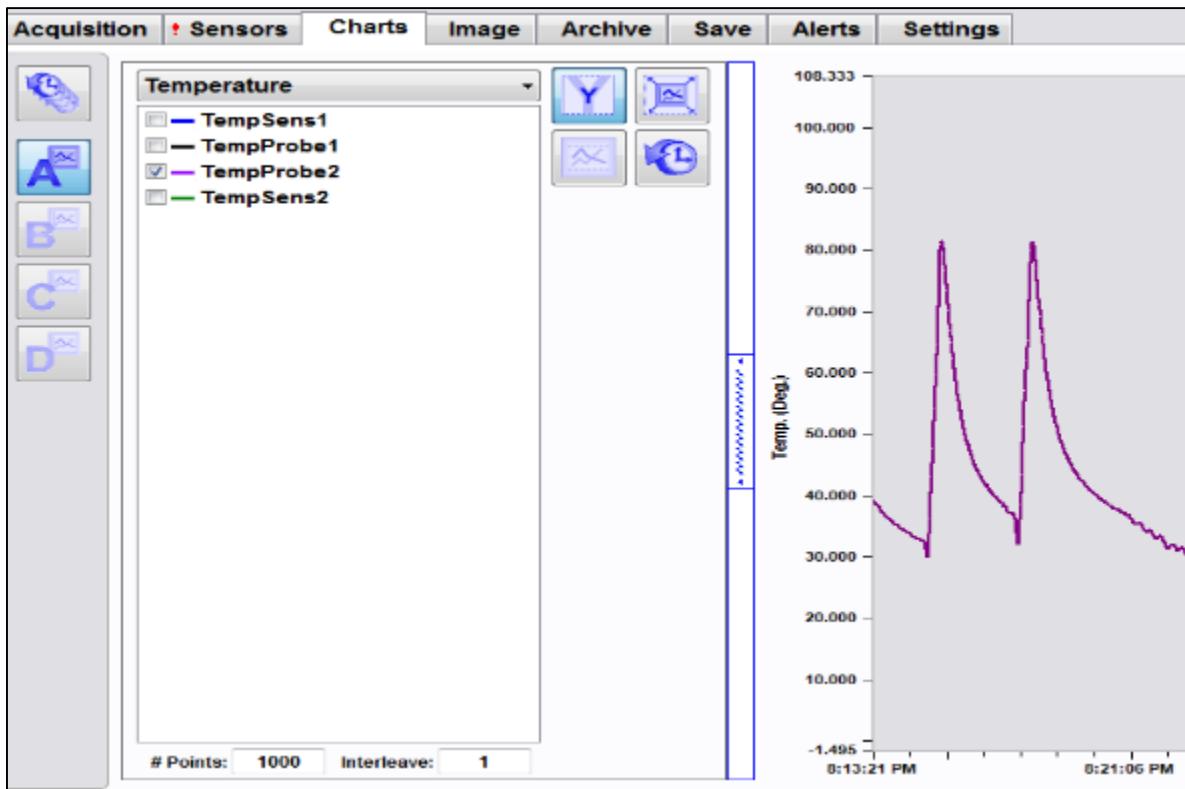


Figure D.6 Charts window with live temperature data.

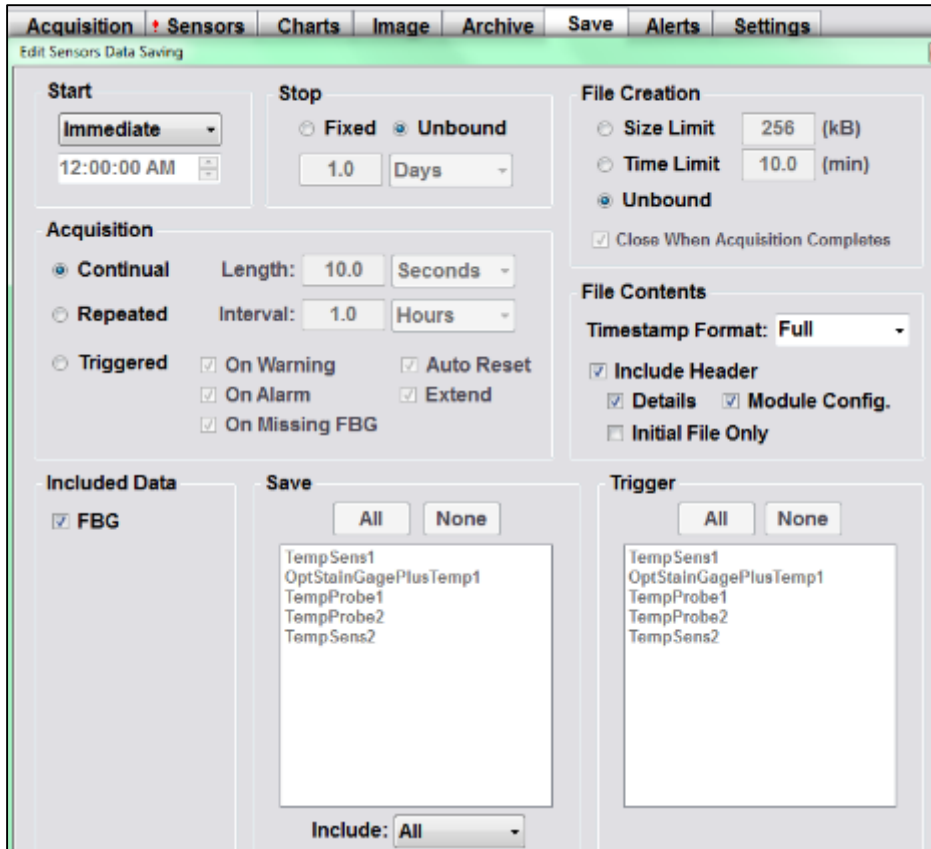


Figure D.7 Edit sensors data saving option under “Save” window.



Figure D.8 Thin stainless steel substrate (0.09” x 1.378” x 4.2875”) pre-blasting.

Appendix E Sample F-test and t-test calculations

Value	A. 4"	B. 6"
Mean	3.887	3.666
Stan. Dev.	0.23243	0.14600
n	10	10
Variance	0.05402	0.02132

$$F = \frac{Var_A}{Var_B}$$

$$F = \frac{0.05402}{0.02131}$$

$$F = 2.535$$

$$t = \frac{\bar{x}_A - \bar{x}_B}{\sqrt{\left[\frac{(n_A - 1) \cdot S_A^2 + (n_B - 1) \cdot S_B^2}{(n_A + n_B - 2)} \right] \cdot \left[\frac{[n_A + n_B]}{[n_A \cdot n_B]} \right]}}$$

$$t = \frac{3.887 - 3.666}{\sqrt{\left[\frac{(10 - 1) \cdot (0.2324^2) + (10 - 1) \cdot (0.1460)^2}{(10 + 10 - 2)} \right] \cdot \left[\frac{[10 + 10]}{[10 \cdot 10]} \right]}}$$

$$t = \frac{0.221}{\sqrt{[0.03766] \cdot [0.2]}}$$

$$t = 2.546$$

Figure E.1 Sample F_{calc} and t_{calc} for F-test and t-test for 4" and 6" blasts on Ra comparison.

$$F = \frac{Var_A}{Var_B}$$

$$F = \frac{16.7223}{12.4025}$$

$$F = 1.348$$

$$t = \frac{\bar{x}_A - \bar{x}_B}{\sqrt{\left[\frac{(n_A - 1) \cdot S_A^2 + (n_B - 1) \cdot S_B^2}{(n_A + n_B - 2)} \right] \cdot \left[\frac{[n_A + n_B]}{[n_A \cdot n_B]} \right]}}$$

$$t = \frac{29.099 - 19.922}{\sqrt{\left[\frac{(5 - 1) \cdot (4.0892^2) + (5 - 1) \cdot (3.5217)^2}{(5 + 5 - 2)} \right] \cdot \left[\frac{[5 + 5]}{[5 \cdot 5]} \right]}}$$

$$t = \frac{9.177}{\sqrt{[14.562] \cdot [0.4]}}$$

$$t = 3.802$$

Figure E.2 Sample F_{calc} and t_{calc} for F-test and t-test for 4" and 6" blasts on 304 SS T comparison.

Appendix F Roughness F-tests and t-tests Data

Data	1. 4"	2. 6"	F-Test Two-Sample for Variances			t-Test: Two-Sample Assuming Equal Variances		
Ra #1	3.77	3.96		Variable 1	Variable 2		Variable 1	Variable 2
Ra #2	3.8	3.52	Mean	3.887	3.668	Mean	3.887	3.668
Ra #3	3.96	3.75	Variance	0.0540	0.0216	Variance	0.0540	0.0216
Ra #4	3.81	3.53	Observations	10	10	Observations	10	10
Ra #5	3.8	3.64	df	9	9	Pooled Variance	0.0378	
Ra #6	3.78	3.5	F	2.496		Hypothesized Mean Diff.	0	
Ra #7	4.52	3.72	P(F<=f) one-tail	0.0946		df	18	
Ra #8	3.72	3.7	F Critical one-tail	3.179		t Stat	2.518	
Ra #9	3.9	3.56	Fcalc < Fcritical			P(T<=t) two-tail	0.0215	
Ra #10	3.81	3.8	Variances are equal.			t Critical two-tail	2.101	
Standard Deviation	0.232	0.147						
Standard Error	0.0735	0.0465						

Figure F.1 F-test and t-test results for 4" and 6" blasts on Ra comparison.

Data	2. 6"	3. 8"	F-Test Two-Sample for Variances			t-Test: Two-Sample Assuming Equal Variances		
Ra #1	3.96	3.41		Variable 1	Variable 2		Variable 1	Variable 2
Ra #2	3.52	3.45	Mean	3.668	3.446	Mean	3.668	3.446
Ra #3	3.75	3.34	Variance	0.0216	0.0188	Variance	0.0216	0.0188
Ra #4	3.53	3.24	Observations	10	10	Observations	10	10
Ra #5	3.64	3.6	df	9	9	Pooled Variance	0.0202	
Ra #6	3.5	3.7	F	1.148		Hypothesized Mean Diff.	0	
Ra #7	3.72	3.52	P(F<=f) one-tail	0.420		df	18	
Ra #8	3.7	3.48	F Critical one-tail	3.179		t Stat	3.489	
Ra #9	3.56	3.31	Fcalc < Fcritical			P(T<=t) two-tail	0.00262	
Ra #10	3.8	3.41	Variances are equal.			t Critical two-tail	2.101	
Standard Deviation	0.147	0.137						
Standard Error	0.0465	0.0434						

Figure F.2 F-test and t-test results for 6" and 8" Ra comparison.

Data	9. 42 psi	10. 60 psi	F-Test Two-Sample for Variances			t-Test: Two-Sample Assuming Equal Variances		
Ra #1	5.07	4.81		Variable 1	Variable 2		Variable 1	Variable 2
Ra #2	5.19	4.65	Mean	5.012	4.675	Mean	5.012	4.675
Ra #3	5.33	4.72	Variance	0.0566	0.0407	Variance	0.0566	0.0407
Ra #4	5.37	4.98	Observations	10	10	Observations	10	10
Ra #5	4.99	4.45	df	9	9	Pooled Variance	0.0486	
Ra #6	4.74	4.86	F	1.391		Hypothesized Mean Diff.	0	
Ra #7	4.82	4.61	P(F<=f) one-tail	0.315		df	18	
Ra #8	4.77	4.84	F Critical one-tail	3.179		t Stat	3.418	
Ra #9	4.75	4.43	F calc < Fcritical			P(T<=t) two-tail	0.00307	
Ra #10	5.09	4.4	Variances are equal.			t Critical two-tail	2.101	
Standard Deviation	0.238	0.202						
Standard Error	0.0752	0.0638						

Figure F.3 F-test and t-test results for 42 psi and 60 psi Ra comparison.

Data	6. 5/16" Straight	18. 3/16" Venturi	F-Test Two-Sample for Variances			t-Test: Two-Sample Assuming Unequal Variances		
				Variable 1	Variable 2		Variable 1	Variable 2
Ra #1	4.16	4.64	Mean	4.234	4.24	Mean	4.24	4.234
Ra #2	4.33	4.23	Variance	0.0572	0.0121	Variance	0.0121	0.0572
Ra #3	4.46	4.19	Observations	10	10	Observations	10	10
Ra #4	4.29	4.41	df	9	9	Hypothesized Mean Diff.	0	
Ra #5	4.07	4.54	F	4.721		df	13	
Ra #6	4.27	4.23	P(F<=f) one-tail	0.0151		t Stat	0.0721	
Ra #7	4.15	3.92	F Critical one-tail	3.179		P(T<=t) two-tail	0.944	
Ra #8	4.20	4.14	F calc > Fcritical			t Critical two-tail	2.160	
Ra #9	4.28	4.13	Variances are not equal.					
Ra #10	4.19	3.91						
Standard Deviation	0.110	0.239						
Standard Error	0.0348	0.0756						

Figure F.4 F-test and t-test results for 5/16" straight and 3/16" Venturi nozzle Ra comparison.

Data	18. No Pulsation	2. Pulsation	F-Test Two-Sample for Variances			t-Test: Two-Sample Assuming Equal Variances		
				Variable 1	Variable 2		Variable 1	Variable 2
Ra #1	4.64	3.96	Mean	4.234	3.668	Mean	4.234	3.668
Ra #2	4.23	3.52	Variance	0.0572	0.0216	Variance	0.0572	0.0216
Ra #3	4.19	3.75	Observations	10	10	Observations	10	10
Ra #4	4.41	3.53	df	9	9	Pooled Variance	0.0394	
Ra #5	4.54	3.64	F	2.642		Hypothesized Mean Diff.	0	
Ra #6	4.23	3.5	P(F<=f) one-tail	0.0820		df	18	
Ra #7	3.92	3.72	F Critical one-tail	3.179		t Stat	6.375	
Ra #8	4.14	3.7	F calc < Fcritical			P(T<=t) two-tail	5.275E-06	
Ra #9	4.13	3.56	Variances are equal.			t Critical two-tail	2.101	
Ra #10	3.91	3.8						
Standard Deviation	0.239	0.147						
Standard Error	0.0756	0.0465						

Figure F.5 F-test and t-test results for no pulsation and pulsation Ra comparison.

Data	13. Old	18. New	F-Test Two-Sample for Variances			t-Test: Two-Sample Assuming Equal Variances		
				Variable 1	Variable 2		Variable 1	Variable 2
Ra #1	5.12	4.64	Mean	4.697	4.234	Mean	4.697	4.234
Ra #2	5.07	4.23	Variance	0.0580	0.0572	Variance	0.0580	0.0572
Ra #3	4.61	4.19	Observations	10	10	Observations	10	10
Ra #4	4.79	4.41	df	9	9	Pooled Variance	0.0576	
Ra #5	4.63	4.54	F	1.014		Hypothesized Mean Diff.	0	
Ra #6	4.6	4.23	P(F<=f) one-tail	0.492		df	18	
Ra #7	4.52	3.92	F Critical one-tail	3.179		t Stat	4.314	
Ra #8	4.33	4.14	F calc < Fcritical			P(T<=t) two-tail	0.000417	
Ra #9	4.61	4.13	Variances are equal.			t Critical two-tail	2.101	
Ra #10	4.69	3.91						
Standard Deviation	0.241	0.239						
Standard Error	0.0761	0.0756						

Figure F.6 F-test and t-test results for newer media and old (recycled media) Ra comparison.

Data	9. Day A	13. Day B	F-Test Two-Sample for Variances			t-Test: Two-Sample Assuming Equal Variances		
				Variable 1	Variable 2		Variable 1	Variable 2
Ra #1	5.07	5.12	Mean	4.697	5.012	Mean	5.012	4.697
Ra #2	5.19	5.07	Variance	0.0580	0.0566	Variance	0.0566	0.0580
Ra #3	5.33	4.61	Observations	10	10	Observations	10	10
Ra #4	5.37	4.79	df	9	9	Pooled Variance	0.0573	
Ra #5	4.99	4.63	F	1.025		Hypothesized Mean Diff.	0	
Ra #6	4.74	4.6	P(F<=f) one-tail	0.485		df	18	
Ra #7	4.82	4.52	F Critical one-tail	3.179		t Stat	2.943	
Ra #8	4.77	4.33	F calc < Fcritical			P(T<=t) two-tail	0.00869	
Ra #9	4.75	4.61	Variances are equal.			t Critical two-tail	2.101	
Ra #10	5.09	4.69						
Standard Deviation	0.238	0.241						
Standard Error	0.0752	0.0761						

Figure F.7 F-test and t-test results for Day A and Day B Ra comparison.

Data	17. VT	1. CCAM	F-Test Two-Sample for Variances			t-Test: Two-Sample Assuming Equal Variances		
				Variable 1	Variable 2		Variable 1	Variable 2
Ra #1	4.52	3.77	Mean	4.345	3.887	Mean	4.345	3.887
Ra #2	4.7	3.80	Variance	0.0576	0.0540	Variance	0.0576	0.0540
Ra #3	4.74	3.96	Observations	10	10	Observations	10	10
Ra #4	4.27	3.81	df	9	9	Pooled Variance	0.0558	
Ra #5	4.1	3.8	F	1.065		Hypothesized Mean Diff.	0	
Ra #6	4.37	3.78	P(F<=f) one-tail	0.463		df	18	
Ra #7	4.29	4.52	F Critical one-tail	3.179		t Stat	4.336	
Ra #8	4.06	3.72	F calc < Fcritical			P(T<=t) two-tail	0.000398	
Ra #9	4.28	3.9	Variances are equal.			t Critical two-tail	2.101	
Ra #10	4.12	3.81						
Standard Deviation	0.240	0.232						
Standard Error	0.0759	0.0735						

Figure F.8 F-test and t-test results for VT and CCAM cabinet Ra comparison.

Data	12. Operator A	16. Operator B	F-Test Two-Sample for Variances			t-Test: Two-Sample Assuming Equal Variances		
				Variable 1	Variable 2		Variable 1	Variable 2
Ra #1	4.82	4.65	Mean	4.476	4.675	Mean	4.675	4.476
Ra #2	4.89	4.4	Variance	0.0541	0.0473	Variance	0.0473	0.0541
Ra #3	4.7	4.59	Observations	10	10	Observations	10	10
Ra #4	4.24	4.35	df	9	9	Pooled Variance	0.0507	
Ra #5	4.67	4.74	F	1.145		Hypothesized Mean Diff.	0	
Ra #6	4.63	4.72	P(F<=f) one-tail	0.422		df	18	
Ra #7	5	4.35	F Critical one-tail	3.179		t Stat	1.976	
Ra #8	4.53	4.21	F calc < Fcritical			P(T<=t) two-tail	0.0637	
Ra #9	4.77	4.07	Variances are equal.			t Critical two-tail	2.101	
Ra #10	4.5	4.68						
Standard Deviation	0.217	0.233						
Standard Error	0.0688	0.0736						

Figure F.9 F-test and t-test results for Operator A and Operator B Ra comparison.

Appendix G Temperature F-tests and t-tests data

Data	SS304 40psi 4"	SS304 40psi 6"	F-Test Two-Sample for Variances			t-Test: Two-Sample Assuming Equal Variances			
Point #1	24.6	25.7		Variable 1	Variable 2		Variable 1	Variable 2	
Point #2	26.3	20.3	Mean	29.1	19.92	Mean	29.1	19.92	
Point #3	35.2	19.2	Variance	16.825	12.537	Variance	16.825	12.537	
Point #4	28.9	18.0	Observations	5	5	Observations	5	5	
Point #5	30.5	16.4	df	4	4	Pooled Variance	14.681		
Standard Deviation	4.102	3.541	F	1.342		Hypothesized Mean Diff.	0		
Standard Error	1.834	1.583	P(F<=f) one-tail	0.391		df	8		
T crit is based on df = 8, at 95% confidence level it equals 2.31.			F Critical one-tail	6.388		t Stat	3.788		
			F calc < Fcritical				P(T<=t) two-tail	0.005325	
			Variances are equal.				t Critical two-tail	2.306	

Figure G.1 F-test and t-test results for 4” and 6” blasts on 304 SS temperature comparison.

Data	SS304 40psi 8"	SS304 40psi 6"	F-Test Two-Sample for Variances			t-Test: Two-Sample Assuming Equal Variances			
Point #1	23.9	25.7		Variable 1	Variable 2		Variable 1	Variable 2	
Point #2	23.0	20.3	Mean	19.92	21.74	Mean	21.74	19.92	
Point #3	23.1	19.2	Variance	12.537	8.943	Variance	8.943	12.537	
Point #4	22.2	18.0	Observations	5	5	Observations	5	5	
Point #5	16.5	16.4	df	4	4	Pooled Variance	10.74		
Standard Deviation	2.990	3.541	F	1.402		Hypothesized Mean Diff.	0		
Standard Error	1.337	1.583	P(F<=f) one-tail	0.376		df	8		
			F Critical one-tail	6.388		t Stat	0.878		
			F calc < Fcritical				P(T<=t) two-tail	0.405	
			Variances are equal.				t Critical two-tail	2.306	

Figure G.2 F-test and t-test results for 6” and 8” blasts on 304 SS temperature comparison.

Data	SS304 50psi 6"	SS304 40psi 6"	F-Test Two-Sample for Variances			t-Test: Two-Sample Assuming Equal Variances			
Point #1	37.5	25.7		Variable 1	Variable 2		Variable 1	Variable 2	
Point #2	34.0	20.3	Mean	19.92	35.16	Mean	35.16	19.92	
Point #3	32.0	19.2	Variance	12.537	6.593	Variance	6.593	12.537	
Point #4	38.1	18.0	Observations	5	5	Observations	5	5	
Point #5	34.2	16.4	df	4	4	Pooled Variance	9.565		
Standard Deviation	2.568	3.541	F	1.902		Hypothesized Mean Diff.	0		
Standard Error	1.148	1.583	P(F<=f) one-tail	0.274		df	8		
			F Critical one-tail	6.388		t Stat	7.791		
			F calc < Fcritical				P(T<=t) two-tail	0.00005279	
			Variances are equal.				t Critical two-tail	2.306	

Figure G.3 F-test and t-test results for 40 psi and 50 psi blasts on 304 SS temperature comparison.

Data	SS304 60psi 6"	SS304 50psi 6"	F-Test Two-Sample for Variances			t-Test: Two-Sample Assuming Equal Variances		
				Variable 1	Variable 2		Variable 1	Variable 2
Point #1	49.5	37.5	Mean	45.08	35.16	Mean	45.08	35.16
Point #2	38.7	34	Variance	23.707	6.593	Variance	23.707	6.593
Point #3	44.8	32	Observations	5	5	Observations	5	5
Point #4	42.2	38.1	df	4	4	Pooled Variance	15.15	
Point #5	50.2	34.2	F	3.596		Hypothesized Mean Diff.	0	
Standard Deviation	4.869	2.568	P(F<=f) one-tail	0.121		df	8	
Standard Error	2.177	1.148	F Critical one-tail	6.388		t Stat	4.030	
			F calc < Fcritical			P(T<=t) two-tail		
			Variances are equal			t Critical two-tail		
						2.306		

Figure G.4 F-test and t-test results for 50 psi and 60psi blasts on 304 SS temperature comparison.

Data	SS304 90°	SS304 45°	F-Test Two-Sample for Variances			t-Test: Two-Sample Assuming Unequal Variances		
				Variable 1	Variable 2		Variable 1	Variable 2
Point #1	25.7	7.9	Mean	19.92	8.3	Mean	19.92	8.3
Point #2	20.3	7.7	Variance	12.537	0.895	Variance	12.537	0.895
Point #3	19.2	7.6	Observations	5	5	Observations	5	5
Point #4	18	8.4	df	4	4	Hypothesized Mean Diff.	0	
Point #5	16.4	9.9	F	14.008		df	5	
Standard Deviation	3.541	0.946	P(F<=f) one-tail	0.01273		t Stat	7.090	
Standard Error	1.583	0.423	F Critical one-tail	6.388		P(T<=t) two-tail	0.0008646	
			Fcalc > Fcrit			t Critical two-tail		
			Variances are unequal			2.571		

Figure G.5 F-test and t-test results for 45° and 90° blasts on 304 SS temperature comparison.

Data	SSThin 40psi 6"	SSThin 40psi 8"	F-Test Two-Sample for Variances			t-Test: Two-Sample Assuming Unequal Variances		
				Variable 1	Variable 2		Variable 1	Variable 2
Point #1	26.8	16.4	Mean	24.14	14.3	Mean	24.14	14.3
Point #2	20.3	15.6	Variance	20.478	2.815	Variance	20.478	2.815
Point #3	30.8	13.3	Observations	5	5	Observations	5	5
Point #4	22	12.3	df	4	4	Hypothesized Mean Diff.	0	
Point #5	20.8	13.9	F	7.275		df	5	
Standard Deviation	4.525	1.678	P(F<=f) one-tail	0.04029		t Stat	4.559	
Standard Error	2.024	0.750	F Critical one-tail	6.388		P(T<=t) two-tail	0.006063	
T crit is based on df = 5, at 95% confidence level it equals 2.57.			F calc > Fcritical			t Critical two-tail		
			Variances are not Equal			2.571		

Figure G.6 F-test and t-test results for 6" and 8" blasts on thin SS temperature comparison.

Data	SSThin 60psi 6"	SSThin 40psi 6"	F-Test Two-Sample for Variances			t-Test: Two-Sample Assuming Equal Variances		
Point #1	32.6	26.8		Variable 1	Variable 2		Variable 1	Variable 2
Point #2	27.3	20.3	Mean	24.92	24.14	Mean	24.92	24.14
Point #3	23.2	30.8	Variance	25.807	20.478	Variance	25.807	20.478
Point #4	21.4	22	Observations	5	5	Observations	5	5
Point #5	20.1	20.8	df	4	4	Pooled Variance	23.1425	
Standard Deviation	5.080	4.525	F	1.260		Hypothesized Mean Diff.	0	
Standard Error	2.272	2.024	P(F<=f) one-tail	0.414		df	8	
			F Critical one-tail	6.388		t Stat	0.256	
			F calc < Fcritical			P(T<=t) two-tail	0.804	
			Variances are equal			t Critical two-tail	2.306	

Figure G.7 F-test and t-test results for 40 psi and 60 psi blasts on thin SS temperature comparison.

Data	SSThin 40psi 6"	SSThin 40psi 6" 45°	F-Test Two-Sample for Variances			t-Test: Two-Sample Assuming Equal Variances		
Point #1	26.8	23.6		Variable 1	Variable 2		Variable 1	Variable 2
Point #2	20.3	20.9	Mean	24.14	23.52	Mean	24.14	23.52
Point #3	30.8	23.4	Variance	20.478	5.607	Variance	20.478	5.607
Point #4	22	27.3	Observations	5	5	Observations	5	5
Point #5	20.8	22.4	df	4	4	Pooled Variance	13.0425	
Standard Deviation	4.525	2.368	F	3.652		Hypothesized Mean Diff.	0	
Standard Error	2.024	1.059	P(F<=f) one-tail	0.119		df	8	
			F Critical one-tail	6.388		t Stat	0.271	
			F calc < Fcritical			P(T<=t) two-tail	0.793	
			Variances are equal.			t Critical two-tail	2.306	

Figure G.8 F-test and t-test results for 45° and 90° blasts on thin SS temperature comparison.

Data	SSThin 40psi 6"	SS304 40psi 6"	F-Test Two-Sample for Variances			t-Test: Two-Sample Assuming Equal Variances		
Point #1	26.8	25.7		Variable 1	Variable 2		Variable 1	Variable 2
Point #2	20.3	20.3	Mean	24.14	19.92	Mean	24.14	19.92
Point #3	30.8	19.2	Variance	20.478	12.537	Variance	20.478	12.537
Point #4	22	18	Observations	5	5	Observations	5	5
Point #5	20.8	16.4	df	4	4	Pooled Variance	16.5075	
Standard Deviation	4.525	3.541	F	1.633		Hypothesized Mean Diff.	0	
Standard Error	2.024	1.583	P(F<=f) one-tail	0.323		df	8	
			F Critical one-tail	6.388		t Stat	1.642	
			F calc < Fcritical			P(T<=t) two-tail	0.139	
			Variances are equal.			t Critical two-tail	2.306	

Figure G.9 F-test and t-test results for 6", 40 psi blasts of both substrates for T comparison.

Data	SS304 40psi 8"	SSThin 40psi 8"	F-Test Two-Sample for Variances			t-Test: Two-Sample Assuming Equal Variances		
Point #1	23.9	16.4		Variable 1	Variable 2		Variable 1	Variable 2
Point #2	23	15.6	Mean	21.74	14.3	Mean	21.74	14.3
Point #3	23.1	13.3	Variance	8.943	2.815	Variance	8.943	2.815
Point #4	22.2	12.3	Observations	5	5	Observations	5	5
Point #5	16.5	13.9	df	4	4	Pooled Variance	5.879	
Standard Deviation	2.990	1.678	F	3.177		Hypothesized Mean Diff.	0	
Standard Error	1.337	0.750	P(F<=f) one-tail	0.145		df	8	
			F Critical one-tail	6.388		t Stat	4.852	
			F calc < Fcritical			P(T<=t) two-tail	0.001269	
			Variances are equal.			t Critical two-tail	2.306	

Figure G.10 F-test and t-test results for 8", 40 psi blasts of both substrates for T comparison.

Data	SS304 60psi 6"	SSThin 60psi 6"	F-Test Two-Sample for Variances			t-Test: Two-Sample Assuming Equal Variances		
Point #1	49.5	32.6		Variable 1	Variable 2		Variable 1	Variable 2
Point #2	38.7	27.3	Mean	24.92	45.08	Mean	45.08	24.92
Point #3	44.8	23.2	Variance	25.807	23.707	Variance	23.707	25.807
Point #4	42.2	21.4	Observations	5	5	Observations	5	5
Point #5	50.2	20.1	df	4	4	Pooled Variance	24.757	
Standard Deviation	4.869	5.080	F	1.089		Hypothesized Mean Diff.	0	
Standard Error	2.177	2.272	P(F<=f) one-tail	0.468		df	8	
			F Critical one-tail	6.388		t Stat	6.406	
			F calc < Fcritical			P(T<=t) two-tail	0.0002077	
			Variances are equal.			t Critical two-tail	2.306	

Figure G.11 F-test and t-test results for 6", 60 psi blasts of both substrates for T comparison.

Data	SSThin 40psi 6" 45°	SS304 40psi 6" 45°	F-Test Two-Sample for Variances			t-Test: Two-Sample Assuming Equal Variances		
Point #1	23.6	7.9		Variable 1	Variable 2		Variable 1	Variable 2
Point #2	20.9	7.7	Mean	23.52	8.3	Mean	23.52	8.3
Point #3	23.4	7.6	Variance	5.607	0.895	Variance	5.607	0.895
Point #4	27.3	8.4	Observations	5	5	Observations	5	5
Point #5	22.4	9.9	df	4	4	Pooled Variance	3.251	
Standard Deviation	2.368	0.946	F	6.265		Hypothesized Mean Diff.	0	
Standard Error	1.057	0.420	P(F<=f) one-tail	0.0516		df	8	
			F Critical one-tail	6.388		t Stat	13.347	
			F calc < Fcritical			P(T<=t) two-tail	9.495 x 10-7	
			Variances are equal.			t Critical two-tail	2.306	

Figure G.12 F-test and t-test results for 45°, 40 psi blasts of both substrates for T comparison.

Appendix H Figures and Tables Permissions

Figure 2.1 [2, used with permission]

No Author. "Technical Reference: Surface Preparation." Blast One. 2014. <http://www.blast-one.com/weekly-tips/the-difference-between-surface-profile-and-class-of-blast> (accessed May 14, 2014) Used with permission from Blast One; email attached.

Table 2-1 [5, used with permission]

Momber A. *Blast Cleaning Technology: Chapter 1: Introduction*, 2008. p. 3.

http://vt.summon.serialsolutions.com/link/0/eLvHCXMwY2BQSDK1MDBNTgFmnETTFHNgg98C2OpIARZdjUxSk9PSTFB2vCOV5m6iDGZuriHOHrqwOcn4AsiRC_GISXxz0LyZrimwyQqsWE3iQav0jQzFGHgTQQvC80rAG8dS-JI4LvXUxfgmLD09V8ppeRo3AOU_KUc (accessed March 31, 2013) Used with permission from Copyright Clearance Center; letter attached.

Figure 2.2 [6, used with permission]

No Author. "Blast Cabinets." Norton Sandblasting Equipment, 2014. Date Obtained: May 14, 2014. Online: <http://www.nortonsandblasting.com/nsbcontact.html> (accessed May 14, 2014) Used with permission from Norton Sandblasting Equipment; email attached.

Figure 2.3 [8, used with permission]

Momber A. *Blast Cleaning Technology: Chapter 2: Abrasive Materials*, 2008. p. 19.

http://link.springer.com/chapter/10.1007%2F978-3-540-73645-5_2 (accessed March 31, 2013) Used with permission from Copyright Clearance Center; letter attached.

Figure 2.4 [11, 12 used with permission]

Momber A. *Blast Cleaning Technology: Chapter 2: Abrasive Materials*, 2008. p. 21.

http://link.springer.com/chapter/10.1007%2F978-3-540-73645-5_2 (accessed March 31, 2013) Used with permission from Copyright Clearance Center; letter attached.

Figure 2.5 [14, used with permission]

Momber A. *Blast Cleaning Technology: Chapter 2: Abrasive Materials*, 2008. p. 20.

http://link.springer.com/chapter/10.1007%2F978-3-540-73645-5_2 (accessed March 31, 2013) Used with permission from Copyright Clearance Center; letter attached.

Figure 2.6 [15, used with permission]

Momber A. *Blast Cleaning Technology: Chapter 2: Abrasive Materials*, 2008. p. 18.

http://link.springer.com/chapter/10.1007%2F978-3-540-73645-5_2 (accessed March 31, 2013) Used with permission from Copyright Clearance Center; letter attached.

Figure 2.7 [18, used with permission]

Momber A. *Blast Cleaning Technology: Chapter 2: Abrasive Materials*, 2008. p. 26.

http://link.springer.com/chapter/10.1007%2F978-3-540-73645-5_2 (accessed March 31, 2013) Used with permission from Copyright Clearance Center; letter attached.

Figure 2.8 [23, used with permission]

Day, James; Huang, Xiao; and Richards, N.L. "Examination of a Grit-Blasting Process for Thermal Spraying Using Statistical Methods." *Journal of Thermal Spray Technology*, 2005/Vol.

14, p. 477. <http://link.springer.com/article/10.1361%2F105996305X76469> (accessed November 2012) Used with permission from Copyright Clearance Center; letter attached.

Figure 2.9 [24, used with permission]

Maruyama T, Akagi K, Kobayashi T. "Effects of Blasting Parameters on Removability of Residual Grit." *Journal of Thermal Spray Technology*. 2006/Vol. 15, no. 4. p. 820. <http://link.springer.com/article/10.1361%2F105996306X147018> (accessed November 2, 2012) Used with permission from Copyright Clearance Center; letter attached.

Table 2-2 [27, used with permission]

Momber A. *Blast Cleaning Technology: Chapter 2: Abrasive Materials*, 2008. p. 14. http://link.springer.com/chapter/10.1007%2F978-3-540-73645-5_2 (accessed April 1, 2013) Used with permission from Copyright Clearance Center; letter attached.

Figure 2.10 [34, used with permission]

Momber A. *Blast Cleaning Technology: Chapter 6: Surface Preparation Process*, 2008. p. 280. http://link.springer.com/chapter/10.1007/978-3-540-73645-5_6 (accessed March 31, 2013) Used with permission from Copyright Clearance Center; letter attached.

Figure 2.11 [36, used with permission]

Makova, I., Sopko, M. "Effect of Blasting Material on Surface Morphology of Steel Sheets." *Acta Metallurgica Slovaca*. 2010/ Vol. 16, no. 2, p. 111. (accessed March 07, 2013) Used with permission from Act Metallurgica Slovaca; email attached.

Figure 2.12 [38, 39 used with permission]

Momber A. *Blast Cleaning Technology: Chapter 2: Abrasive Materials*, 2008. p. 11, 12. http://link.springer.com/chapter/10.1007%2F978-3-540-73645-5_2 (accessed March 31, 2013) Used with permission from Copyright Clearance Center; letter attached.

Figure 2.13 [50, used with permission]

Fang, C.K., Chuang, T.H. "Erosion of SS41 Steel by Sand Blasting." *Metallurgical and Materials Transactions A*. 1999/Vol. 30A, p. 944. (accessed January 11, 2013) Used with permission from Copyright Clearance Center; letter attached.

Figure 2.14 [50, used with permission]

Fang, C.K., Chuang, T.H. "Erosion of SS41 Steel by Sand Blasting." *Metallurgical and Materials Transactions A*. 1999/Vol. 30A, p. 944. (accessed January 11, 2013) Used with permission from Copyright Clearance Center; letter attached.

Figure 2.15 [51, used with permission]

Mellalia, M., Grimaud, A., Leger, A.C., Fauchais, P., and Lu, J. "Alumina Grit Blasting Parameters for Surface Preparation in the Plasma Spraying Operation." *Journal of Thermal Spray Technology*. 1997/Vol 6. No. 2. p 219. (accessed October 22, 2012) Used with permission from Copyright Clearance Center; letter attached.

Figure 2.16 [53, used with permission]
Chander, K. Poorna, Vashita, M., Sabiruddin, Kazi, Paul, S., Bandyopadhyay, P.P. "Effects of Grit Blasting on Surface Properties of Steel Substrates." *Materials and Design*. 2009. p. 2901. (accessed November 2012) Used with permission from Copyright Clearance Center; letter attached.

Figure 2.17 [53, used with permission]
Chander, K. Poorna, Vashita, M., Sabiruddin, Kazi, Paul, S., Bandyopadhyay, P.P. "Effects of Grit Blasting on Surface Properties of Steel Substrates." *Materials and Design*. 2009. p. 2899. (accessed November 2012) Used with permission from Copyright Clearance Center; letter attached.

Figure 2.18 [51, used with permission]
Mellalia, M., Grimaud, A., Leger, A.C., Fauchais, P., and Lu, J. "Alumina Grit Blasting Parameters for Surface Preparation in the Plasma Spraying Operation." *Journal of Thermal Spray Technology*. 1997/Vol 6. No. 2. p 221. (accessed October 22, 2012) Used with permission from Copyright Clearance Center; letter attached.

Figure 2.19 [54, used with permission]
Amada, Shigeyasu, Hirose, Tohru. "Influence of grit blasting pre-treatment on the adhesion strength of plasma sprayed coatings: fractal analysis of roughness." *Surface and Coatings Technology*. 1998/Vol. 102. p. 134. [http://dx.doi.org/10.1016/S0257-8972\(97\)00628-2](http://dx.doi.org/10.1016/S0257-8972(97)00628-2) (accessed October 29, 2012) Used with permission from Copyright Clearance Center; letter attached.

Figure 2.20 [55, used with permission]
Carter, G., Bevan I.J., Katardjiev I.V., Nobes, M.J. "The Erosion of Copper by Reflected Sandblasting Grains." *Materials Science Engineering*. 1991/Vol. A. no. 132. P. 232. (accessed October 22, 2012) Used with permission from Copyright Clearance Center; letter attached.

Figure 2.21 [56, used with permission]
Celik, E., Demirkiran, A.S., Avci, E. "Effect of Grit Blasting of Substrate on the Corrosion Behaviour of Plasma-Sprayed Al₂O₃ Coatings." *Surface and Coatings Technology*. 1999/Vol. 116-119. p. 1062. (accessed October 29, 2012) Used with permission from Copyright Clearance Center; letter attached.

Figure 2.22 [59, used with permission]
Wigren, Jan. "Technical Note: Grit Blasting as Surface Preparation Before Plasma Spraying." *Surface and Coatings Technology*. 1988/Vol 34. p. 107. (accessed January 15, 2013) Used with permission from Copyright Clearance Center; letter attached.

Figure 2.23 [60, used with permission]
Mombber A. *Blast Cleaning Technology: Chapter 2: Abrasive Materials*, 2008. p. 38. http://link.springer.com/chapter/10.1007%2F978-3-540-73645-5_2 (accessed March 31, 2013) Used with permission from Copyright Clearance Center; letter attached.

Figure 2.24 [62, used with permission]

Momber A. *Blast Cleaning Technology: Chapter 2: Abrasive Materials*, 2008. p. 47, 48.
http://link.springer.com/chapter/10.1007%2F978-3-540-73645-5_2 (accessed March 31, 2013)
Used with permission from Copyright Clearance Center; letter attached.

Figure 2.25 [64, used with permission]

Tabenkin, Alex. "The Basics of Surface Finish Measurement." *Quality Magazine*. 2014.
http://www.deterco.com/products/Mahr%20Federal/newsletter/finish_measure_10_19_04.htm
(accessed May 14, 2014) Used with permission from Mahr Federal Inc.; email attached.

Figure 2.26 [66, used with permission]

Pickrell, G., Homa, D, Mills, R. "Abrasive Blasting Deliverable No.3." CCAM. 2014. (accessed April 2, 2014) Used with permission from Robert Mills.

Figure 2.27 [67, used with permission]

Sosale, G., Hackling S.A., and Vengallatore, S. "Topography Analysis of Grit-Blasted and Grit-Blasted-Acid Etched Titanium Implant Surfaces Using Multi-scale Measurements and Multi-Parameter Statistics." *Journal of Materials Research*. 2011/Vol. 23, Issue 10. p. 2709. (accessed June 6, 2014) Used with permission from Copyright Clearance Center; letter attached.

Table A-1 [35, used with permission]

No Author. "Blast Media Chart." Norton Sandblasting Equipment. 2014.
<http://www.nortonsandblasting.com/nsbabrasives.html> (accessed June 9, 2014) Used with permission from Norton Sandblasting Equipment; email attached.

Figure B.1 [63, used with permission]

No Author. "Abrasive Blast Nozzles." Kennametal Inc. 2012 page 9.
http://www.kennametal.com/content/dam/kennametal/kennametal/common/Resources/Catalogs-Literature/Advanced%20Materials%20and%20Wear%20Components/B-12-02861_KMT_Blast_Nozzles_Catalog_EN.pdf (accessed June 9, 2014) Used with permission from Kennametal, Inc.; email attached.